POLITECNICO DI MILANO

SCUOLA INTERPOLITECNICA DI DOTTORATO

Doctoral Program in Electrical Engineering

Final Dissertation

Design and Optimization of Reflectarray Antennas

Bui Van Ha

Tutor
Prof: Riccardo Enrico Zich

Co-ordinator of the Research Doctorate Course
Prof: Alberto Berizzi

February, 2014

Abstract

REFLECTARRAY antennas are nowadays a quite popular technology, used in several applications, thanks to their advance features e.g. low-cost, conformal deployment, and the reconfigurability. Nevertheless, they still suffer for some limitations, that are partially due to their intrinsic reduced bandwidth, that could be enlarged, but generally with a drastic increase of the structure complexity. Therefore, in this thesis new types of re-radiating element for reflectarray design will be presented. Moreover, the design will exploit the capability of optimization algorithms to support the design of RAs and enhance their bandwidth.

The developed activity was mainly focused on the following two research areas:

- the development of enhanced optimization techniques;
- the study of innovative, wide bandwidth printed Reflectarray Antennas (RAs).

For what concerns the activity on the optimization algorithms, different available solutions, including evolutionary algorithms (e.g. PSO, GA), Bayesian optimization algorithm (BOA), and compact genetic algorithm (cGA), have been firstly investigated. Modified versions of BOA and cGA, which greatly improved their performances with respect to the original algorithms, have been then developed. These modified algorithms have been successfully applied to array synthesis problems, as the design of thinned arrays and sparse arrays, revealing promising features also for more complex applications as the optimized design of reflectarray antennas.

Passive reflectarrays are flat arrays of passive printed elements, whose resonant behavior allows a phase shaping of a beam incident on the array, thus replacing the curvature of a conventional reflector. Despite of their advantages, RAs present also some drawbacks, the main of which is their narrow bandwidth. In order to enhance the bandwidth, new possible configurations of reflectarray unit elements have been studied. After an exhaustive analysis of different types of elements, the most promising have been used to design entire RAs; their full-wave numerical analysis shows the obtained bandwidth improvement.

Reconfigurable reflectarray antenna (RRA) have been also investigated in the thesis. RRA offer the possibility of dynamically control and reconfigure the antenna's beam

patterns, feature which is highly demanded in radar and satellite communication applications. The research has been focused on the design of a RRA unit cell, simple and easy to implement in RRA. The selected configuration shows its characteristics, that make it suitable for the design of a whole RRA.

Acknowledgments

I would like to give my thanks firstly to Prof. Riccardo Enrico Zich, my supervisor through these years, for his advice, kindness and for his support through some hard times. I wholeheartedly thank Prof. Paola Pirinoli at Politecnico di Torino for her supervise, her care over my development as my second advisor.

I would like to give big thanks to Dr. Marco Mussetta for his supports over multiple topics. To Dr. Francesco Grimaccia for his help over my university stuffs. To Prof. Alberto Berizzi, the director of Electrical Engineering PhD program, who has allowed me to participate to valuable conferences, courses.

I wish to thank Prof. Fan Yang and Prof. Sean Victor Hum for accepting the role of international reviewers of my thesis. With your valuable comments, advise, the thesis has been improved. It is certain that within this work is exclusively my own.

Concerning chapter 5, I would like to thank Prof. Sean Victor Hum for the results of my visiting at the University of Toronto, Canada under his supervision. Thank to his deep knowledge about Reflectarray, I have learned a lot from him through the weekly meeting.

I also deeply thank Prof. Dao Ngoc Chien at Hanoi University of Science and Technology, Vietnam for his guidance, encouragement when I first joined with his Electromagnetic group. To my colleges at Politecnico di Milano, and University of Toronto, for your sharing during the time I stayed.

Finally, big hug to my family, friends, and my girlfriend, for your supports, your encouragements, you have given me in these years. To you, I dedicate this thesis.

Contents

CHAPTER 1

General Introductions

Antennas are essential components of any wireless communication system, transmitting and receiving electromagnetic signals from one point to the other. They have been designed in all kinds of shapes and sizes integrating themselves into several applications, such as personal communications and wireless connection.

In many applications, such as satellite or radar, the radiated power need to focus at a specific direction to maximize the signal at the receivers. In these cases, antennas with high gain are required. Generally, there are two approaches to achieve high gain antennas: Big aperture antennas, or forming arrays of small antennas. The aperture antennas have been the first structures that achieved high gain by creating large illuminated apertures. The larger the aperture and the more uniform field phases and amplitude on the aperture, the higher the directivity will be. The horn antennas and the reflector are two typical examples of this type. The aperture antennas, however, often have very large physical dimension, which requires a supporting structure. Therefore, aperture antennas are usually bulky and heavy, which limits their applications to modern communication systems.

The second approach is to group several small antennas into an array, in which each antenna is excited with a specific phase, to effectively create a large aperture of uniform field. The array antennas also offer reconfigurability since the array phase can be electrically tuned by controlling the excitation, i.e., the phased arrays. Moreover, the elements of the array can be planar or conformal, therefore the phased arrays are often less bulky than the aperture antennas. However, the phased arrays have their own drawbacks, which are the design of the feeding network and the losses. Since each element is excited individually by transmission line, the arrays need a complex feeding network to excite their elements. The losses over the transmission line will increase when the array's size increases. The losses and complexity associated with the feed

network are major limitations of the phased arrays.

Both approaches have their own advantages and limitations. The idea of combining their advantages, i.e., spatial techniques for exciting an array using single feed antenna and an array of passive scatters, has been implemented, for example reflectarray antennas [1]. The reflectarray antennas usually consist of an array of passive elements, which are spatially excited by a feed antenna, and reflect the wave to create uniform phase in the same way as an aperture antenna does. Compared to traditional reflectors, the RAs have the major advantage of being planar, which enables the RAs to be integrated into structures such as walls and roofs, and they are even more portable. Furthermore, they may be designed on conformal surface as well.

1.1 Evolution of Reflectarray Antennas

As it is well known, reflectarray (RA) antennas consist of one or more feed antennas illuminating a usually flat reflecting surface, whose electromagnetic reflecting features have to be suitably designed in order to obtain the required performances of the whole radiating system. Reflectarray antennas have first been proposed in 1963 by Kennedy et al. [2], where the reflecting surface consisted of a planar array of variable-length shorted waveguide components, as shown in Fig. 1.1. So, the original reflectarray antenna was definitively not a low cost, easy to manage, light-weight antenna, allowing foldability or any other of the interesting features that nowadays are typical properties of reflectarray solutions.

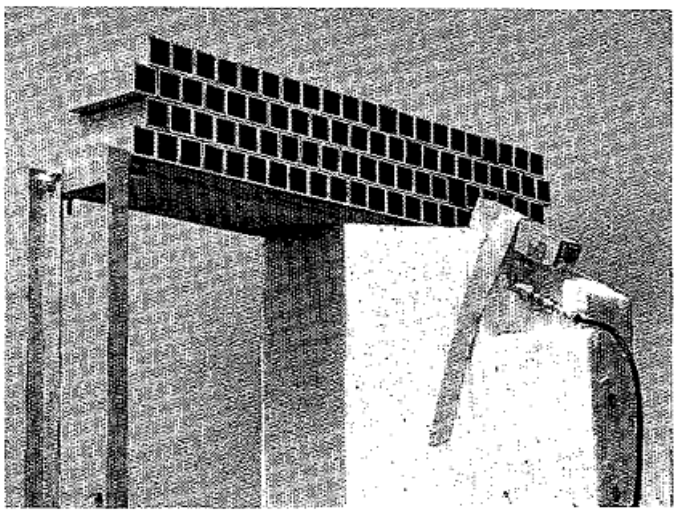

Figure 1.1: *Waveguide Reflectarray Antenna (from [2]).*

This probably is the reason why for more than a decade this solution, without apparent advantages but with evident drawbacks compared to parabolic reflectors for example, has not been considered again, until 1975, when the feasibility of a reflectarray with scanning possibilities has been claimed in a US patent [3]. In this case, a reflecting surface consisting of spiral antenna elements has been proposed, where each re-radiating element uses a suitable set of diodes to manage properly the phase of the

reflected wave allowing beam scanning of the whole system. So, it is possible to say that from the very beginning, the usual way of enhancing reflectarray antenna electromagnetic performances in order to introduce them in real life application, is to exploit complexity at most.

The real breakthrough in reflectarray technology came with the evolution of printed circuit technology and high frequency laminates synthesis allowed low-profile, lightweight implementations. In fact, even if the first reflectarray patent introducing a microstrip patch antenna based reflecting surface has been published in 1977 [4], it is only from the late eighties that this kind of solution spread out. Furthermore, in order to achieve good antenna performances, a very large array of patches has to be suitably designed exploiting in the proper way all the possible geometrical free parameters, requiring the adoption of numerical electromagnetic solvers, sophisticated numerical optimization tools and in any case a significant numerical effort.

These, i.e., the enabled technology and the numerical modeling tool availability, are the reasons why only nowadays printed reflectarrays technology became well-assessed, and in the last years it substituted other technologies in many fields of applications, in particular where it is of paramount importance to fulfill constrains such as high gain, narrow beam with low side lobes, lightweight and smaller volume, easiness of deployment and foldability.

The main limitation now to a complete diffusion of this kind of solutions is due to the fact that the most recent antenna systems require a very large bandwidth, typically even the multi-band operability, or the possibility of beam steering: features that are still difficult goals to be achieved with a printed reflectarray.

In fact, for what concerns the bandwidth, it is intrinsically limited for two different reasons: the poor bandwidth of printed radiating elements themselves, usually no larger than the $3-6\%$, and, most importantly, the frequency-dependence of the phase delay of the incident field. In particular, this second aspect is quite critical and becomes dominant in large RAs [5, 6], since it requires that the RA elements should be able to compensate different phase delays at different operating frequencies

The usual way to enhance the RA bandwidth is to use radiating elements that consist of two or more stacked printed single radiators (see for instance [7–10]). However, this technique results in a heavier, bulkier and more complex re-radiating structure, as depicted in Fig. 1.2, requiring a careful and expensive manufacturing and presenting some difficulties for its foldability.

Recently, alternative solutions have been proposed, in which the RA elements are single-layer printed patches of non conventional shape [11–16]. These shapes are chosen properly in order to present more degrees of freedom as compared to the one usually adopted for multilayer stacked structures: these can be used to compensate the frequency variation of the phase, allowing the bandwidth enhancement.

More recently, design of reflectarray antennas also involved the use of sub-wavelength element as unit cell to enhance their bandwidth [17–21]. Initially, the term "artificial impedance surfaces" was used to express the structure of closely spaced electrically small patches [17], and later on was changed to sub-wavelength reflectarray antennas. The idea is to reduce the element's size to avoid the near-resonance operation of conventional $\lambda/2$ unit cells. Reported results have shown an improvements of reflectarray bandwidth to $17-19\%$ 1 dB gain bandwidth. However, the main drawback of this

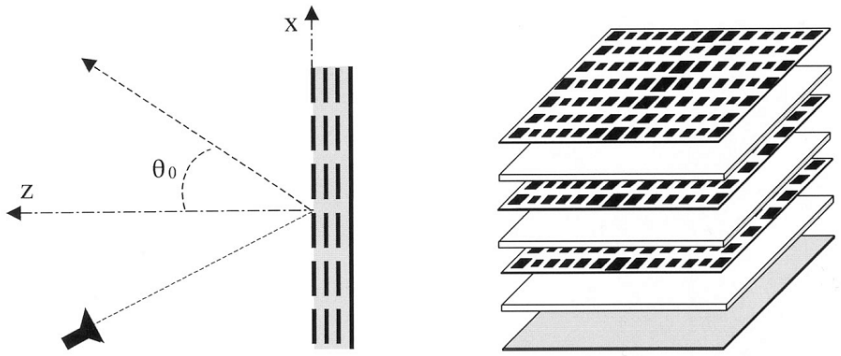

(a) Reflectarray illuminated by feed. (b) Multilayer structure.

Figure 1.2: *Multi-layers Reflectarray Antenna (from [8]).*

approach is the limited phase range of these elements. As the cell's size decreases, the phase range decreases, and consequently, the antenna gain and performance are also decreased.

In recent years, there is another trend in RA design, which integrates electronic devices into RA in order to change the electrical properties of RA elements to reconfigure the RA pattern. These RAs are classified as reconfigurable reflectarray antennas (RRAs). In fact, the first RRA has been designed a long time ago, when Phelan [3] implemented rotation technique to spiral cell of reflectarray to reconfigure circularly polarized wave. However, until recent years, with enabled technologies, several alternative solutions for RRAs have been proposed including the use of varactor diodes, PIN diodes, and also MEMS. The RRAs offer dynamically switching beam capabilities, which allow RRAs to be applied to several applications such as radars. RRAs can also be reconfigured at different frequencies, which would increase their bandwidth. The limitations of RRAs, however, are the lack of phase availability and the complexity of the designs. The first factor contributes to the discrepancies in RRA performances, while the second factor results in a complex or multi-layer design, which includes the controlling networks of RRAs. The RRA designs, therefore, need a simple structure with continuous phase which allow to apply different design methods for the whole RRA design.

1.2 Optimization of Reflectarray Antennas

The design of RAs for modern applications often involves hundreds of elements, which requires an accurate design method for properly selecting RA elements. The use of an indirect synthesis procedure based on an optimization scheme could be convenient since it can handle a large number of degrees of freedom and provide a configuration that satisfies different constraints.

In general, the optimization of RAs often uses phase-only optimization techniques, which involves two steps: the phase-only synthesis (POS) is carried out first to find the phase distribution of all RA elements to attain desired beam, then the RA element's dimension is selected to provide the required phase calculated in the first step. The second step is often based on the analysis of the RA element which usually takes the local

periodic (LP) assumption, i.e., element is analyzed in an infinite environment [22]. The LP analysis is able to capture the mutual coupling effects between identical elements. However, the final RA design consists of different elements, which potentially vary strongly in geometries, thereby changing the interaction between elements. Therefore, this leads to significant changes in the measured performances of the RA respect to the numerically presented ones.

Recently, direct optimization technique (DOT) [23] has been proposed to directly relate the element's physical dimension to the RA performance. The surface current corresponding to the element's geometries is calculated first and then the far-field pattern, which is used for evaluating the fitness function of the optimization algorithm, is calculated using the equivalent theorem. The method, however, is still based on the LP assumption for element analysis, i.e., calculating the surface current. Moreover, the optimization is a gradient-based minimax, which greatly depends on starting points and is a local optimization algorithm. Finally, the optimization procedure requires a "look-up table" to store the surface current for calculating the RA pattern to proceed the optimization routine.

The application of the global optimizations to RA design has been also proposed [24, 25], and deeply investigated. Genetic Algorithm (GA) has been first applied to the design of RA [24] to maximize the gain in the desired direction and minimize the side-lobe level. In that work, RA elements have been represented by simplified models to accelerate the optimization procedure. Particle Swarm Optimization (PSO) has also been applied to RA design [25]. The RA has been synthesized to generate multi-beams with single feed, and in this case it has been applied array theory to calculate the far-field radiation, introducing suitable approximated modals of both the feed and the elements. Although, these methods were efficient to optimize the RAs, they ignored the interaction between elements, by using the ideal pattern for every elements or the simplified models. As a result, the obtained patterns show significant discrepancies with respect to measurements.

1.3 Motivations and Objectives

From these view points, a single-layer element, which offers enough phase range and several degrees of freedom to compensate the required phase at different frequencies, is needed for the design of passive RA. For active reconfigurable RAs, a simple structure with continuous tuning phase is desired to introduce electronic components and manage the RRA. Moreover, effective optimization algorithms are desired to solve complex Electromagnetic problems, especially RA. Finally, an accurate optimization procedure for RA design is also needed to efficiently handle the design process.

Given the issues outlined above, the goal of this thesis is to develop new optimization algorithms and apply to design and optimize reflectarray antennas with improved bandwidth performance for passive RA, and effectively controlling the design parameters for RRA. To achieve this goal, the following steps need to be done:

- Develop new optimization algorithms (by introducing suitable modifications to existing algorithms to improve their performances), which are applicable to electromagnetic (EM) problems, and able to manage a large number of parameters.

- Investigate non-conventional single-layer broadband elements with several degrees of freedom for application in passive RAs.
- Design entire passive RAs implementing a new design method to handle all degrees of freedom in order to improve the bandwidth of the RA.
- Propose a new, simple RRA element which offers continuously controllable phase, and it is easy to integrate with electronic devices.
- Design the entire RRA by means of optimization to effectively control the RRA performances.

1.4 Outline

The outline of this thesis is as follows. Chapter 2 is dedicated to the electromagnetic backgrounds of the reflectarray antennas. The chapter presents the theory of array antennas including thinned and sparse arrays. Reflectarray theory is also introduced, which is extensively employed for the design of RAs later. In Chapter 3, two new modified optimization algorithms: The improved compact Genetic Algorithm, and the modified Bayesian Optimization Algorithm, are presented. Their performances have been tested with mathematical and EM problems. In Chapter 4, the design of passive RAs implementing a simple structure of double square rings as elementary, is carried out. The double parameter design method is also introduced, and its application to design entire RAs has been presented. In Chapter 5, a new RRA element has been presented, and its implementation to design of entire RRA has also been shown. Finally, Chapter 6 presents the thesis's conclusions.

CHAPTER 2

Electromagnetic Background

In this chapter, some basic principles that have been used to analyze and design reflectarrays will be presented. Starting from the array theory, the definition of element pattern and array factor will be introduced. In the design of reflectarrays, since the arrays often consist of hundreds of elements, the array patterns are sometimes approximated as the product of the element pattern and the array factor. Next, the concept of phased array and phase shift, which are used to calculate the required phase for reflectarray design, will be presented. Finally, background on thinned and spares arrays are introduced, which are used to exemplify the effectiveness of the newly developed optimization algorithms.

In the second section, the concept and theory for designing reflectarray will be presented. The coordinate system that will be used to design RA is defined first. The incident fields is then derived from the feed to each array's element, where it is reflected back. Following, the radiation pattern of reflectarray antenna is calculated using the array theory presented in the previous section.

The third section will be dedicated to the Floquet analysis, which is used for analyzing periodic apertures. The expression of periodic function will be presented first as the expansion of Floquet series through the Fourier transform. Analogously, the electromagnetic fields of periodic structure will be derived. From this analysis, it will be shown that, for infinite structures, the electromagnetic fields will radiate at discrete directions, instead of everywhere as the case for finite structures. The analysis is useful the for design of reflective surface in Chapter 5. Finally, some conclusions will be drawn at the end of this chapter.

2.1 Antenna Array Principles

An antenna array is a spatially extended collection of similar radiating elements oriented in the same direction in 3-D space and usually with the same radiation patterns. The elements are usually spaced on a regular grid, and they are fed with currents usually differing in both amplitude and phase, in order to properly shape the far-field radiation pattern. In this section, some basic properties of antenna array such as the element pattern, array pattern, definition of phased array, thinned array and sparse array will be presented. For more detail on array theory, please refer to [26, 27].

2.1.1 Element Pattern

Element pattern is the radiation pattern of a single antenna of which the array consists. It is the fundamental element for estimating the radiated power of an antenna array, which is the superposition of all element patterns. The element pattern is defined as the field intensity distribution of a radiating element as function of two far-field coordinates, while the radial distance remains constant. The radiated electric field in the far-field region can be expressed as

$$\vec{E}(r,\theta,\phi) = A\frac{e^{-jk_0 r}}{r}\vec{e}(\theta,\phi) \tag{2.1}$$

where A is a constant, which is related to the input excitation of the antenna, $\vec{e}(\theta,\phi)$ is the element pattern, (r,θ,ϕ) is the spherical coordinate of far-field point, i.e., observation point, and k_0 is the wave number in free space.

The other term, which is related to element far-field pattern, is the directivity. The directivity is the far-field intensity pattern normalized with respect to the square root of the average radiated power per unit angle, as it follows:

$$\vec{D}(\theta,\phi) = \sqrt{\frac{4\pi}{\eta P_r}}A\vec{e}(\theta,\phi) \tag{2.2}$$

where η denotes the free space impedance, which is approximated to 120π Ohms, and P_r is the total radiated power, which is determined by integrating the Poynting vector on a closed surface covering the antenna:

$$P_r = \iint\limits_{\Omega}\frac{|\vec{E}^2|}{\eta}r^2\mathrm{d}\Omega = \frac{|A|^2}{\eta}\int_0^{2\pi}\int_0^{\pi}|\vec{e}(\theta,\phi)|^2\sin\theta\,\mathrm{d}\theta\,\mathrm{d}\phi \tag{2.3}$$

The directivity of an element represents the relative power flux per solid angle with respect to that of an isotropic radiator that radiates an equal amount of power. A more practical term that relates the far-field intensity pattern to the incident power at the input instead of radiated power is antenna gain, which is expressed as:

$$\vec{G}(\theta,\phi) = A\sqrt{\frac{4\pi}{\eta P_{inc}}}\vec{e}(\theta,\phi) \tag{2.4}$$

Since the total radiated power is less than the incident power, because of Ohmic loss, the gain is always smaller than the directivity.

2.1.2 Array Pattern

By the array's definition, i.e., array is a group of elements, all array pattern is the summation of the element fields. It is shown that the far-field pattern of an array of identical elements can be presented as a product of the *element pattern* and the *array factor*, i.e., *pattern multiplication*. Considering an array of N identical elements uniformly distributed on X-axis with excitation coefficients, A_n (where $n = 1, \ldots, N$) , and separation d, the total radiated field of the array is expressed as:

$$\vec{E}_{\text{array}} = A_1 \frac{e^{-jk_0 r_1}}{r_1} \vec{e}(\theta, \phi) + A_2 \frac{e^{-jk_0 r_2}}{r_2} \vec{e}(\theta, \phi) + \ldots + A_N \frac{e^{-jk_0 r_N}}{r_N} \vec{e}(\theta, \phi) \tag{2.5}$$

where r_n is the distance from the n^{th} element to the observation point located on the far-field region.

Eqn. 2.5 can be written as:

$$\vec{E}_{\text{array}} = \frac{e^{-jk_0 r_1}}{r_1} \vec{e}(\theta, \phi) \left[A_1 + A_2 \frac{r_1}{r_2} e^{-jk_0(r_2 - r_1)} + \ldots + A_N \frac{r_1}{r_N} e^{-jk_0(r_N - r_1)} \right] \tag{2.6}$$

Since the distance from the observation point to array element is much greater than the distance between elements, two approximations are made $r_1 \approx r_n$ and $r_n - r_1 \approx (n-1)d \sin\theta \cos\phi$. Eqn. 2.6 reduces to:

$$\vec{E}_{array} \approx \frac{e^{-jk_0 r_1}}{r_1} \vec{e}(\theta, \phi) \left[A_1 + A_2 e^{-jk_0 d \sin\theta \cos\phi} + \ldots + A_N e^{-jk_0(N-1)d \sin\theta \cos\phi} \right] \tag{2.7}$$

In Eqn. 2.7, the quantity inside the square bracket is called the *array factor*, while the rest on the right is the *element pattern* as written in Eqn. 2.1. From Eqn. 2.7, it is shown that the total radiated field of the array is the product of array factor and element pattern. For the $2-D$ planar array, the array factor can be derived in the same way as:

$$AF(\theta, \phi) = \sum_{n=1}^{N} A_n e^{[-jk_x x_n - jk_y y_n]} \tag{2.8}$$

where (x_n, y_n) represents the coordinate of the n^{th} element and k_x, k_y are

$$k_x = k_0 \sin\theta \cos\phi \quad k_y = k_0 \sin\theta \sin\phi \tag{2.9}$$

2.1.3 Phased Array

One of the main advantage of antenna arrays is their possibility to scan the beam by controlling the phase of excitation to each array element, this type of array is called phased array. This section, the theory to scan such phased arrays is presented. For sake of simplicity, it is assumed to have a uniform array, which consists of identical elements all of identical magnitude and each with a progressive phase. Assuming each succeeding element has β progressive phase, the *array factor* in Eqn. 2.7 can be expressed as:

$$AF = \left[A_1 + A_2 e^{-j(k_0 d \sin\theta\cos\phi+\beta)} + \ldots + A_N e^{-j(N-1)(k_0 d \sin\theta\cos\phi+\beta)}\right] \quad (2.10)$$

$$= A\sum_{n=1}^{N} e^{-j(n-1)(k_0 d \sin\theta\cos\phi+\beta)} \quad (2.11)$$

here, the amplitude of excitation is identical, i.e., $A_n = A$. The array factor, therefore, can be reduced to:

$$AF = \sum_{n=1}^{N} e^{-j(n-1)\psi} \quad (2.12)$$

where $\psi = kd\sin\theta\cos\phi + \beta$

The array factor in Eqn. 2.12 is the summation of exponential, it can be represented by the vector sum of N phasors each of unit amplitude and progressive phase ψ relative to the previous one. It appears that by controlling the phase of excitation the maximum radiation can be oriented in any direction, forming a scanning array. For example, we want the main beam is at direction of (θ_0, ϕ_0), the phase shift β between the elements will be determined by:

$$\psi = (kd\sin\theta\cos\phi + \beta)\big|_{\theta=\theta_0,\phi=\phi_0} = kd\sin\theta_0\cos\phi_0 + \beta = 0$$
$$\Rightarrow \beta = kd\sin\theta\cos\phi \quad (2.13)$$

Therefore, by controlling the phase shift between the elements, the main beam radiation can be tilted in desired direction to form a scanning array. In practice, the phase shift can be adjusted by using electronic devices such as ferrite or diode phase shifters. This is the basic principle of electronically scanning phased array.

For planar arrays, the scanning technique is similar as for linear arrays. In this case, the progressive phase for each element will be determined in both x- and y- directions. The array factor in Eqn. 2.8 will be written as:

$$AF(\theta,\phi) = \sum_{n=1}^{N}\sum_{n=1}^{N} e^{-j(n-1)(k_0 d_x \sin\theta\cos\phi+\beta_x)} e^{-j(m-1)(k_0 d_y \sin\theta\sin\phi+\beta_y)} \quad (2.14)$$

where d_x, d_y are the distances between elements, and β_x, β_y are the phase shift along $x-$ and $y-$ directions respectively.

By controlling the phase shift β_x, β_y independently, it is possible to scan the main beam in $x-$ and $y-$ directions differently. However, in practical applications, it often requires to have only one main beam. Assuming the main beam is at the (θ_0, ϕ_0) direction, the phase shifts between elements in the $x-$ and $y-$ directions are determined as:

$$\beta_x = k_0 d_x \sin\theta_0\cos\phi_0 \quad (2.15a)$$

$$\beta_y = k_0 d_y \sin\theta_0\sin\phi_0 \quad (2.15b)$$

2.1.4 Thinned Array

Traditionally, antenna arrays are designed with uniformly spaced and weighted element (usually of 0.5λ separation), which allow to easily calculate the array pattern and predict the side-lobe level of the array, e.g. using array factor as in Eqn. 2.10. Recently, the

synthesis of unequally spaced array has received a great attention in the Electromagnetic community. With respect to equally spaced arrays, unequally spaced arrays provide more degree of freedom, i.e. the element's position; thanks to this, the unequally spaced can provide lower side-lobe levels (SLL) even with uniformly excitation [28]. Generally, there are proposed two approaches to obtain this kind of arrays: Thinned array and sparse array. Both approaches are presented in the following subsections, and will be used as optimization problems to test proposed optimization algorithms.

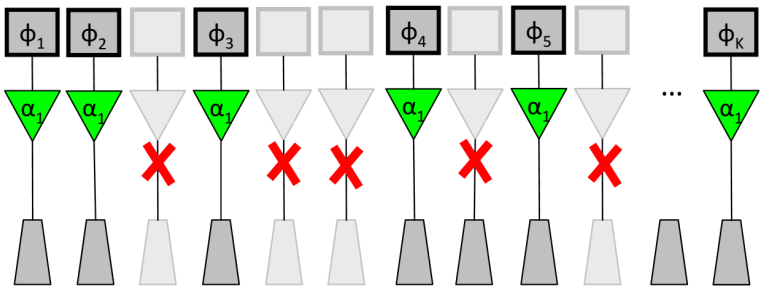

Figure 2.1: *Thinned array from a regular array.*

Thinned arrays, where some elements in the regular grid are turned off as shown in Fig. 2.1, is the first proposed approach to achieve unequally spaced array. Compared to the equally spaced array, the thinned arrays offer several advantages such as the power consumption, and array weight. Moreover, thinned arrays provide an extra design parameter, i.e. turned off/on position, to control the SLL in thinned arrays. Massively thinned arrays, i.e. thinned array in which almost half of the elements is switched off, are recently become more and more popular, since the reduced number of switched on elements allows a strong reduction of the array weight and of the complexity of the feeding network. The reduction of the number of array elements has however also some drawbacks, the main of which is the decreasing of the maximum gain that is proportional to the total number of array elements [29].

The synthesis of thinned array, i.e. involving the procedure of removing some radiating elements by terminating them with matched loads, can be considered as a binary problem, where the excitation of each element can be assigned a value of 1/0 corresponding to the state "ON/OFF" of that element in the array. From the array theory, the array factor of thinned array is calculated as:

$$AF = \sum_{n=1}^{N} A_n e^{-j(n-1)\psi} \tag{2.16}$$

where A_n is the excitation, could be assigned a value of 1 or 0, and $\psi = kd \sin\theta \cos\phi + \beta$.

The determination of turn ON/OFF elements results heavily in the affection of the performance of the thinned array, especially the behavior of peak side-lobe level (PSL). As an example, Fig. 2.2 plots the normalized array factor of different 100-element thinned arrays with 50% of elements turned off randomly. Compared to the normalized

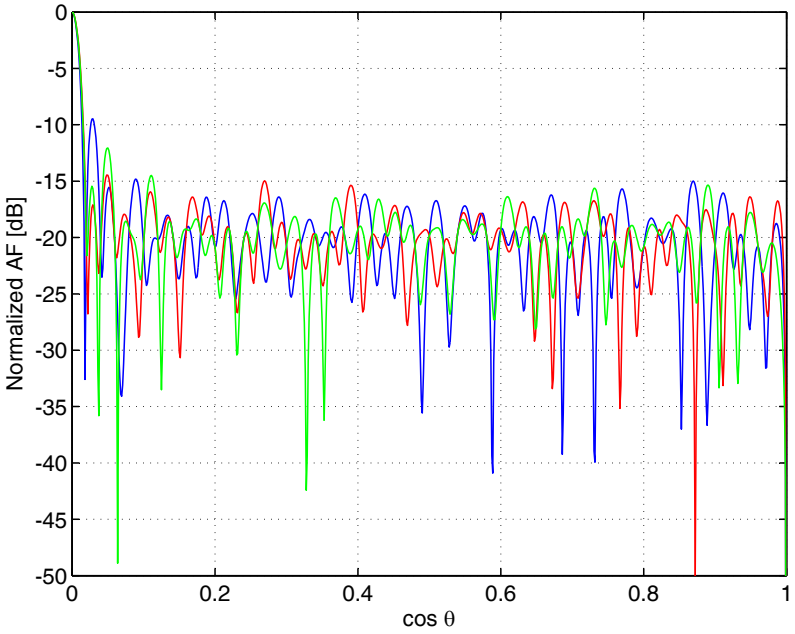

Figure 2.2: *Normalized array factor of 3 different 100 element linear thinned array with* 50% *turn off randomly.*

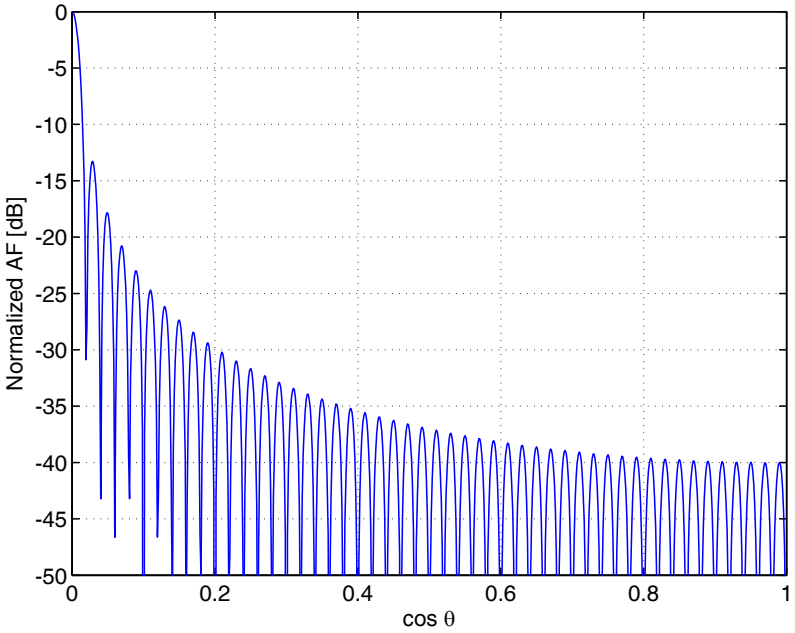

Figure 2.3: *Normalized array factor of 100 element linear array uniformly separation of* 0.5λ .

array factor of a fully populated array of 0.5λ spacing shown in Fig. 2.3, the PSLs of thinned arrays fluctuate around the PSL of the regular array, which indicates the possibility of minimizing the PSL of thinned array. While the beam widths are kept almost the same. The synthesis of the thinned array, therefore, can be considered as an optimization problem, and will be presented in the Section 3.4.1 as the validation of the proposed optimization algorithm.

2.1.5 Sparse Array

Another type of unequally spaced array is the sparse array, where the element's positions are varied in a limited range in the array. Generally, the separation between elements in sparse array is greater than 0.5λ and smaller than a wavelength λ to avoid the grating lobes [27]. The sparse arrays, therefore, reduces the number of elements in the array compared with equally spaced arrays of 0.5λ spacing, which in turn brings several practical advantages such as the reduction of cost, weight. Moreover, the positions of elements can be varied continuously, which adds an additional degree of freedom for the design that allow the array to achieve low side-lobe level.

Compared to the thinned array approach, the sparse array is more flexible since element's positions are not fixed, however for a large planar array, the design of sparse array requires a lot of effort to define the best configuration. In practice, the sparse arrays have been proposed for different applications including the square kilometer array (SKA) for radio telescope applications, as shown in Fig. 2.4.

Figure 2.4: *Square Kilometer Array.*

The synthesis of the sparse array is to determine the positions of all elements in the array with the pre-defined constraint, e.g. the inter-element separation, normally $0.5\lambda \leq d \leq \lambda$, to produce the required beam pattern. As shown in Fig. 2.5, the coordinate of planar sparse array, each element's position is controlled in both $x-$ and $y-$axis, therefore, a special procedure is needed to control these constraints. Several

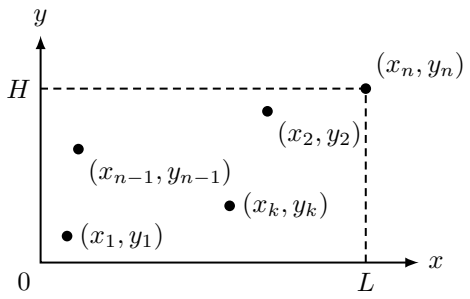

Figure 2.5: *Coordinates of elements of sparse planar array.*

methods have been proposed to design sparse arrays including the inversion algorithm, and the application of optimization algorithms such as the differential evolution algorithm. In the scope of the thesis, synthesis of sparse array is considered as an optimization test problem to prove the performance of the proposed optimization algorithm in Section 3.4.3.

2.2 Reflectarray Theory

In the chapter introduction, the approach to and the evolution of reflectarray have been presented. In order to provide a deep understanding of the operational mechanism of the RA, in this section the theory for RA design is presented, which includes the model of the incident field and the reflected field, the array pattern, which is calculated using the array theory, and finally the array phasing, which describes the beam forming procedure.

The considered geometry for an off-set planar reflector antenna is reported in Fig. 2.6, when a point source, with linear polarization, has been considered as a feed. The reflector consists of a surface covered by suitable printed elements and it is backed by a conductive ground plane.

2.2.1 Coordinate systems

The relations between the different coordinate systems in Figure 2.6 are the following:

$$\begin{bmatrix} \hat{r}_f \\ \hat{\theta}_f \\ \hat{\phi}_f \end{bmatrix} = \begin{bmatrix} \sin\theta\cos\phi & \sin\theta\sin\phi & \cos\theta \\ \cos\theta\cos\phi & \cos\theta\sin\phi & -\sin\theta \\ -\sin\phi & \cos\phi & 0 \end{bmatrix} \cdot \begin{bmatrix} \hat{x}_f \\ \hat{y}_f \\ \hat{z}_f \end{bmatrix} \tag{2.17}$$

$$\begin{bmatrix} \hat{x}_f \\ \hat{y}_f \\ \hat{z}_f \end{bmatrix} = \begin{bmatrix} 0 & 1 & 0 \\ \cos\alpha_0 & 0 & \sin\alpha_0 \\ \sin\alpha_0 & 0 & -\cos\alpha_0 \end{bmatrix} \cdot \begin{bmatrix} \hat{x} \\ \hat{y} \\ \hat{z} \end{bmatrix} \tag{2.18}$$

therefore:

$$\begin{bmatrix} \hat{r}_f \\ \hat{\theta}_f \\ \hat{\phi}_f \end{bmatrix} = \begin{bmatrix} \sin\theta\sin\phi\cos\alpha_0 + \cos\theta\sin\alpha_0 & \sin\theta\cos\phi & \sin\theta\sin\phi\sin\alpha_0 - \cos\theta\cos\alpha_0 \\ \cos\theta\sin\phi\cos\alpha_0 - \sin\theta\sin\alpha_0 & \cos\theta\cos\phi & \cos\theta\sin\phi\sin\alpha_0 + \sin\theta\cos\alpha_0 \\ \cos\phi\cos\alpha_0 & -\sin\phi & \cos\phi\sin\alpha_0 \end{bmatrix} \cdot \begin{bmatrix} \hat{x} \\ \hat{y} \\ \hat{z} \end{bmatrix} \tag{2.19}$$

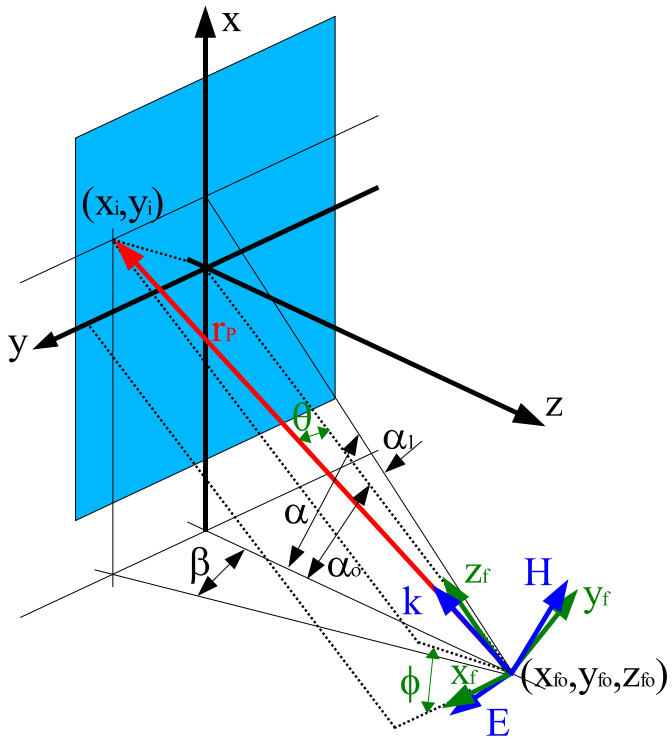

Figure 2.6: *Geometry of the considered reflectarray antenna.*

2.2.2 Incident Field

The incident field may be written as:

$$\vec{E}^{inc}(\vec{r}) = E_0(\vec{r})\hat{p}(\vec{r})e^{-jk_0 r} \tag{2.20}$$

where:

$$E_0(\vec{r}) = -jk_0 Z_0 \frac{1}{4\pi r} E_0(\theta,\phi) \tag{2.21}$$

$$\hat{p}(\vec{r}) = \hat{p}(\theta,\phi) \tag{2.22}$$

and $E_0(\theta,\phi)$ is the radiation pattern of the feed. ($\hat{r}$,$\hat{\theta}$,$\hat{\phi}$) are the unit vectors of the spherical coordinate system centered in the feed point.

At a point $\vec{P}$, on the reflector surface, the incident field will be given by:

$$\vec{E}^{inc}(\vec{P}) = E_0(\vec{r}_P)\hat{p}(\vec{r}_P)e^{-jk_0 r_P} \tag{2.23}$$

where it has been shown the dependence of both the magnitude and the polarization of the field from the point. In general, the reflector is in the far-field region of the feed, thus the incident field can be written as

$$\vec{E}^{inc}(\vec{P}) = E_0(r_0,\hat{\theta}_P,\hat{\phi}_P)\hat{p}(\hat{\theta}_P,\hat{\phi}_P)e^{-jk_0\hat{k}_P\cdot\vec{r}'_P} \tag{2.24}$$

where

$$E_0(r_0,\hat{\theta}_P,\hat{\phi}_P) = -jk_0 Z_0 \frac{e^{-jk_0 r_0}}{4\pi r_0} E_0(\theta,\phi) \tag{2.25}$$

and r_0 is the distance between the feed and the origin of the Cartesian coordinate system (x, y, z) and $\vec{r}'_P$ is the vector that locates the point $\vec{P}$ in the same coordinate system. Locally, the incident field represented by Eqn. 2.24 is a plane wave: in fact

$$\hat{p} = p_\theta \hat{\theta} + p_\phi \hat{\phi} \tag{2.26}$$
$$\vec{k}(\vec{P}) = k_0 \hat{k}(\vec{P}) \tag{2.27}$$

i.e., the polarization unit vector and the propagation unit vector are orthogonal and the impedance relation between the electric and magnetic field is satisfied

$$\vec{H}^{inc}(\vec{P}) = \frac{1}{Z_0} \hat{k}(\vec{P}) \times \vec{E}^{inc}(\vec{P}) \tag{2.28}$$

It is important now to express the field, i.e., $\hat{p}$ and $\hat{k}$ in the coordinate system (x, y, z). This can be done using the relation reported in Section 2.2.1:

$$\hat{k} = k_x \hat{x} + k_y \hat{y} + k_z \hat{z} \tag{2.29}$$
$$\hat{p} = p_x \hat{x} + p_y \hat{y} + p_z \hat{z} \tag{2.30}$$

Therefore the incident field has, in general, three components, i.e., it can be seen as the superposition of a TE and a TM plane wave. This field may be decomposed in the TE and TM waves, both of them will have an x and a y component:

$$\vec{E}^{TE}(\vec{P}) = E_x^{TE} \hat{x} + E_y^{TE} \hat{y} \tag{2.31}$$
$$\vec{E}^{TM}(\vec{P}) = E_x^{TM} \hat{x} + E_y^{TM} \hat{y} + E_z^{TM} \hat{z} \tag{2.32}$$

This is correct since both TE and TM belong to the plane orthogonal to $\hat{k}$, but TE has no components parallel to $\hat{z}$, then TM lays in the plane that contains $\hat{k}$ and $\hat{z}$ (*incident plane*) and, generally, it has three components along $\hat{x}$, $\hat{y}$ and $\hat{z}$.

Usually, both the TE and the TM plane waves interact with the elements on the reflecting surface;this means that the TE and the TM reflection coefficient have to be computed and combined to have the *total* reflected field:

$$E_{r,y}^{TE} = \Gamma^{TE} \cdot E_{i,y}^{TE} \tag{2.33}$$
$$E_{r,y}^{TM} = \Gamma^{TM} \cdot E_{i,y}^{TM} \tag{2.34}$$
$$E_{r,y}^{TOT} = E_{i,y}^{TE} + E_{i,y}^{TM} \tag{2.35}$$

2.2.3 Reflected Field

In the spherical coordinate system $\{r, \theta, \phi\}$ with the origin at the center of the reflector surface, the far-field power radiation pattern is

$$P(\theta, \phi) = \frac{1}{2}[E_\theta^2(\theta, \phi) + E_\phi^2(\theta, \phi)]/\eta, \tag{2.36}$$

where E_θ and E_ϕ are the components of the field radiated by the reflectarray antenna, and $\eta = \sqrt{\mu_0/\varepsilon_0}$ is the free space characteristic impedance. This electric field can

be found following a standard procedure by means of the electric and magnetic vector potentials, $\vec{F}$ and $\vec{A}$ [26]. Specifically, the far-field radiation is approximated as

$$\vec{E}^{\text{far}-\text{field}} \simeq -j\omega\vec{A} + j\omega Z_0 \hat{r} \times \vec{F}, \tag{2.37}$$

where ω is the angular frequency and $\hat{r}$ is the unit vector in the radial direction. The potentials, in turn, are given by

$$\vec{A} = \frac{\mu_0}{4\pi} \iint_S \vec{J}^e G \, ds, \qquad \vec{F} = \frac{\varepsilon_0}{4\pi} \iint_S \vec{J}^m G \, ds, \tag{2.38}$$

where $\vec{J}^e$ and $\vec{J}^m$ are equivalent electric and magnetic surface current densities, respectively, on the reflector surface S, and G is the free space Green's function. Integrations in the Eqn. 2.38 are carried out on the upper reflector surface. Equivalent surface current densities can be determined by means of Love's equivalence principle [26] as

$$\vec{J}^e = \hat{n} \times \vec{H}^{\text{total}}, \qquad \vec{J}^m = -\hat{n} \times \vec{E}^{\text{total}}, \tag{2.39}$$

where $\hat{n}$ is the outward unit normal vector to the reflector surface. $\vec{E}^{\text{total}}$ and $\vec{H}^{\text{total}}$ in the Eqn. 2.39 are total electric and magnetic fields on the reflector surface, which are sum of incident fields from the feed $\vec{E}^{\text{inc}}$ and $\vec{H}^{\text{inc}}$ and the reflected fields by the system of the re-radiating elements together with the ground plane. In fact, the total fields can be represented as

$$\vec{E}^{\text{total}} = (1 + e^{j\psi})\vec{E}^{\text{inc}}, \qquad \vec{H}^{\text{total}} = (1 - e^{j\psi})\vec{H}^{\text{inc}}, \tag{2.40}$$

since the ground plane in our model is assumed to be a perfect electric conductor (PEC) and it reflects the incident wave completely. Therefore, the reflection coefficient of this system is represented by the phase factor $\psi = \psi(\vec{P})$ only, where $\vec{P}$ is some point on the upper surface of the reflector.

2.2.4 Radiation Pattern of the Reflectarray Antenna

The radiated field strength at a certain point in the space, assumed to be in the far-field, is calculated by adding the contributions of each element to the total radiated fields. Therefore, assuming all the element patterns, EP, taken individually, are identical (within a certain tolerance) and that the patterns are all aligned in the same direction in azimuth and elevation, then the total array antenna pattern is attained by multiplying the array pattern by the element pattern. In fact, given an array of identical $M \times N$ elements, for an identical elements with uniform spacing placed on the plane, the far-field radiation pattern is therefore given by:

$$FF(\theta, \phi) = \sum_{m=1}^{M} \sum_{n=1}^{N} A_{m,n} \cdot EP(\theta, \phi) \cdot e^{j(\psi_x + \psi_y)} \tag{2.41}$$

where

$$\psi_x = 2\pi \frac{x_{m,n}}{\lambda} \sin\theta \cos\phi \tag{2.42}$$

$$\psi_y = 2\pi \frac{y_{m,n}}{\lambda} \sin\theta \sin\phi \tag{2.43}$$

being $x_{m,n}$ and $y_{m,n}$ the coordinates of the element m, n, $A_{m,n}$ the complex local excitation for each element, $EP(\theta, \phi)$ is the element pattern, and being λ the free space wavelength of the radiation.

2.2.5 Beam Forming

A printed reflectarray often consists of a feed and a planar array of printed elements at the far-field region of the feed. The incident field from the feed to each reflectarray element can be considered as a plane wave with a phase proportional to the distance from that element to the feed. To produce a focus beam, the reflected field at each element needs to be adjusted to create a progressive phase distribution on the planar surface that generate pencil beam in a give direction as presented in phased array section. In order to obtain this phase distribution, each element is incorporated a certain phase shift when it is illuminated by a feed. The phase shift is adjusted independently for each element by particular techniques such as varying one of the geometrical parameters in the reflectarray elements, or attaching phase shifters.

In this section, the procedure to generate pencil beam is described. For other beams, e.g. contoured beams, can be generated by implementing an appropriate phase distribution. Considering the coordinate system shown in Fig. 2.6, the progressive phase distribution on the reflectarray surface that produces a beam in the direction (φ_0, θ_0), calculated using array theory, is expressed as:

$$\phi(x_i, y_i) = -k_0(x_i \cos\varphi_b + y_i \sin\varphi_b) \sin\ \theta_b \tag{2.44}$$

where k_0 is the propagation constant in vacuum, and (x_i, y_i) the coordinate of the element i. On the other hand, the phase of the reflected field at each reflectarray element is equal to the phase of the incident field from the feed and the phase-shift introduced by each element:

$$\phi(x_i, y_i) = -k_0 d_i + \phi_{shift}(x_i, y_i) \tag{2.45}$$

From Eqn. 2.44, 2.45, the phase shift required at each is element is calculated as:

$$\phi_{shift}(x_i, y_i) = k_0 d_i - k_0(x_i \cos\varphi_b + y_i \sin\varphi_b) \sin\ \theta_b \tag{2.46}$$

Fig. 2.7 shows an example of required phase shift of a 32×32 reflectarray to create a pencil beam scanning 18° in $X - Y$ plane, which is designed in Section 4.5.2.

2.3 Floquet Analysis

The design of reflectarray antennas is often based on the analysis of the unit cell. To understand how the unit cell will behave in the array, it is common to assume an infinite array of identical cells [22]. In this section, the Floquet analysis approach to analyze such infinite arrays will be presented. Before starting Floquet analysis, it is important to introduce the Fourier transform of a periodic function in terms of a Floquet series expansion.

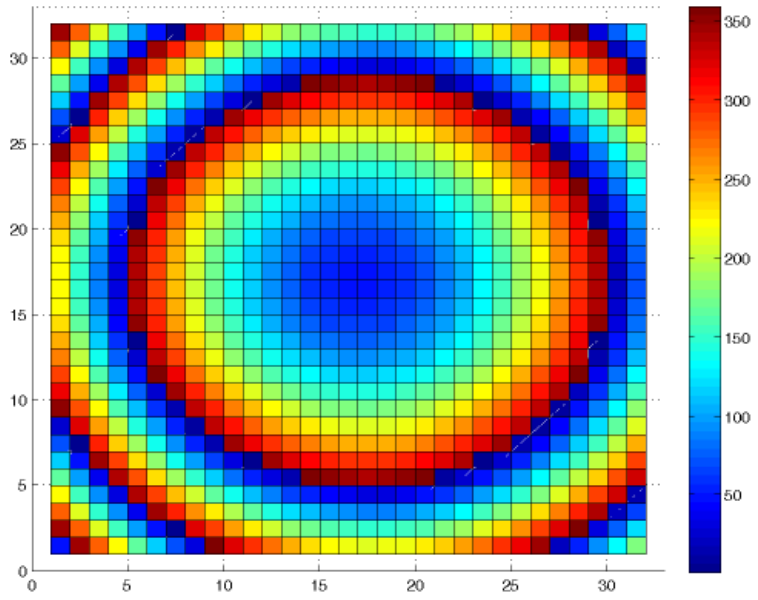

Figure 2.7: *The required phase phase distribution of a reflectarray.*

2.3.1 Floquet Series

Given a function $f(x)$, the Fourier transform of $f(x)$ is defined as:

$$\tilde{f}(k_x) = \frac{1}{2\pi} \int_{-\infty}^{\infty} f(x) e^{jk_x x} \mathrm{d}x \tag{2.47}$$

where $\tilde{f}(k_x)$ is the Fourier transform of $f(x)$, and k_x is the spectral frequency. The function $f(x)$ can be found by using inverse Fourier transform as follows:

$$f(x) = \int_{-\infty}^{\infty} \tilde{f}(k_x) e^{-jk_x x} \mathrm{d}k_x \tag{2.48}$$

In case of a periodic function, $g(x)$, in general both the phase and the amplitude are periodic, with different periodicities, given by:

$$g(x) = \sum_{n=-\infty}^{\infty} f(x - na) e^{-jn\varphi} \tag{2.49}$$

The Fourier transform of $g(x)$ can be expressed as:

$$\tilde{g}(k_x) = \frac{1}{2\pi}\int_{-\infty}^{\infty} g(x)e^{jk_x x}\mathrm{d}x \tag{2.50}$$

$$= \frac{1}{2\pi}e^{-jn\varphi}\sum_{n=-\infty}^{\infty}\int_{-\infty}^{\infty} f(x-na)e^{jk_x x}\mathrm{d}x \tag{2.51}$$

$$= \tilde{f}(k_x)\sum_{n=-\infty}^{\infty} e^{jn(k_x a-\varphi)} \tag{2.52}$$

The infinite series summation can be substituted by an infinite series of Dirac delta functions using the identity [27]

$$\sum_{n=-\infty}^{\infty} e^{jnk_x a} = \frac{2\pi}{a}\sum_{n=-\infty}^{\infty}\delta\left(k_x - \frac{2n\pi}{a}\right) \tag{2.53}$$

Therefore, the Fourier transform of $g(x)$ will be:

$$\tilde{g}(k_x) = \frac{2\pi}{a}\tilde{f}(k_x)\sum_{n=-\infty}^{\infty}\delta\left(k_x - \frac{2n\pi}{a} - \frac{\varphi}{a}\right) \tag{2.54}$$

From Eqn. 2.48, the periodic function $g(x)$ can be represented alternatively using inverse Fourier transform:

$$g(x) = \int_{-\infty}^{\infty}\tilde{g}(k_x)e^{-jk_x x}\mathrm{d}k_x$$

$$= \int_{-\infty}^{\infty}\frac{2\pi}{a}\tilde{f}(k_x)\sum_{n=-\infty}^{\infty}\delta\left(k_x - \frac{2n\pi}{a} - \frac{\varphi}{a}\right)k_x e^{-jk_x x}\mathrm{d}k_x \tag{2.55}$$

Since the Dirac-delta function has nonzero value only at discrete point, the periodic function $g(x)$ will have a set of discrete values, leaving

$$g(x) = \frac{2\pi}{a}\sum_{n=-\infty}^{\infty}\tilde{f}\left(\frac{2n\pi+\varphi}{a}\right)e^{-\frac{j(2n\pi+\varphi)x}{a}} \tag{2.56}$$

The right-hand side of Eqn. 2.56 is the Floquet series expansion of $g(x)$ [27]. In case $\varphi = 0$, Floquet series are the Fourier series.

2.3.2 Floquet Analysis

In the previous section, the periodic function has been represented in terms of the Floquet series expansion, given in Eqn. 2.56. In this section, the same procedure is derived for the electromagnetic fields of a periodic array of current sources in the same way. The considered infinite array is assumed to have both the magnitude and phases of the cells are periodic, with different periodicities, such that the phase can be shifted by a constant value from one cell to the next. Therefore, the analysis can assist the analysis of phase-shifted cells to produce plane-waves in different directions as it will be shown in Section 5.3.

For sake of simplicity, an 1-D array has been considered here, expressions of an infinite 2-D array can be derived in similar manner. The considered array is assumed to have $y-$directed current sources in the $z-$ plane with spacing a in $x-$direction. The current sources have identical magnitudes and their phases are shifted progressively by constants k_{x_0} along $x-$ direction. If the current distribution at each element is expressed as $f(x)$, the total current density is given by:

$$J_y(x) = \sum_m f(x - ma)e^{-j(k_{x0}ma)} \tag{2.57}$$

where $\sum_m$ denotes for $\sum_{m=-\infty}^{\infty}$. Since the total current density is a periodic function, the Fourier transform of $J_y(x)$ will be:

$$\begin{aligned}
\tilde{J}_y(k_x) &= \frac{1}{2\pi}\int_{-\infty}^{\infty} J_y(x)e^{jk_x x} \\
&= \frac{1}{2\pi}\sum_m e^{-jk_{x0}ma}\int_{-\infty}^{\infty} f(x-ma)e^{jk_x x}\mathrm{d}x \\
&= \sum_m e^{-jk_{x0}ma}\tilde{f}(k_x)e^{jk_x ma} \\
&= \tilde{f}(k_x)\sum_m e^{j(k_x-k_{x0})ma}
\end{aligned} \tag{2.58}$$

Using the identity in Eqn. 2.53, it can be written as:

$$\tilde{J}_y(k_x) = \frac{2\pi}{a}\tilde{f}(k_x)\sum_m \delta\left(k_x - k_{x0} - \frac{2m\pi}{a}\right) \tag{2.59}$$

Therefore, the Fourier spectrum for $J(x)$ exists only at discrete points in k_x-axis. These points are given by

$$k_{xm} = k_{x0} + \frac{2m\pi}{a} \tag{2.60}$$

Similar to Eqn. 2.55, Eqn.2.56, the current density can be expressed as

$$\begin{aligned}
J_y(x) &= \int_{-\infty}^{\infty}\tilde{J}_y(k_x)e^{-jk_x x}\mathrm{d}k_x \\
&= \int_{-\infty}^{\infty}\frac{2\pi}{a}\tilde{f}(k_x)\sum_m \delta(k_x - k_{xm})e^{-jk_x x}\mathrm{d}k_x \\
&= \frac{2\pi}{a}\sum_m \tilde{f}(k_{xm})e^{-jk_{xm}x}
\end{aligned} \tag{2.61}$$

where k_{xm} are defined in Eqn. 2.60. Eqn. 2.61 represents the total current density as Floquet series expansion. The current density may be then used to determine the electric field as [27]

$$E_y = -\frac{\pi\omega\mu_0}{a}\sum_{m=-\infty}^{\infty}\frac{\tilde{f}(k_{xm})}{k_{zm}}e^{-jk_{xm}x - jk_{zm}z} \tag{2.62}$$

with k_{xm} is defined as Eqn. 2.60, and $k_{zm} = k_0^2 - k_{xm}^2$.

The electric field produced by the current source in Eqn. 2.57 may be expressed in terms of an infinite series. The exponential term inside the summation sign is known as a Floquet modal function or a Floquet mode. The vector represents the propagation direction of the n^{th} Floquet mode:

$$\vec{p}_n = \hat{x}k_{xm} + \hat{z}k_{zm} \tag{2.63}$$

With respect to a finite aperture where radiated power is in every direction, an infinite periodic structure only radiates plane waves in discrete directions for some particular values of m in Eqn. 2.60. A Floquet mode becomes a propagating mode if the following condition is satisfied

$$k_{xm}^2 + k_{zm}^2 < k_0^2 \tag{2.64}$$

The direction of propagation is determined as $\theta_m = \tan^{-1}(\frac{k_{xm}}{k_{zm}})$. If the condition is not satisfied, then the Floquet mode is an evanescent mode that decay along $z-$direction.

CHAPTER 3

Optimization Algorithms

In this chapter, two recently developed optimization algorithms, potentially applicable to reflectarray design, will be presented. The application of evolutionary algorithms such as Genetic Algorithms (GA), Particle Swarm Optimization Algorithm (PSO) to Electromagnetic (EM) problems is reviewed to discuss their advantages and limitations. A new trend of optimization algorithms based on the estimation of good solutions will be presented.

Then, in the second section, an improved version of the compact Genetic algorithm (cGA), hereafter denoted as M-cGA, is introduced. The M-cGA is recently developed by implementing more than one probability vector (PV) and integrating a learning mechanism into cGA. The M-cGA shows its superior performances compared with its ancestors when tested with mathematical problems as well as practical EM problems.

Following, in the third section, another algorithm, the modified Bayesian optimization Algorithm (M-BOA), will be presented. A suitable mutation scheme is introduced inside the original BOA to overcome the drawbacks of BOA, which limit its performance when the starting points are not sufficiently good. The modified version has been tested by benchmark functions at the end of this section, and the results have been compared with the original BOA and the PSO as well.

Finally, in the forth section, some numerical results of the applications of the M-cGA and the M-BOA to EM problems are presented. The M-cGA has been applied to thinning array problems, while the M-BOA has been used to synthesize sparse arrays. Their applications to large array syntheses show promising features for different possible applications to EM problems, and reflectarray design in particular.

3.1 Introduction

The design of complex electromagnetic (EM) structures for real life applications often requires to exploit the features of evolutionary computation techniques such as the classic Genetic Algorithms (GA) [30], Particle Swarm Optimization (PSO) [31], Ant Colony Optimization (ACO) [32] as well as more recently developed population-based approaches such as Meta-PSO [33], Memetic Algorithm [34], the Invasive Weed Optimization (IWO) [35], the Biogeography-Based Optimization [36] or other hybrid techniques [37–39]. All these population-based techniques share the same basic idea, i.e., they attempt to reach the optimum solution acting at each step of the iterative process on the current population, i.e., on a considered set of candidate solutions, through general, problem-independent operators. These, however, could be insufficiently effective and therefore they could lead to lose the best solutions, or, at least, to slow down the convergence.

Obviously this risk is greater in case of complex optimization problems, as the EM ones are, but it can occur also in simpler cases. To improve the performances of population-based optimization algorithms such as GA, increasing the population size could help for long-term performance of the algorithm [40]. The cost, however, will be paid at the expense of computational performance, i.e., number of evaluations per generation. Even increasing the population size, these algorithms are able to solve only for low-order building blocks (BBs), while for a higher-order problem, they often get stuck at a local minimum, as it will be shown later in section 3.2.4, the validation of the modified compact Genetic algorithm.

In literature, another approach has been proposed to tackle this limitation of the pseudo-stochastic algorithms. That approach is based on the idea of using the information already available from the entire set of the most promising solutions to generate new offspring, as opposed to what is done for instance in the GA, where only the genes of two parents concur to the chromosome structure of a child. This principle has been introduced in the Estimation of Distribution Algorithms (EDAs) [41], based on the estimate of the distribution of the promising solutions and on the generation of a new population according to this estimate.

EDAs, in general, try to get the distribution of good solutions, and they work effectively for problems where knowledge of these problems is already available. However, when the information about the problems is unavailable or the starting points are not good, these algorithms could be trapped at local minimas. In this chapter, different modifications will be introduced to two EDAs in order to enhance their performances. New algorithms, based on the compact Genetic Algorithm (cGA) and Bayesian optimization algorithm (BOA), will be presented. By introducing a learning scheme and a mutation scheme to the original cGA and BOA respectively, the modified cGA and modified BOA showed significant improvements in their performances and are promising for application in EM problems.

3.2 Compact Genetic Algorithm

Genetic Algorithms (GAs) [30] are a class of the most well-known optimization algorithms for applied engineering thanks to their ease of implementation. Their concepts are based on the idea that the next generation would perform better than the current

population. The creation of next generation depends on two main operators: Selection and mutation. Depending on the selection methods, there are two general approaches to GAs: Generational update and steady-state update, as depicted in Fig. 3.1. Generational approach selects a large number of individuals and makes a "big" update of population, while steady-state approach only selects two individuals and makes "small" update to the population.

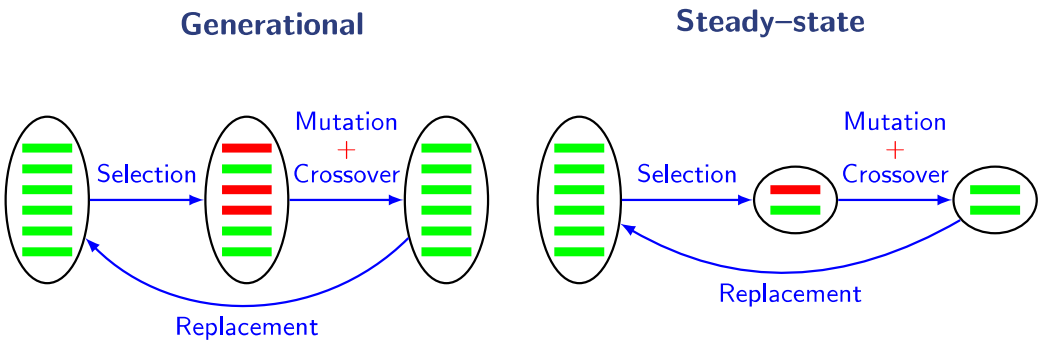

Figure 3.1: *Generational update vs. Steady-state update.*

Both of these approaches have their own advantages and drawbacks, e.g. generational scheme evaluates more individuals per one iteration, but requires less iterations than steady-state scheme. The generational scheme seems to gain popularity since most of current GA versions are applying this concept. The steady-state scheme, however, reduces computer resources needed to store and evaluate the population of GAs since every iteration the algorithm just needs to store and evaluate only two new generated individuals. In [42], Harik implemented this idea and created a new algorithm, named compact Genetic Algorithm – cGA. The cGA uses a probability vector (PV) to represent the population, therefore it greatly reduces the memory storage required by the algorithm (that is also why it is called compact). However, the cGA's performances are generally similar to the simple GA (sGA). Therefore, there is a need to improve its capability, and in the next section, the ideas for cGA's modifications are presented in detail.

3.2.1 Concepts of cGA

Compact Genetic Algorithm, cGA, first presented in [42], uses a probability vector (PV) to represent a possible solution. In cGA, instead of using a real population as in traditional Genetic Algorithm, it manages the PV to get the distribution of good solutions. The length of the PV corresponds to the number of variables of the problem, and the value of the PV measures the probability of one variable to get particular value e.g. the proportion of "1" in case of a binary problem. A full treatment of the method can be found in [42, 43], but for sake of clarity and uniformity of notation it is briefly summarized in the following section.

The pseudo code of cGA is described in Fig. 3.2. Initially, the PV is set to 0.5, i.e., assuming uniform distribution for every position. In each generation, two individuals

are generated from the current PV. They are left to compete, and the winner will be responsible for updating the PV. The updating rule will increase or decrease the probability vector by a factor $1/n$ (where n is the population size) according to the value of the winner. The cGA will stop when the PV reaches a value of 0 or 1 at all positions, i.e., when the optimal solution has been found.

Step 1: Initial PV: `PV=0.5*ones(1,N)`

Step 2: Generate two individuals: a & b

Step 3: Compete between individuals

```
winner, loser:= compete(a,b)
```

Step 4: Update PV:

```
for i = 1:N
 if winner(i)#loser(i)
   if winner(i)==1
          PV(i)=PV(i)+1/n;
   else   PV(i)=PV(i)-1/n;
end
```

Step 5: Check convergence

Parameters: n: population size
N: chromosome length

Figure 3.2: *Pseudo code of the compact Genetic Algorithm, cGA.*

The procedure described above is for a binary problem where the PV is initially set to 0.5 at all position, representing a uniform distribution. The cGA has been also modified for continuous variables as proposed in [44], where the author implemented two PVs to represent solutions, for the mean, μ, and the standard deviation, σ. The variables have been assumed to have normal distribution, and the updating process implements the same idea as the original cGA. The original cGA, however, only performs equivalent to the first-order behavior of the simple GA with uniform crossover. In the next section, some improved versions of the cGA will be presented and their performances will be reviewed.

3.2.2 Improved Compact Genetic Algorithms

The first modification of the standard cGA has been introduced in [42], by increasing the number of generated offspring and applying a tournament competition, i.e., simulating higher selection pressure. The concept is similar to improving the performance of GAs by generating larger populations [40]. This modification therefore results in a high computational cost since it needs to store and evaluate a considerable number of individuals.

In [43], Ahn proposed new versions of cGAs introducing the elitism scheme. He created two different approaches: The persistent elitism cGA (pe-cGA) and the non-

persistent elitism cGA (ne-cGA). In the first iteration, the pe-cGA selects the winner as the leader, and keeps the leader until the algorithm finds a new generated individual with a better fitness score. The ne-cGA, on the contrary, will replace its leader by a new random individual if the algorithm couldn't find a better candidate after a certain number of iterations. The cGA scheme has been modified as reported in [43], in which pe-cGA and ne-cGA only generate one new individual for the next generation. The new cGAs, therefore, only evaluate one individual per iteration. The elitism-based cGAs outperform the original cGA in terms of computational cost, i.e., the number of function evaluations. The reason for this is the elitism can prevent the loss of low salience genes of chromosomes which is equivalent to increasing the selection pressure. Unfortunately, pe-cGA and ne-cGA do not perform better in term of solution quality.

Step 4: Update PVs:

```
% local update
    for i = 1:P & for j = 1:N
     if winner(i,j)#loser(i,j)
       if winner(i,j)==1
              PV(i,j)=PV(i,j)+1/n;
       else   PV(i,j)=PV(i,j)-1/n;
     end
% global update
    pv_best = best(PVs)
    for i = 1:P
      PV(i) = PV(i)+c*(pv_best-PV(i))
     end
```

Parameters: N: length of PV n: populationsize P: number of PVs c: learning factor

Figure 3.3: *New updating rules for M-cGA.*

In population-based optimization algorithms, the learning scheme plays an important role to the algorithm's performance as shown in the PSO and the recent hybrid Genetic Swarm Optimization (GSO) [37]. This scheme has been implemented in this thesis, and is presented in [45] to further improve the performance of the ne-cGA. The ne-cGA has been modified by implementing more PVs and integrating a learning scheme (the new modified cGA is hereafter called M-cGA). The concept is to use more than one PV to enhance the exploration properties of the algorithm and increase the ability to avoid local optimums. Since the new algorithm incorporates more PVs, a new updating rule has to be applied. Fig. 3.3 describes the new updating rules for M-cGA, replacing step 4 in Fig. 3.2, where a learning scheme is added as global update that allows PVs to learn from each other. The PVs, therefore, are updated not only by their generated individuals, but also by the best PV. In the next section, M-cGA will be tested and compared with its ancestors to prove its performances.

3.2.3 Implementation of M-cGA

3.2.4 Mathematical Validation

In this section, the performance of M-cGA is tested and compared with its predecessors, i.e., cGA, pe-cGA and ne-cGA, on mathematical test functions. The proposed problems here include high-order building blocks (BB) problems, and continuous problems, which purposefully demonstrate M-cGA's ability of dealing with both discrete and continuous variables. In all cases, the M-cGA implements 4 PVs, while the population, relating to the updating $1/n$, for each cGA version is chosen to provide the best convergence.

The first test function with high-order BBs is the Minimum Deceptive Problem (MDP), consisting of concatenating ten copies of minimum deceptive functions, i.e., 2 bits as follows:

$$f_{MDP} = \sum_{i=1}^{10} f(x_{2i}) \tag{3.1}$$

where

$$f(x_{2i}) = \begin{cases} 0.7 & \text{if} \quad x_{2i} = 00 \\ 0.4 & \text{if} \quad x_{2i} = 01 \\ 0.0 & \text{if} \quad x_{2i} = 10 \\ 1.0 & \text{if} \quad x_{2i} = 11. \end{cases}$$

Fig. 3.4 reports the results of the MDP with 10 BBs performed by different algorithms, where the quality of solution and speed of convergence of all cGAs are considered (the M-cGA is denoted as "new"). With low-order problems the M-cGA is close to the cGA performances in terms of population size as plotted in Fig. 3.4(a), while, as shown in Fig. 3.4(b) reporting the comparison of the quality of the solution in terms of the number of function evaluations, the M-cGA outperforms cGA, pe-cGA, and ne-cGA.

Fully deceptive problems have been then considered for testing the M-cGA. The problems involving trap functions are ideal cases for testing the capability to deal with high order BBs. A simple 3-deceptive problem, formed by concatenating ten copies of the three bit trap function has been considered, each three bits trap function has deceptive to optimal ratio of 0.7 as plotted in Fig. 3.5 and defined below:

$$f_{3-bit} = \sum_{i=1}^{10} f(x_{3-bit}) \tag{3.2}$$

where

$$f(x_{3-bit}) = \begin{cases} 0.7 & \text{if sum}(3-bit) = 0 \\ 0.4 & \text{if sum}(3-bit) = 1 \\ 0.0 & \text{if sum}(3-bit) = 2 \\ 1.0 & \text{if sum}(3-bit) = 3 \end{cases}$$

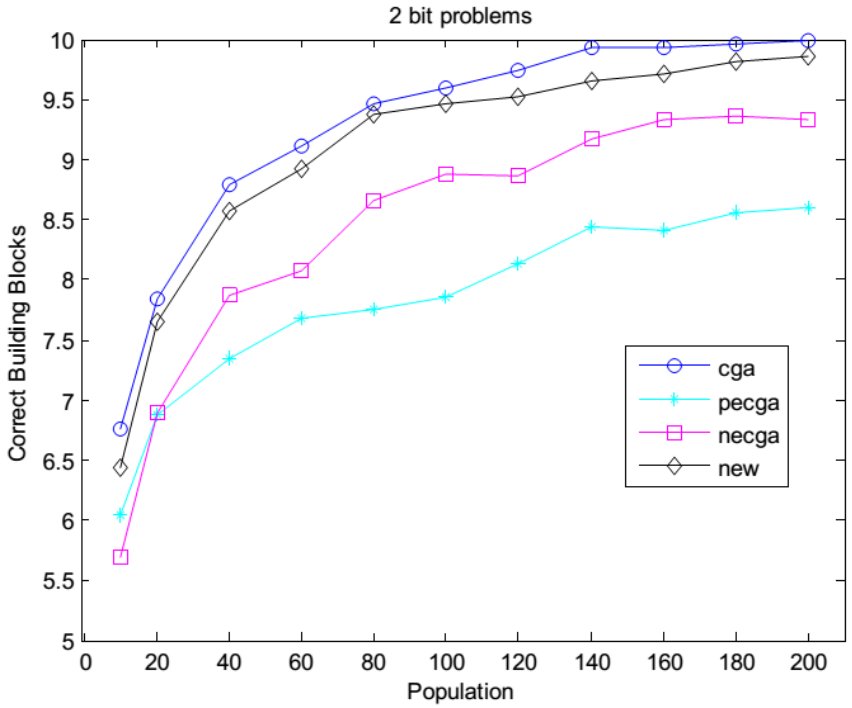

(a) Number of corrected BBs vs. population size.

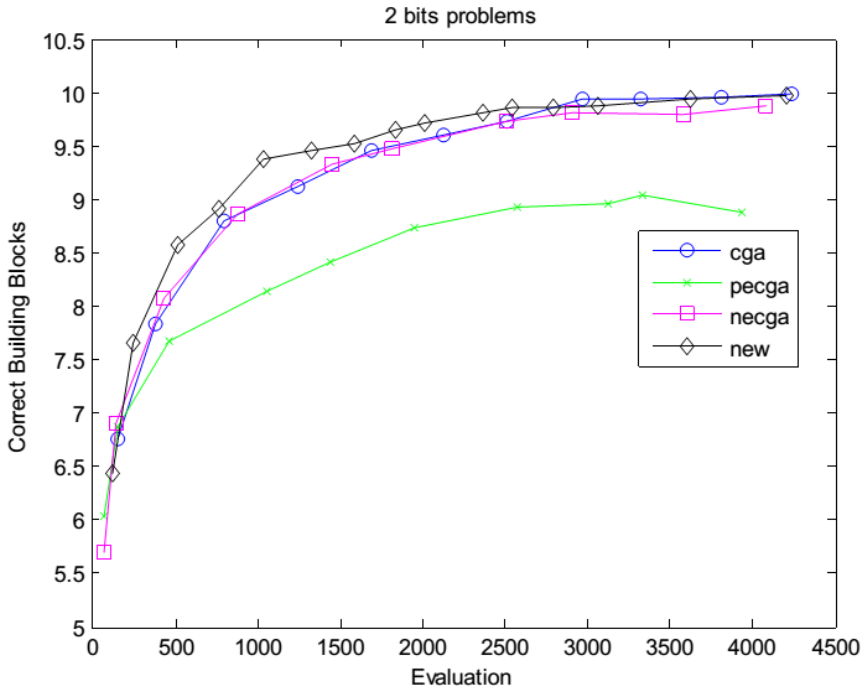

(b) Number of corrected BBs vs. number of function evaluations.

Figure 3.4: *Performance of the algorithms on MDP problem.*

In Fig. 3.6(a), the cGA fails to solve the problem, while the performance of pe-cGA and ne-cGA can be considered close to the one of cGA with high selection pressure

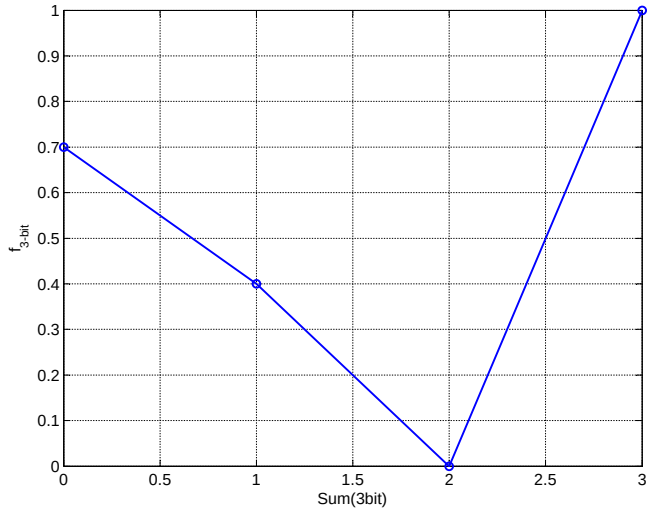

Figure 3.5: *3-bit deceptive problem.*

$s = 8$ and $s = 16$ respectively. The M-cGA generally shows better performances to achieve best solutions both in terms of quality of the solution vs. population size and vs. function evaluations, which indicates the superior performance of M-cGA with respect to its ancestors.

The last considered mathematical test is the Sinc problem to illustrate the ability of the newly proposed algorithm when dealing with continuous problems. The cGA versions are modified for continuous variables as described in [44], where the normal distribution is applied. The Sinc function is expressed as follows:

$$f(X) = \prod_{i=1}^{N} \frac{\sin(\pi(x_i - q_i))}{\pi(x_i - q_i)} \tag{3.3}$$

For this problem, the M-cGA's performances have been compared with two most recent improved versions of cGA, i.e., the pe-cGA and the ne-cGA. The comparison have been made on the achieved results and number of function evaluations required by each algorithm.

Fig. 3.7 shows the performance of pe-cGA, ne-cGA and M-cGA on the Sinc problem for cases of $N = 10$ and $N = 20$. Apparently, pe-cGA is the worst one among them, while ne-cGA could not converge when the problem's dimension increases, as shown in Fig. 3.7(b). For both considered cases, M-cGA outperforms pe-cGA and ne-cGA in term of achieved results and in term of the function evaluation as well. The results on the continuous problems again confirm the higher performance of M-cGA with respect to other cGA versions. In the next section, its application to thinned array syntheses will be presented and compared with previous reported results by other methods.

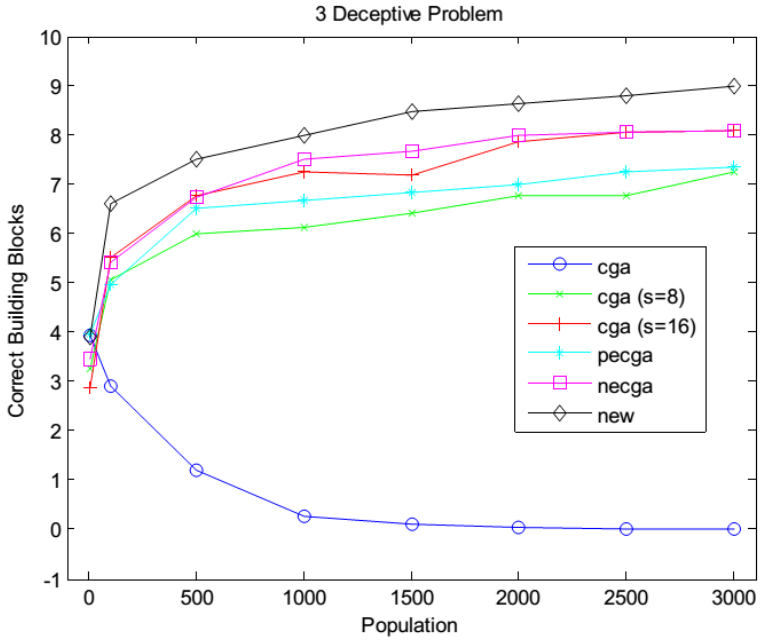

(a) Number of corrected BBs vs. population size.

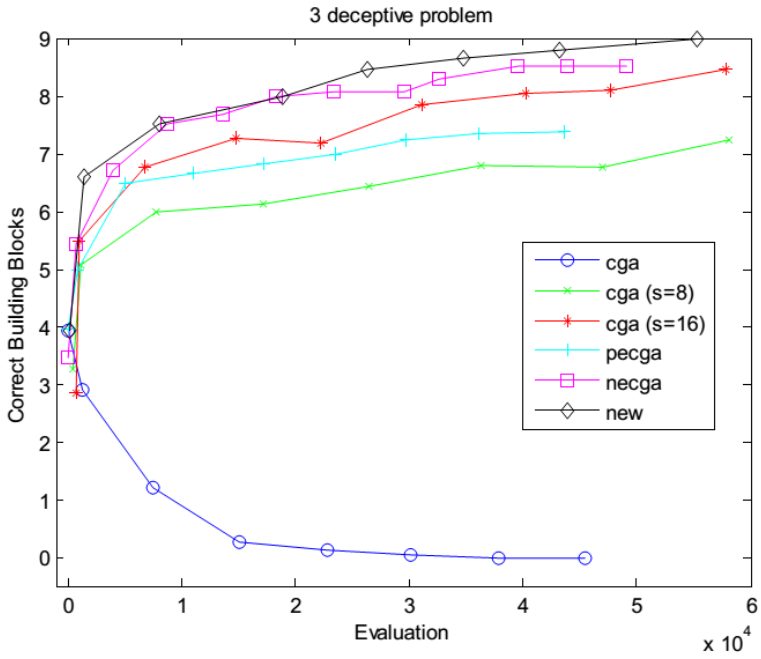

(b) Number of corrected BBs vs. number of function evaluations.

Figure 3.6: *Performance of the algorithms on 3-Deceptive problem.*

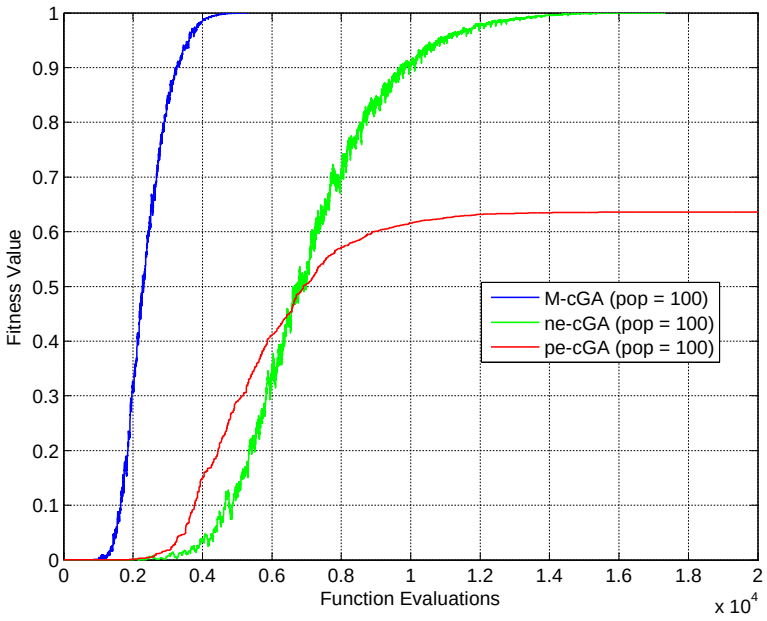

(a) $N = 10$

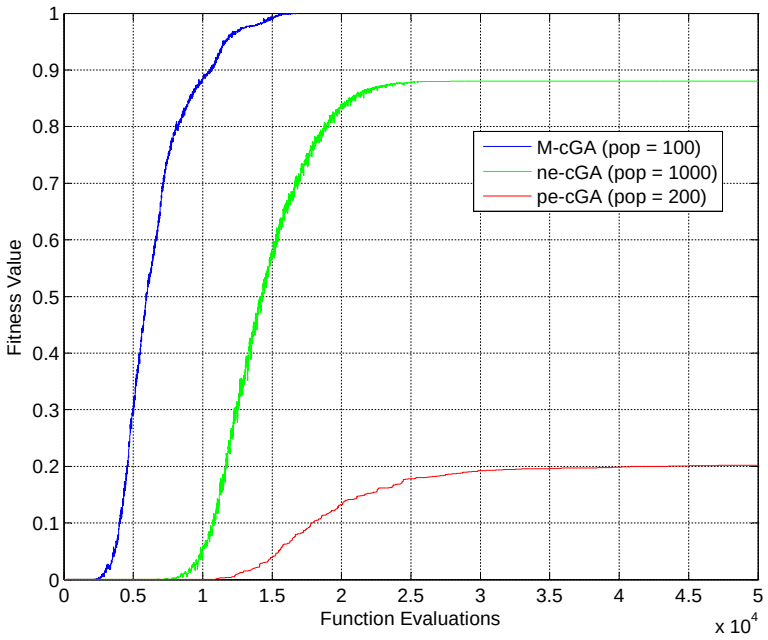

(b) $N = 20$

Figure 3.7: *Performance of the algorithms on Sinc problem.*

3.3 Bayesian Optimization Algorithm

The Bayesian Optimization Algorithm (BOA), introduced in [46], uses probability theory for estimating the distribution of promising solutions for the considered problem. In the BOA, the interaction between parameters (i.e. variables) are investigated in order to build a probabilistic model, i.e., a Bayesian Network (BN), that evolves during an iterative process towards increasingly good solutions, until the achievement of a global optimum.

In the BOA procedure the BN is built taking advantages of the information from the selected most promising solutions and eventually the prior knowledge on the problem to be optimized, if already available. At each iteration, new candidate solutions are generated by sampling the BN, and then they are included in the population, in place of its worst elements. A thorough description of BOA can be found in [46, 47], but for sake of clarity and uniformity of the notation it is briefly summarized in the following, before introducing its modifications, the M-BOA.

3.3.1 Standard BOA

The BOA starts with randomly generating an initial population as a set of strings. The best solutions in the current population are then selected using a specific selection method such as the truncation selection or the tournament selection. A Bayesian Network is then constructed to fit the selected set of strings. In the process of building the network, a metric and a search method are used to measure and maximize the quality of the Bayesian network. The new offspring is generated using the information encoded in the BN. Finally, a new population is obtained, substituting in the older one the worst strings with the new ones. The iterative algorithm proceeds until the stopping criteria are satisfied. The pseudo-code of the BOA could be summarized in the following steps:

Step 1:	Randomly generate initial population (P)
Step 2:	Select a set of promising solutions (S) from (P)
Step 3:	Construct the network (B) using the information from the set of solutions at step 2 and the prior knowledge of the problem, if available
Step 4:	Generate a new Offspring (O) by sampling B
Step 5:	Create a new population (P') by replacing some instances from (P) with (O)
Step 6:	If the stopping criteria are not met, go to Step 2.

Figure 3.8: *Pseudo code of the Bayesian Optimization Algorithm, BOA.*

In the above pseudo-code, steps (3) and (4) are the most important and critical, since the accuracy and the effectiveness of the entire algorithm depends on them.

The Bayesian Network [48], as shown in Fig. 3.9, represents the structure of the problem, since it is essentially a mathematical graphical model that combines proba-

bilistic theory with graph theory to encode the relationship between variables contained in the modeled data. In the graph, each node represents one variable and the edges between the nodes correspond to the conditional dependencies between two variables. Once constructed, the BN is used to generate new instances, resorting the conditional probability of each variable.

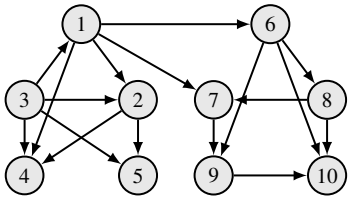

Figure 3.9: *Bayesian Network.*

Mathematically, a BN encodes the joint probabilistic distribution:

$$p(X) = \prod_{i=1}^{l} p(X_i|\pi_i) \tag{3.4}$$

where $\mathbf{X} = (X_1, X_2, \ldots, X_l)$ is the vector of variables of problem, π_i is the set of parents of variable X_i, and $p(X_i|\pi_i)$ is the conditional probability of X_i conditioned on the variables π_i.

In the BOA procedure, the BN has to be trained in order to properly fit the promising solutions which satisfy the design requirements. There are two basic components of the algorithm to perform the learning of the BN: the scoring metric and the search procedure.

The scoring metric quantifies the quality of the given network. As already mentioned, all the prior knowledge about the problem can be included into the metric as well. The search engine is used to explore the space of all possible networks in order to maximize the value of the scoring metric. The exploration is usually restricted by the problem constraints such as the maximum number of incoming edge to one node. This number directly influences the complexity of the algorithm in constructing the network and generating the related offspring. In this work, we chose K2 as scoring metric [49] and greedy algorithm as search procedure.

3.3.2 Modified BOA

As described above, the performance of the BOA greatly depends on the distribution of the current good solutions. The critical point is that, in absence of available prior knowledge of the problem, the initial population for the BOA, in order to start to build up the BN, is randomly generated. Therefore, in some cases it could be possible that all the best solutions in the initial population would not provide good enough distribution, e.g. because they do not represent properly the solution space dimensionality, affecting the convergence capability of the algorithm itself.

To overcome this problem, one possibility is to increase the population size: this may increase the quality of the sampling in terms of information quantity, and therefore may improve the distribution modeling of good solutions, but it also increases

the algorithm computational cost. On the contrary, the variation of the standard BOA proposed here, presents the advantage of enhancing the method's performance without increasing its computational cost, since it does not need further sampling of the cost function. The resulting approach will be indicated in the following as Modified BOA (M-BOA).

The basic idea of the M-BOA is using not only the Bayesian Network for generating a new offspring, but also a mutation scheme. Mutation is also characteristic of other optimization algorithms such as the GA [30], Population Based Incremental Learning (PBIL) [50] and the Compact Genetic Algorithm (cGA) [42]. Using mutation, some individuals will be used to explore candidate solutions out of the considered distribution space and therefore, the algorithm:

- will avoid being trapped in local optima;
- could find good solutions out of the initial population, allowing it to have a reduced size.

Referring to the pseudo code of the BOA, the introduction of the mutation essentially affects steps 4 and 5 that are modified as in Fig. 3.10.

Step 4:	Generate a set of new offspring (O) according to the joint distribution encoded by B; generate a set of new offspring (O') applying mutation to the same set of promising solution (S) use to generate (O).
Step 5:	Create a new population (P') by replacing some instances, the worst ones, from (P) with (O) and (O').

Figure 3.10: *The procedure to generate new population in M-BOA.*

The scheme adopted by the M-BOA for generating a new population is therefore the one sketched in Fig. 3.11. It is worth noticing that both the new population elements obtained through the application of the Bayesian Network and through mutation are derived from the same set of selected solutions, i.e., the best ones. This differs from other algorithms that use mutation, since they generally apply it to the worst elements of the population. The new population is therefore given by the sum of the most promising elements of the previous population (S) plus the new offspring obtained applying to S the BN (O) or the mutation (O').

Finally, notice that M-BOA works with variable vectors, which is much preferable for real variable problems or components, instead of probability vectors as for PBIL and cGA. In all the examples and tests problems considered in the following, the M-BOA with tournament selection and individual mutation have been adopted.

3.3.3 M-BOA Validation: Benchmark Functions

Preliminary results for the modified BOA have been presented in [51]. In this section, the results of the testing of the M-BOA through its application to benchmark functions

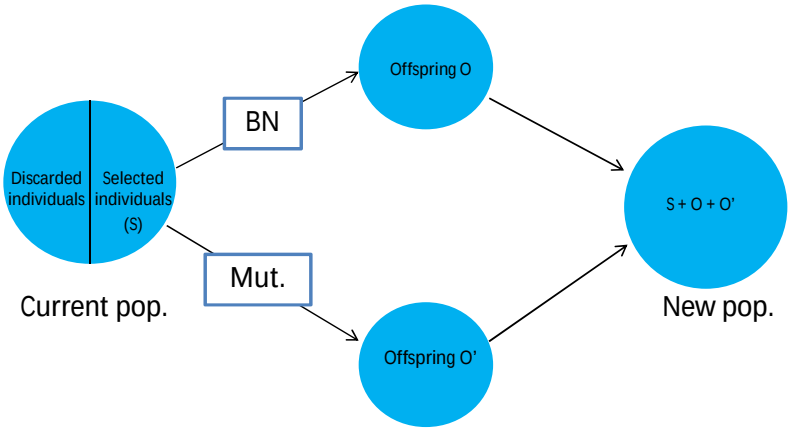

Figure 3.11: *M-BOA new population generation scheme.*

are presented, while in the next section real-life antenna problems will be considered.

In particular, the results shown here refer to the application of the M-BOA to the *Rosenbrock*, the *Rastrigin*, the *Ackley* (all with dimension N = 15) and the *Shenkel* functions and its comparison with the standard BOA and the PSO (the expressions of these benchmark cost functions are reported in the Appendix A for the sake of completeness). The three algorithms have been compared both in terms of speed of convergence and reliability, considering for each of them the results obtained with 50 independent trials, each consisting in 1000 iterations.

The curves of convergence relative to the application of the three optimization methods applied to the *Rosenbrock* function are shown in Fig. 3.12. The blue, green and red lines represent the average curves of convergence over the 50 trials for the BOA, the PSO and M-BOA, respectively. Comparing these three curves, it clearly appears that the M-BOA outperforms the other two schemes, since both BOA and PSO are inclined to stagnate.

Further performance comparisons are shown in Table 3.1, in which the average minimum values obtained by the three algorithms when applied to the different considered benchmark functions are listed, together with the standard deviation (in parenthesis). Both the BOA and the M-BOA outperform the PSO, in terms of convergency and reliability. For what concerns the comparison between these two, they show both an (almost) zero standard deviation, but the average minimum value achieved with the M-BOA is much smaller, and this confirms the results in Fig. 3.12, i.e., the M-BOA achieves better result than the standard BOA.

3.4 Numerical Results

In this section, numerical results of the applications of M-cGA and M-BOA to EM problems are presented. Each of these algorithms is applied to different tasks, in which hundred of variables are needed to be controlled. The performance of M-cGA and M-BOA are compared with results reported in literature, and conclusions are conducted at the end of this chapter.

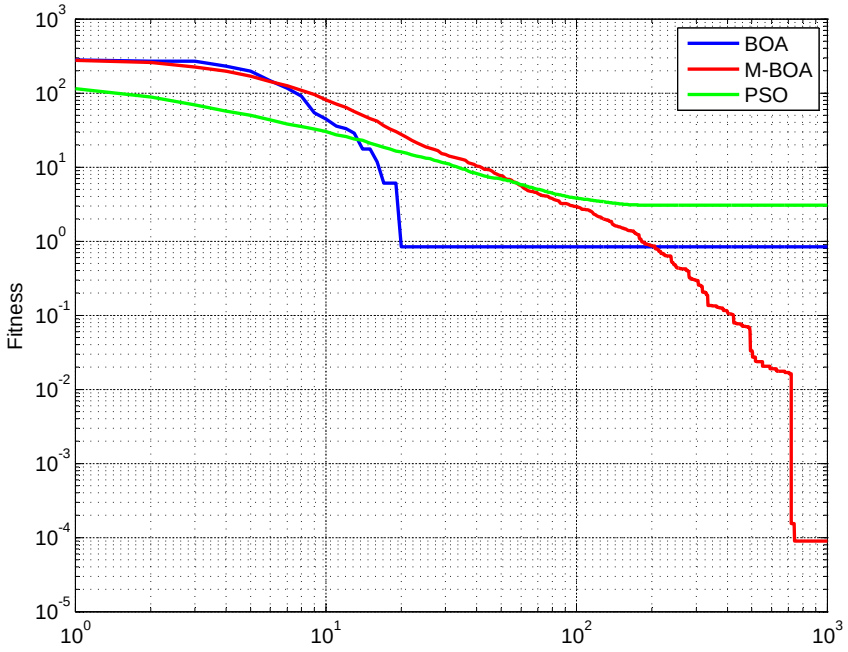

Figure 3.12: *Curves of convergence relative to the PSO (green line), the BOA (blue lines) and M-BOA (red lines) applied to the Rosenbrock function.*

Table 3.1: *Comparison of PSO, BOA AND M-BOA in terms of minimum value and standard deviation (in brackets).*

	Ackley	Rosenbrock	Rastrigin	Shekel
PSO	3.149 (0.164)	0.218 (0.039)	30.062 (9.48)	0.0022 (0.0178)
BOA	0.164 (0)	0.8384 (0)	0.1488 (0)	0.0013 (0)
M-BOA	0.032 (0.02)	0.000085 (0.0000128)	0.0092 (0.0012)	0.000026 (0.000016)

3.4.1 Synthesis of Thinned Arrays using M-cGA

In recent years, thinned arrays, presented in Section 2.1.4, have attracted significant attention from researchers because of their advantages such as the reduction of the array weight and of the complexity of the feeding network. The reduction of the number of array elements has however also some disadvantages, the main of which is the decrease of the maximum gain, that corresponds to an increase of the side-lobe level (SLL) with respect to a fully populated array with the same size [29].

To overcome these drawbacks, several techniques have been proposed, aimed at finding the best configurations of thinned array [52], [53]. Deterministic approaches have been adopted first, but they do not show significant improvements with respect to the random element placement [52,54]. Recently, dynamic program [55] and stochastic

optimization techniques, including Genetic Algorithm (GA) [56], simulated annealing (SA) [57, 58], and Ant Colony Optimization (ACO) [53], have been applied to the optimization of thinned array. The obtained results are remarkable, even if they could be further improved.

The combination of deterministic approaches and stochastic optimization have been proposed exploiting the available knowledge of Different Sets (DS) or Almost Different Sets using GA [59], [60]. The combinations have proved that this procedure is very effective, in most case. However, the operations performed by the optimizer still remain an inherent disadvantage of stochastic based optimization e.g. convergence difficulties.

Recently, M-cGA has been applied to thinned array problem and shown improvements in controlling the peak side-lobe level (PSL) of several linear thinned array [61, 62]. The PVs in M-cGA are used to represent the states (ON/OFF) of all elements in the arrays. The M-cGA manages these PV to find the best configuration of thinned array with minimization of PSL. The performance of M-cGA is good even without the help of deterministic method, i.e., DSs or ADSs. In this section, the use of M-cGA is presented and further investigated for several large linear and planar thinned arrays. The achieved PSLs show the effectiveness of M-cGA to thinning array problems.

Synthesis of Thinned Linear Array

The synthesis of linear thinned array using M-cGA has been presented in [61,62], and it is extended in this section to several different configurations. Two main types of thinned arrays are considered here: configurations with available ADS sequences and extended configurations from available ADS in order to compare with the performance of GA-ADS reported in [60]. In all the tested cases, M-cGA works alone with 4 probability vectors, and the results are compared with those of GA with or without ADS.

The linear arrays considered in this section have different number of elements in the array, with the spacing of 0.5λ (wavelength at considered frequency) in the regular grid. Thus, if the array has N elements, its length is $N \times \lambda/2$, and the side-lobel levels for these regular arrays are -13.3 dB. These arrays are then thinned with different thinned ratio, and the M-cGA is applied to reduce the PSL of these arrays.

The first considered case is a thinned array configuration where 50% of the elements are turned on, and there are ADS sequences available for the GA-ADS optimization. In Table 3.2, the achieved PSL by different methods has been reported. It appears that M-cGA is able to obtain better results than both GA and GA-ADS for all cases. Moreover, the computational cost required by M-cGA is much lower than those by GA or GA-ADS as plotted in Fig. 3.13. When the number of elements in the array increases, the number of function evaluations increases exponentially for the case of GA and GA-ADS, while it shows a linear increase when using M-cGA. Fig. 3.14 and Fig. 3.15 report the normalized pattern of 502 element thinned array by different methods.

Table 3.2: *Achieved PSLs by Different Methods.*

Array	GA [60]	ADS-GA [60]	M-cGA
98	-19.82	-20.4	-20.45
198	-18.20	-19.24	-21.9
502	-20.83	-21.31	-23.53

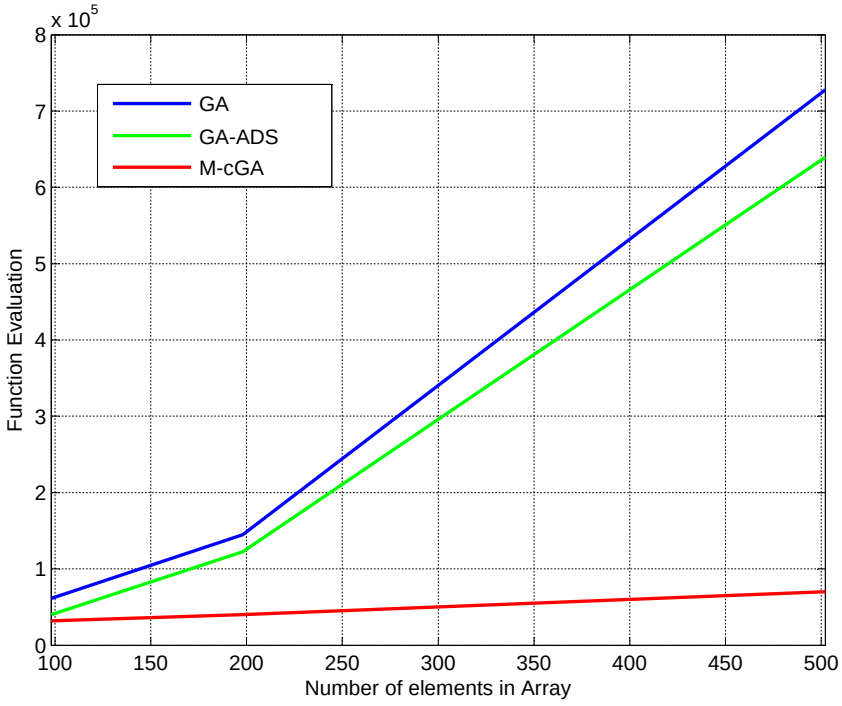

Figure 3.13: *Function evaluation of different thinned arrays.*

Secondly, the performance of M-cGA is compared to those of GA and GA-ADS over the syntheses of arbitrary thinned array configurations where the ADSs are not available, i.e., problem II and III in [60]. Two different arrays are thinned: The first array of 198 elements with 79 elements are off, and the second case, 46 of 200 elements are off, and the results are reported in Table 3.3, and Table 3.4. The optimized PSLs by M-cGA are again lower than PSLs obtained by GA and GA-ADS. Furthermore, the computational cost needed for M-cGA to converge is much lower than those required by GA and GA-ADS as shown in Table 3.4. As an example, the obtained pattern of the 200-element thinned array with 77% turned on is shown in Fig. 3.16, while the thinned arrays obtained by other methods are plotted in Fig. 3.17.

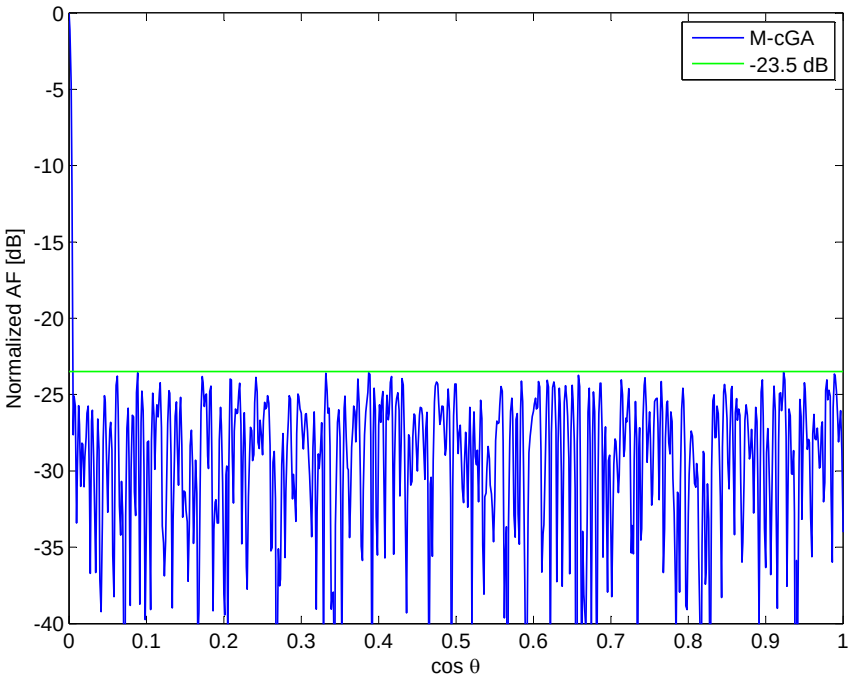

Figure 3.14: *Normalized Array Factor of 502 element thinned array, with* 50% *turn on.*

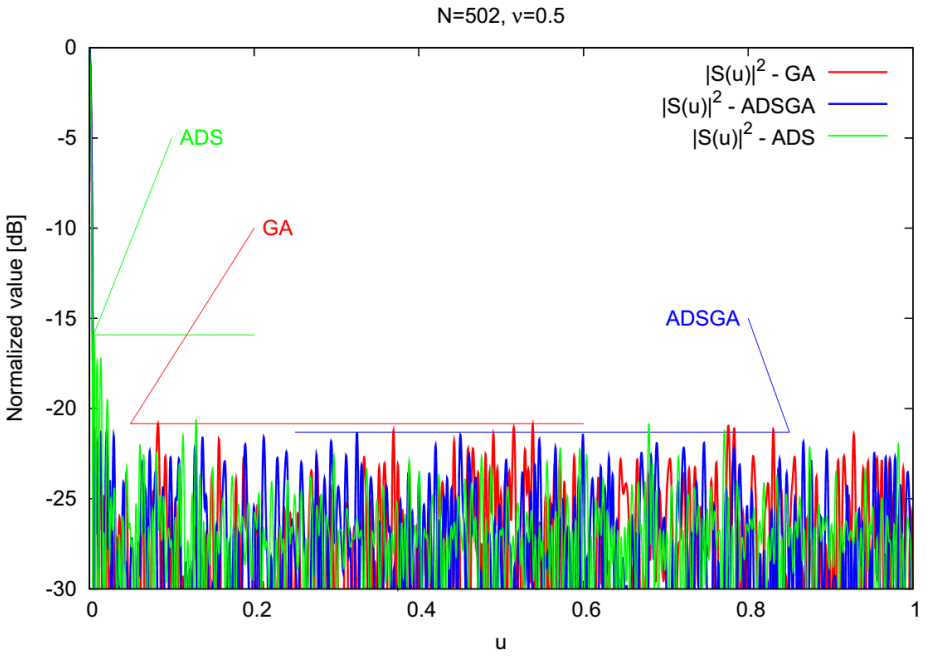

Figure 3.15: *Normalized Array Factor of 502 element thinned array obtained by other methods [60].*

Table 3.3: *Obtained PSL by different methods.*

Array	GA [60]	ADS-GA [60]	M-cGA
$198/79$	-19.95	-20.25	-21.10
$200/46$	-22.47	-23.05	-23.75

Table 3.4: *Function evaluations.*

Array	GA [60]	ADS-GA [60]	M-cGA
$198/79$	$342,540$	$126,126$	$60,000$
$200/46$	$345,000$	$305,600$	$100,000$

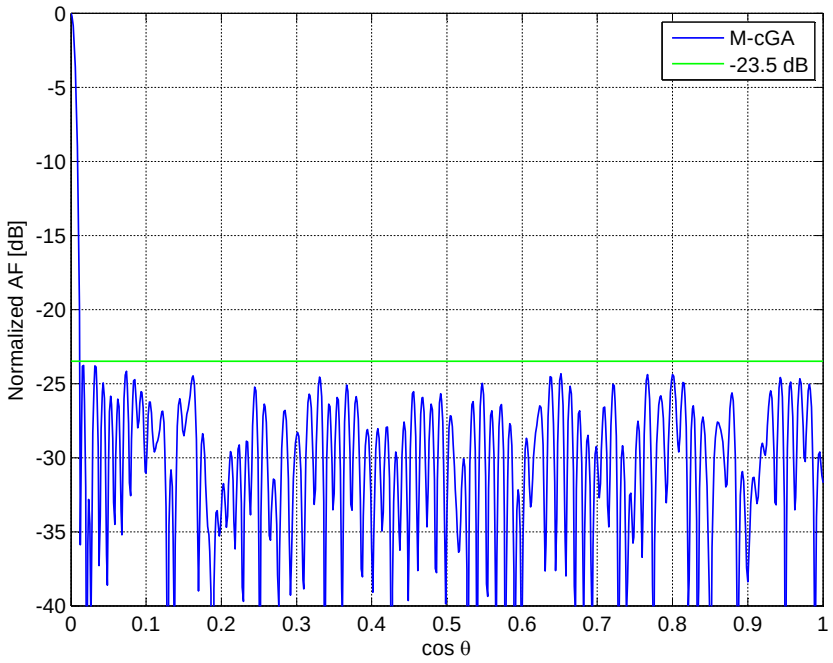

Figure 3.16: *Normalized Array Factor of 200 element thinned array, with 77% turn on.*

Synthesis of Planar Thinned Array

In this section, the 20×10 element planar array is thinned using M-cGA. The probability vectors here are represented as one-dimensional vectors since it would be more convenient for M-cGA operations e.g. learning and updating. The algorithm performs the synthesis in the same way as it did for linear array. The sampled solution is converted to planar array configuration. Even though, two-dimensional probability vector

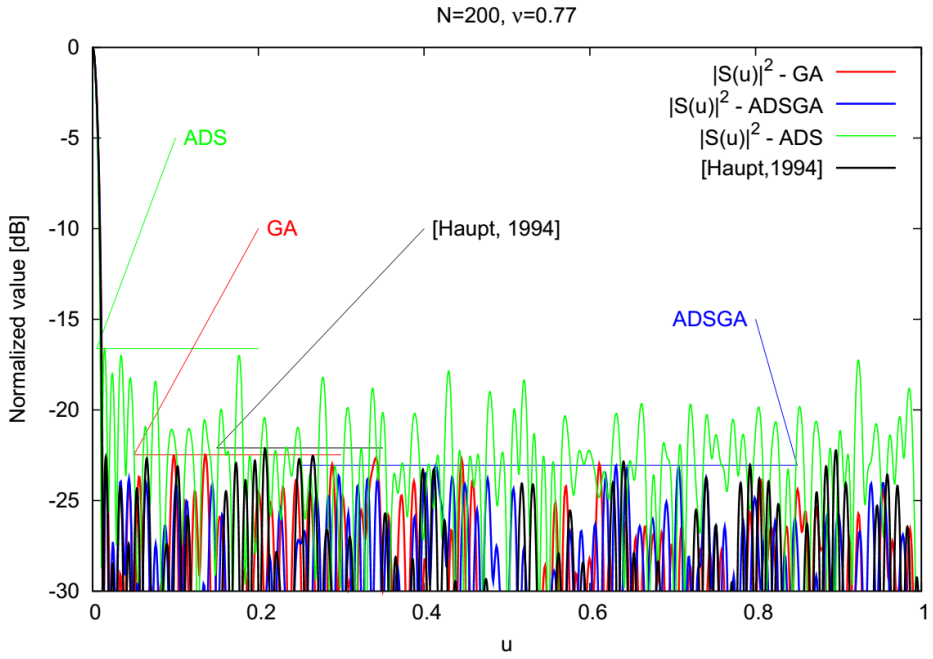

Figure 3.17: *Normalized Array Factor of 200 element thinned array obtained by other methods [60].*

is also applicable to represent the distribution of solution of planar array. The fitness function here is the sum of PSLs at two main plane cuts, i.e., $\phi = 0°$, and $\phi = 90°$.

In Fig. 3.18, the far-field pattern cuts are reported, and Fig. 3.19 shows the average convergence curve (over 30 trials) of the synthesis of the thinned array where 108 elements are turned on. The optimized PSLs are -26.6 dB at $\phi = 0°$ plane, and -23.5 dB at $\phi = 90°$ plane. The achieved results by M-cGA are 10 dB (cost function) lower than the results obtained by GA [56], and even 5 dB lower than the results obtained by modified real genetic algorithm (MGA) which optimized the position of the elements [63]. Moreover, the number of function evaluation required to converge by M-cGA is around 12000 (4 PVs and non-persistent elitism are implemented) which is less than half of that needed by MGA [63].

3.4.2 Microstrip Filter Design

The first application of M-BOA to EM problem is the microstrip filter presented in [51]. In this section, this procedure is detailed, and the optimum results is reported.

The considered microstrip band-pass filter is show in Fig. 3.20, consiting of a cascade of $2P - 1$ segments, each of which with electrical length equal to $\lambda_g/2$ at the central frequency (being λ_g the guided wavelength, given by $\lambda_0/\varepsilon_{eff}$, where ε_{eff} is the effective permitivity, related to the relative permitivity of the substrate ε_r and λ_0 is the free-space wavelength), but different width.

The filter can be easily modeled with its transmission line equivalent model, i.e. with a cascade of $2P - 1$ transmission lines, having the same electrical length $\lambda_g/2$, but different characteristic impedance Z_i, since the later quantity depends on the line

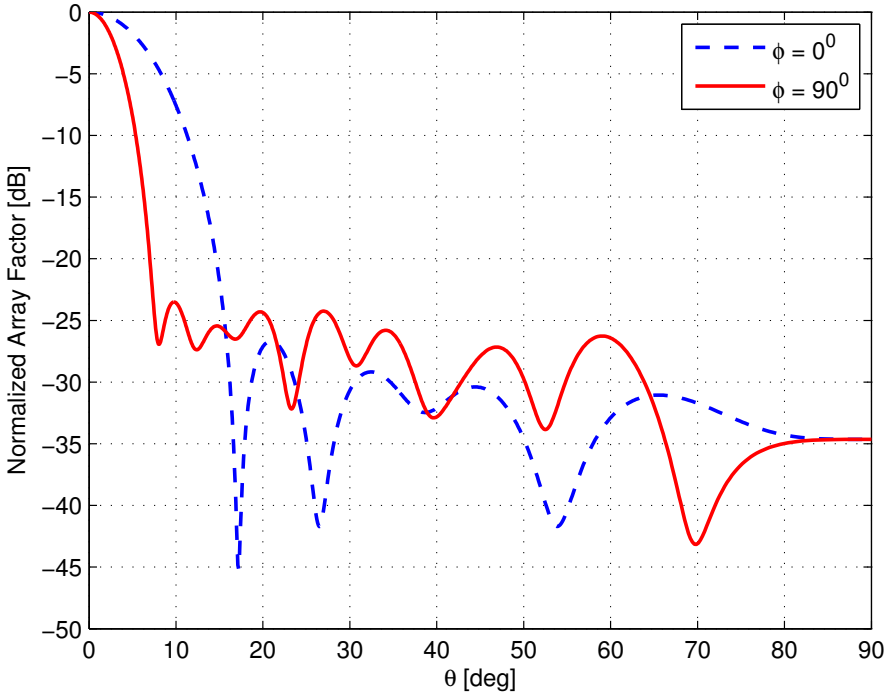

Figure 3.18: *Far-field patterns at two main plane cuts.*

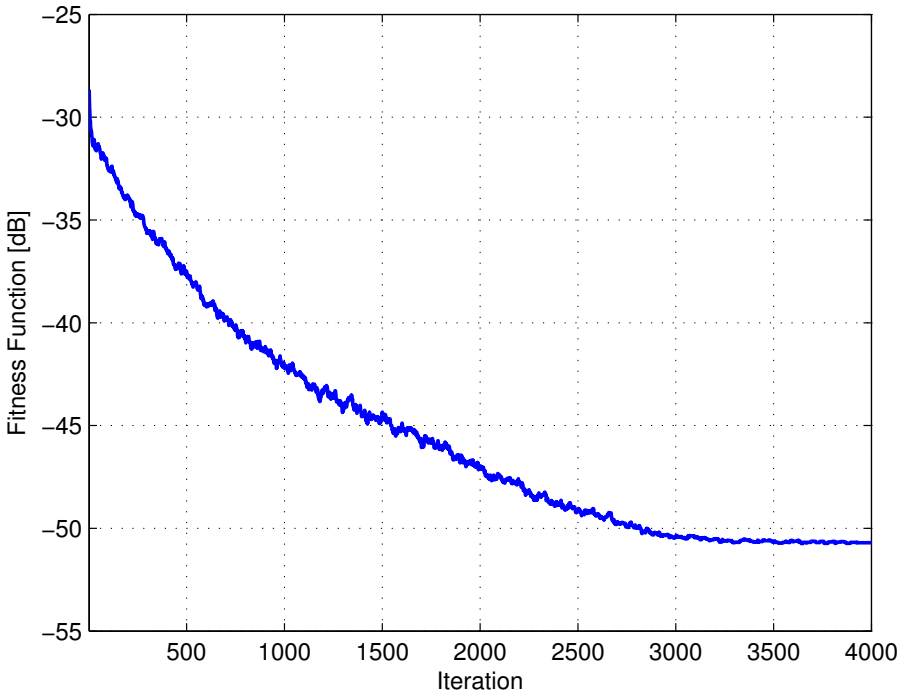

Figure 3.19: *Convergence curve of thinned array optimized by M-cGA.*

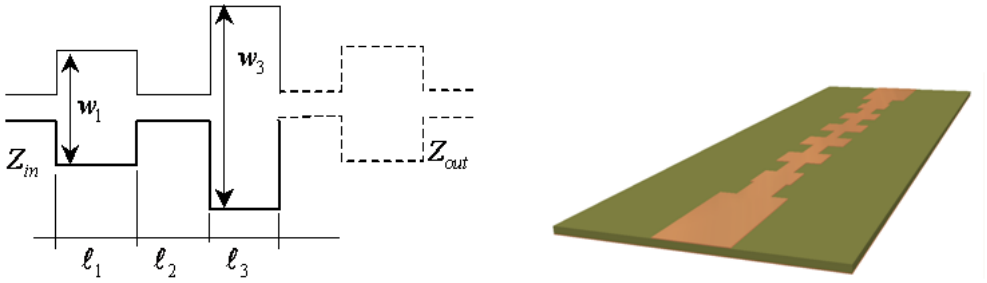

(a) Analytical Modal (b) Printed Design

Figure 3.20: *Microstrip filters.*

width w_i. The filter can be therefore seen as a sequence of two-port networks, each of which can be represented by its chain matrix [64], whose entries depend only on the characteristic impedance and on the electric length. The chain matrix of the entire structure is given by the product of $2P-1$ single chain matrices and the transmission coefficient, i.e. the transfer function, of the filter is expressed in terms of the entries of the chain matrix of the whole structure:

$$S_{21} = \frac{2\sqrt{Z_{\text{out}}/Z_{\text{in}}}}{A_{\text{tot}} + B_{\text{tot}}/Z_{\text{in}} + (Z_{\text{out}}/Z_{\text{in}})(C_{\text{tot}}Z_{\text{in}} + D_{\text{tot}})} \tag{3.5}$$

where Z_{out}, Z_{in} are the reference impedances at the output and input ports of the filter, respectively.

The performances of the filter depend on the number of lines used for its realization (the greater is P, the larger is the bandwidth, but also the longer the filter is), and on the values of the characteristic impedance of the equivalent transmission lines. In the considered case here, P is fixed and the filter widths, w_i, are optimized with the M-BOA following the design constraints:

- the bandwidth that has to be equal or greater than a fixed value, e.g. 0.6;
- minimize the in-band ripple;
- maximize the out of band rejection

Even the model, Eqn. 3.5, doesn't take into account the interactions between the different lines, it represents a good compromise between the accuracy in modeling the filter and the low computational cost that is very important aspect when optimization tools as the M-BOA is applied. Fig. 3.21 show the transfer function of the microwave filter consisting of 17 line segments ($P = 9$). The design satisfies 60% of 3-dB bandwidth required, with in-band ripple less than -0.2dB (shown in the inset). In this case, M-BOA is applied with population of 50, and mutation rate of 0.1. Variables considered are the impedance, Z_i, of each microstrip line segment. Table 3.5 reports the optimum result obtained by the M-BOA. The results can be used to find the width, w_i, of each microstrip line segment which depends on the substrate and considered frequency.

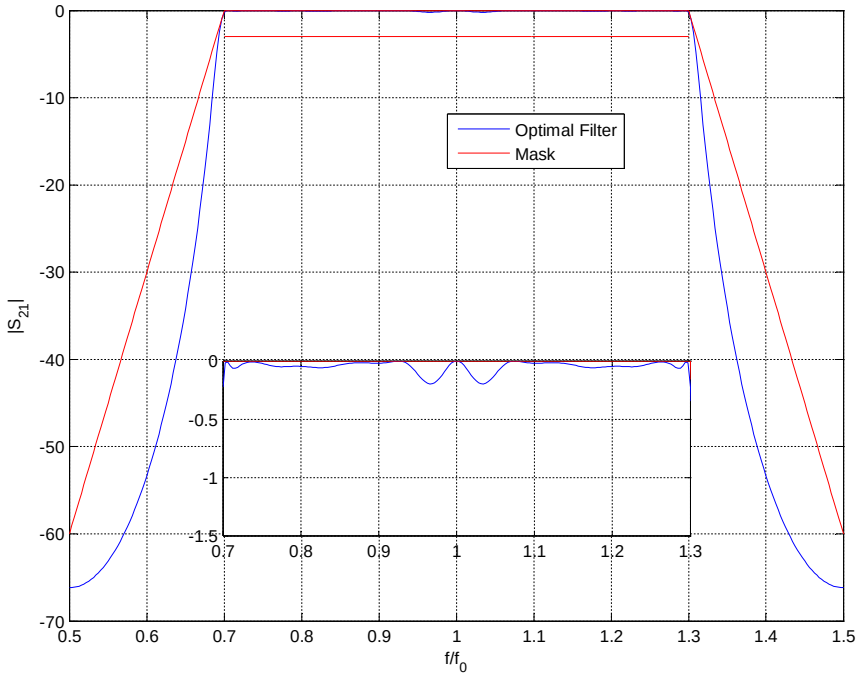

Figure 3.21: *Transfer function of 17 line segment microstrip filter (inset: in-band ripple).*

Table 3.5: *Impedance of each segment of final design.*

Segment #	Impedance (Ω)	Segment #	Impedance (Ω)
1	71.408	6	36.273
2	39.595	7	134.854
3	104.203	8	37.696
4	35.503	9	134.66
5	120.02		

3.4.3 Sparse Array Synthesis using M-BOA

Thank to the promising results obtained over the benchmark functions, the M-BOA has been applied to more realistic antenna problems, i.e., the optimization of the design of three linear antenna arrays. To compare the results obtained by the M-BOA with those provided by other approaches, different examples of linear, broadside, sparse, symmetric arrays, have been considered [65–69]. In all the considered cases, the arrays are symmetric, and the optimization goal is that of determining the array element excitation coefficients, a_n, the position normalized with respect to the wavelength, d_n/λ, and the minimum number, $2N$, of array elements that allows to satisfy the array radiation constraints. Note that the estimation of the lowest number of necessary array elements is an important aspect, as also discussed in [69]. Most of the optimization techniques adopted for array syntheses [65, 70–75] work with a fixed and predetermined number of array elements, which is generally taken larger than the actually needed, in order to

be sure to satisfy the radiation pattern constraints. However, the use of a not redundant number of elements is generally advantageous, since that reduces the feeding network complexity and the antenna weight. For this reason, in the last years, several efforts have been done to propose techniques for the design of arrays, linear and planar, with a reduced number of elements not equally spaced [67–69, 76]. Due to their probabilistic nature, BOA and M-BOA seem particularly suitable to determine, during the optimization process, also the proper number of array elements, and therefore the design of such kind of array seems a particularly suitable test case for comparing their performances.

Chebyshev–like Pattern Synthesis

The first considered example consists the synthesis of an array showing a radiation pattern with the HPBW of at least $6.3°$, the -30 dB beam-width lower than $8°$ and the side lobe level ≤ -30 dB (see the mask plotted later on in Fig 3.25.). Such requirements can be easily obtained with an uniformly spaced Chebyshev array with $2N = 20$ elements (this is the reason why we named "Chebyshev-like" this type of radiation pattern), while in [67, 69] the constraints have been satisfied with unequally spaced arrays with $N = 6$.

Here both the BOA and the M-BOA have been used for the array optimized synthesis, according to the Chebyshev-like constraints specified above. In this test, a population of 100 individuals in both the procedures has been used, considering 1000 independent trials of 200 iterations each. The fitness function that models the problem is defined as:

$$f(X) = \sum_i \varepsilon(\theta_i) \tag{3.6}$$

where $\varepsilon(\theta_i)$ is the the difference between the constraints mask (R_{mask}) and the radiation pattern (R_p) obtained at any iteration of the optimization process:

$$\varepsilon(\theta_i) = R_p(\theta_i) - R_{\text{mask}}(\theta_i) \tag{3.7}$$

It is worthy noticing that Eqn. 3.7 applies only when $R_p(\theta_i) - R_{\text{mask}}(\theta_i) \geq 0$, i.e., when the obtained pattern exceeds the constraints, while $\varepsilon(\theta_i) = 0$ when $R_p(\theta_i) - R_{\text{mask}}(\theta_i) \leq 0$.

The ranges of variation for the optimization variables are set equal to $(0.25 - 5)$ for the normalized array element location (d_n/λ), $(0 - 1)$ for the element excitation coefficient (a_n) and $(5 - 9)$ for the array element pair number (N). In order to have a stronger validation of the M-BOA, it has also been compared with the GA and the PSO.

First, the results of the comparison between the standard BOA and the M-BOA are presented: in Fig. 3.22 the worst (dot-dashed line), the average (continuous line) and the best (dashed line) curves of convergency relative to the two methods are plotted, showing that the M-BOA outperforms the BOA both in terms of capability of convergence (the average curve relative to M-BOA reaches a final value for the cost function that is almost two order of magnitude smaller than the one of the BOA) and reliability (the average curves converge, although with a greater number of iterations, almost to the same value that the best one; moreover, the average curve of convergence for the M-BOA is much closer to the best solution than to the worst one, and this means that

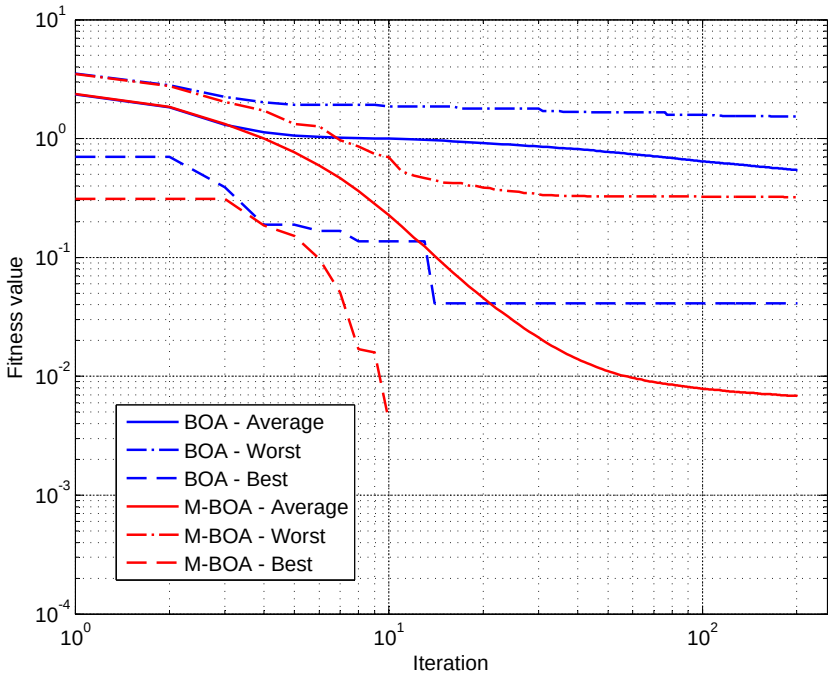

Figure 3.22: *Chebyshev-like pattern synthesis: comparison between the BOA and the M-BOA in terms of convergence.*

the number of trials, in which a solution closed to the best one is reached, is greater than the number of cases in which it is close to the worst one).

In Fig. 3.23 the average curve of convergence obtained with the M-BOA (red solid line in Fig. 3.22) is compared with the best curves of convergence obtained with a decreasing number of array elements: with $N = 6$ the algorithm convergence is still good and fast: this means that it is possible to satisfy the radiation pattern constraints with such a number of radiator pairs. The curve corresponding to $N = 5$ is not plotted since in that case the algorithm does not converge.

The second column of Table 3.6 shows the probability (computed as the ratio between the times in which a good result is obtained and the total number of trials) of obtaining a good solution with different array sizes within a predefined number of iterations. Note that, as it can be also deduced from the above considerations, in that table any row corresponds to $N = 5$, since with such a small number of elements the desired radiation pattern is never achieved (the probability is therefore 0). Moreover, note that the probability to have good solutions first increases and then decreases. This could be explained with the fact that with a high value of N, e.g. 9, the number of variables that the M-BOA has to manage increases and therefore the convergence could not be reached in the considered number of iterations; on the other side, when N is small, i.e., 6, it becomes difficult to find the proper values of a_n and d_n/λ that get the required pattern. In both cases, the algorithm hardly converges and less good solutions are obtained. On the contrary, medium values of N, i.e., 7, 8, represent a good trade-off

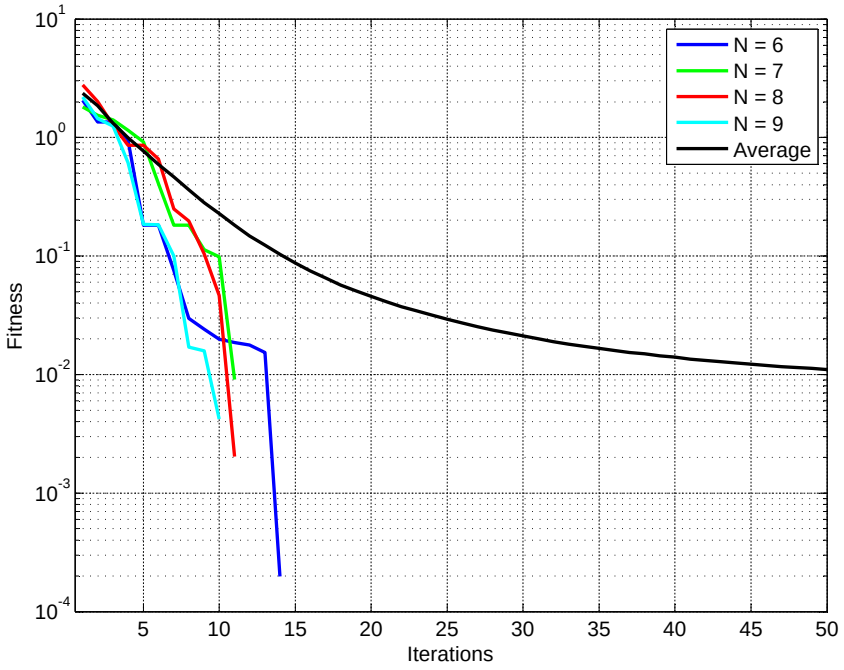

Figure 3.23: *Chebyshev-like pattern synthesis: curves of convergences of the M-BOA, relative to different values of array element pairs.*

between the problem size and the ease of satisfying the pattern constraints. In the third column of the table, the probability values computed in [69] for the same array problem are reported: even if the case $N = 10$ is out of the range of the number of element pairs considered here, its respective row has been added, just to show that also in [69] the sum of the probabilities is equal to 1. It is worth to note that both algorithms shown the ability to obtain the desired array performances with 6 elements, but the probability value relative to M-BOA is higher than that what derived in [69] for the Bayesian Interference (BI), and this confirms the better reliability of the M-BOA with respect to the BI.

Table 3.6: *Probability of good convergence for different values of N.*

N	Convergence Probability	
	M-BOA	BI [69]
6	0.182	0.1327
7	0.349	0.5377
8	0.296	0.2843
9	0.173	0.0393
10		0.006

Finally, the convergence of the M-BOA has been compared with that of the PSO and

the GA. For doing that, N has been fixed to 6, a population of 100 individuals has been considered and the results have been averaged over 30 independent trials, each of 1000 iterations. The resulting average curves of convergence for the M-BOA, the BOA, the PSO and the GA are plotted in Fig. 3.24.

As expected, the BOA could not converge since the number of array elements is too small, while the M-BOA outperforms both the GA and the PSO. The results show that the M-BOA not only has the capability of automatically set the minimum number of elements needed to satisfy the radiation constraints, but, for a fixed N, it also converges faster than the GA and the PSO. Note that the radiation pattern in Fig. 3.25 does not show uniform SLL as that obtained with the Chebyshev synthesis, but in any case the mask is satisfied, with a much smaller number of elements.

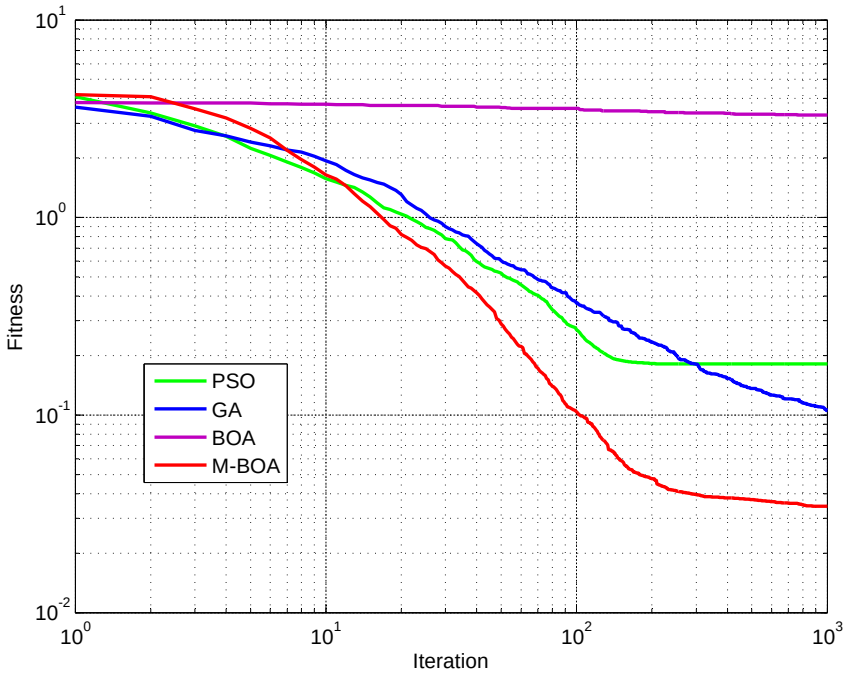

Figure 3.24: *Chebyshev-like pattern synthesis ($N = 6$): average curves of convergency relative to different methods.*

Fig. 3.25 shows the radiation pattern for the $N = 6$ array, designed with the M-BOA, together with the required mask, while the corresponding values of the element positions (d_n/λ) and of the excitation coefficients a_n are listed in Table 3.7.

Flat-beam (sector beam) pattern synthesis

The second considered example is the synthesis of a sector beam pattern with the following requirements: a first region ranging from $78.3°$ to $90°$,where the beam has to be almost flat, with a ripple lower than 0.5 dB, and a second region, ranging from $0°$

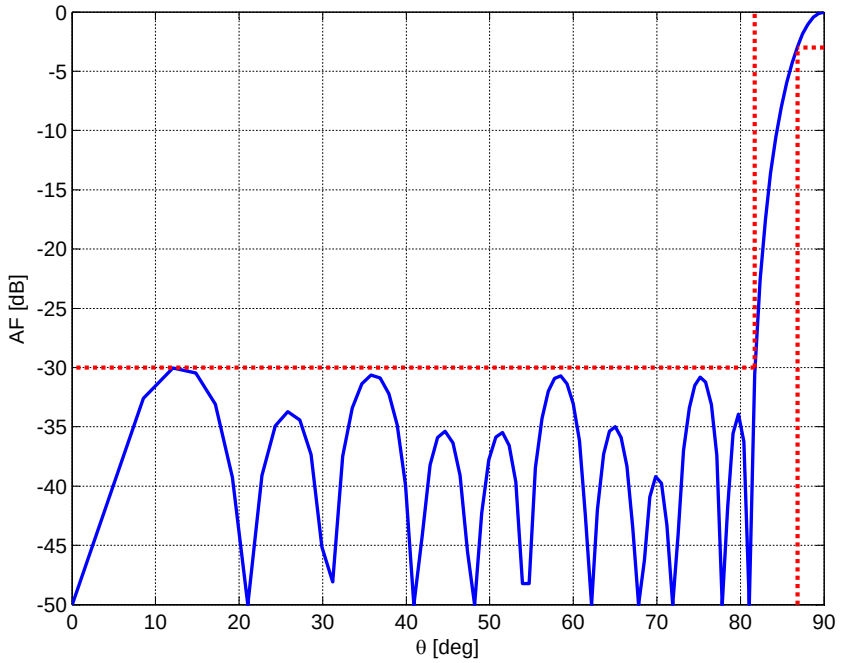

Figure 3.25: *Chebyshev-like pattern synthesis ($N = 6$): best array factor (AF) obtained by M-BOA.*

Table 3.7: *Parameters of the $N = 6$ array design with the M-BOA.*

Element #	d_n/λ	a_n
1	0.4313	0.3657
2	1.3055	0.3282
3	2.1777	0.2769
4	3.0494	0.2037
5	3.9076	0.1316
6	4.7919	0.0815

to $69.3°$, in which the side-lobe level has to be less than -25 dB. Therefore, the cost function is the same as Eqn. 3.6, considering $R_{\text{mask}}(\theta_i)$ defined in Fig. 3.28.

This synthesis problem is effectively solved by controlling the excitation amplitude and the phase of all the array elements [65, 66]. In [66], the use of the Taguchi method allows to fulfill the radiation pattern constraints with an array of $N = 7$ pairs of elements, i.e., with 6 elements less than the one designed in [65] using PSO. As in the previous example, the M-BOA is used also to estimate the minimum number of elements necessary to satisfy the radiation pattern requirements.

Since M-BOA has been shown that it outperformed BOA both in terms of speed of convergence and solution quality, the M-BOA is from here on only compared with the GA and the PSO. In all cases the ranges of variation for the optimization variables are set equal to $(0.25 - 5)$ for the normalized array element location (d_n/λ), $(-0.5 - 0.5)$ for the element excitation coefficient (a_n), while for the M-BOA the number of element

pairs could also vary between 4 and 9, since the problem could be easy solved with 10 pairs of elements.

In Fig. 3.26, the best curves of convergence of the M-BOA for different values of N are reported. They have been obtained using a population of 100 individuals and considering 800 independent trials, each of 200 iterations. From this plot it appears that the problem can be solved even with $N = 5$ pairs of elements, since the convergence of M-BOA with $N = 5$ is really fast, and the pattern requirements are reached with two less pairs of elements than those of the array proposed in [66].

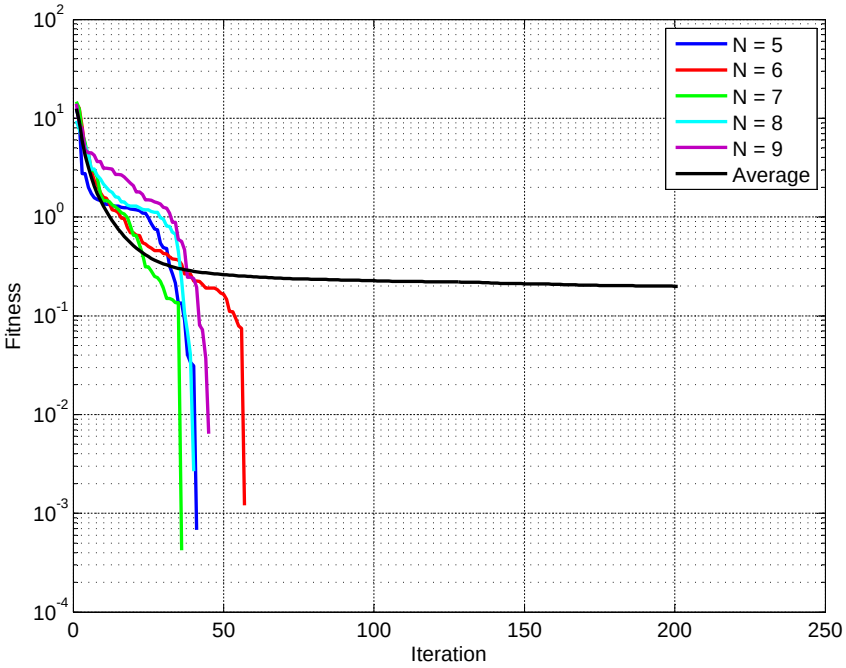

Figure 3.26: *Sector beam pattern synthesis: curves of convergency of the M-BOA, relative to different values of array element pairs.*

Table 3.8: *Probability of good convergence with different values of N.*

N	M-BOA Convergence Probability
5	0.818
6	0.110
7	0.055
8	0.015
9	0.002

In Table 3.8, the probability of obtaining a good solution with different array sizes is listed. For values smaller than 5 (e.g. $N = 4$), the algorithm could not convergence to the desired solution and the probability is 0. The probability for $N = 5$ is the highest,

indicating that this is the sufficient number of element pairs necessary to obtain the desired radiation pattern. Moreover, when N increases, the probability of finding good solution decreases, since the problem complexity increases and probably the population size and/or the number of iterations considered here are not still enough to guarantee the convergence. Finally, note that also in [69] an array of 10 elements satisfying the same constraints as here has been designed, but comparing the probabilities of obtaining good solutions in Table 3.8 with those in ([69], Table III), it is possible to conclude that also in this case the M-BOA outperforms the Bayesian Interference method.

In Fig. 3.27 the average curve of convergence for the M-BOA in the case with $N = 5$, is compared with those relative to the GA and the PSO. For all the three methods, the adopted population has 50 individuals, while 30 independent trials have been considered, each of 1000 iterations. It could be seen that the GA converges better than the PSO, while the M-BOA outperforms both of them. The radiation pattern obtained with the M-BOA is plotted in Fig. 3.28, together with the mask it has to satisfy, while the design parameters are listed in Table 3.9. A very good flat beam has been obtained with a ripple of 0.22 dB, i.e., 0.36 dB less with respect to the ripple of the array designed with the Taguchi method [66].

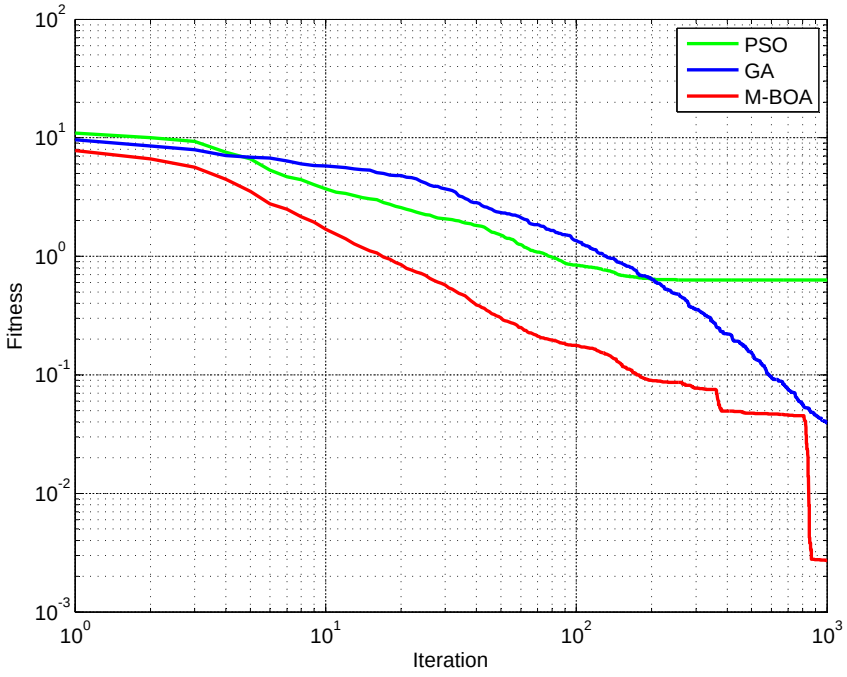

Figure 3.27: *Sector beam pattern synthesis ($N = 5$): average curves of convergence relative to different methods .*

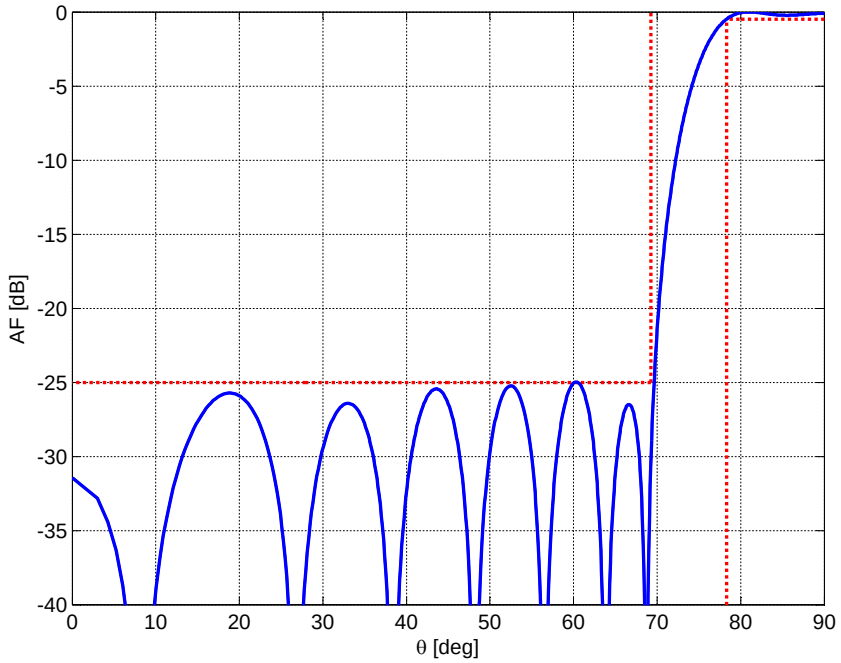

Figure 3.28: *Sector beam pattern synthesis ($N = 5$): best array factor (AF) obtained by M-BOA.*

Table 3.9: *Parameters of the $N = 5$ array design with the M-BOA.*

Element #	d_n/λ	a_n
1	0.3586	0.2767
2	1.0748	0.1420
3	2.4697	- 0.0472
4	3.0955	- 0.0246
5	4.1708	0.0245

Null-controlled Pattern Synthesis

The last considered linear array example is the synthesis of an array whose radiation pattern presents nulls for specific directions [66, 69]. The main beam has to point to $90°$ with a HPBW of $7.4°$, while the side-lobe levels have to be lower than -40 dB. Moreover, two nulls are desired between $50°$ and $60°$. Such a radiation pattern has been obtained using GA, PSO, and Taguchi methods with arrays of 20 elements [66, 73, 74]. Here, the M-BOA is used in order to estimate the sufficient number of element to fulfill the requirements [69].

The ranges of variation are set equal to $(0.25 - 5)$ for the normalized array element location (d_n/λ), $(-0.5 - 0.5)$ for the element excitation coefficient (a_n), and $(5 - 9)$ for the array element pair number (N), assuming to be able to design the array with a number of elements lower than that used in [66, 73, 74].The M-BOA uses a population of 100 individuals, and 800 independent trials, each of 200 iterations, have been con-

sidered. As previously, the cost function is given in Eqn. 3.6, considering $R_{\text{mask}}(\theta_i)$ shown later on in Fig 3.31.

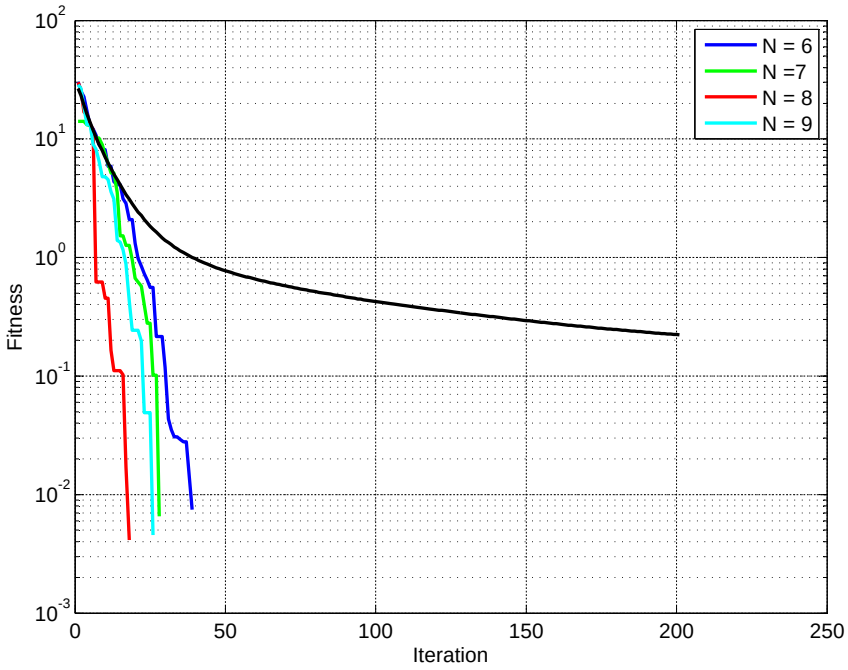

Figure 3.29: *Null-controlled pattern synthesis: curves of convergency of the M-BOA, relative to different values of array element pairs.*

In Fig. 3.29 , the average curve of convergence of M-BOA is plotted along with the best curve of convergence obtained for different values of N. The results reveal that the desired pattern can be obtained even with 6 pairs of elements, i.e., with a reduction of the 40% of the number of elements compared with the one in [66]. It is worth to note that the best result ever achieved for this problem is with $N = 7$ in [69], and this again confirms the better performances of the proposed method with respect to direct sampling from Bayesian Interference.

Table 3.10: *Probability of good convergence with different values of N.*

N	M-BOA Convergency Probability
6	0.105
7	0.255
8	0.327
9	0.313

In Table 3.10, the probability of achieving good solutions with different values of N is shown. For $N = 5$, the desired pattern is never obtained, while the probability increases with N, probably due to the fact that the constraints on the radiation pattern

are harder to fulfill with a too smaller number of elements (as can be seen in Fig. 3.29 that for larger values of N the convergence is faster). However, the probabilities to obtain good solutions with $N = 8$ or $N = 9$ are very close, showing that a further increases of the number of array element will not improve significantly the possibility of having good solutions.

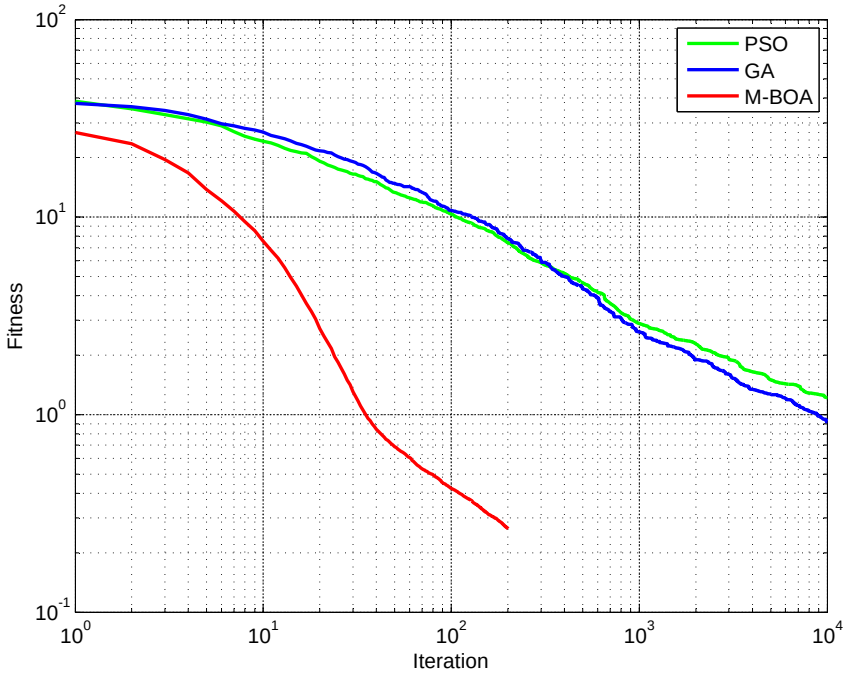

Figure 3.30: *Null-controlled pattern synthesis ($N = 6$): average curves of convergency relative to different methods .*

Finally, the performances of the M-BOA have been tested again against those of the GA and the PSO, setting $N = 6$, using a population of 100 individuals and averaging the results over 30 independent trials; for the M-BOA, it is sufficient to perform 200 iterations to reach the convergence, while both the GA and the PSO needed 10000 iterations; the resulting average curves of convergency are plotted in Fig. 3.30: also in this case the M-BOA outperforms both the GA and the PSO in terms of computational cost and in term of solution quality, i.e., the M-BOA requires less iterations than PSO and GA, to reach a final value of the fitness function that is better than those of the PSO and the GA. The desired pattern for the twelve elements null-controlled array, obtained by M-BOA, is plotted in Fig. 3.31, together with the mask. All the design parameters are instead reported in Table 3.11.

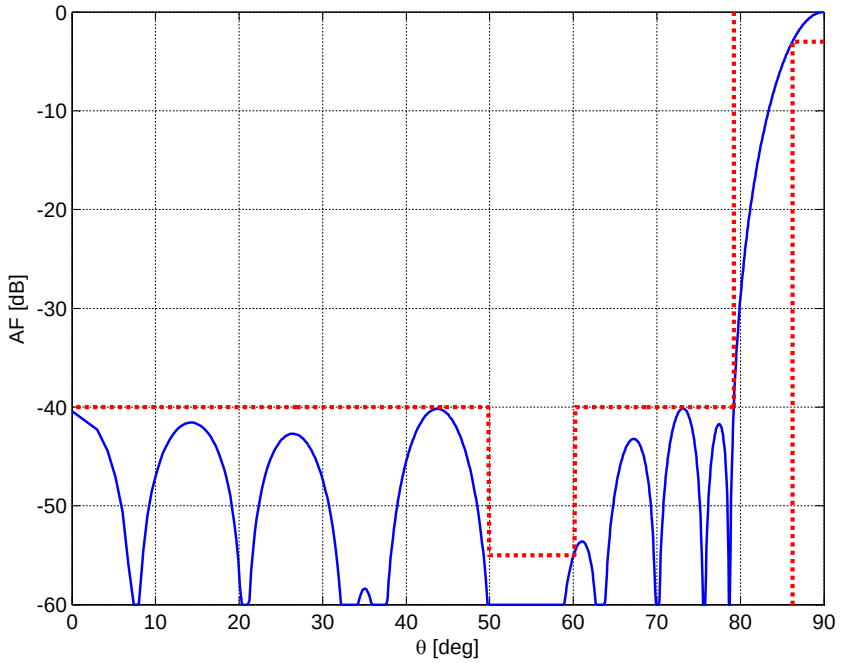

Figure 3.31: *Null-controlled pattern synthesis ($N = 6$): best array factor (AF) obtained by M-BOA.*

Table 3.11: *Parameters of the $N = 6$ array design with the M-BOA.*

Element #	d_n/λ	a_n
1	0.4221	0.2114
2	1.2611	0.1834
3	2.1023	0.1390
4	2.9476	0.0881
5	3.7805	0.0461
6	4.6220	0.0146

Synthesis of planar sparse array

The application of M-BOA to planar sparse array is explored in this sub-section. The considered array consists of 108 elements and satisfies the design constraints [63] as follows:

– Distance between any pair of elements is equal or greater than $d_c = 0.5\lambda$.

– All elements are allocated on a fixed aperture of $9.5\lambda \times 4.5\lambda$.

The array is assumed to be symmetrical along x- and y- axis, which reduces the problem complexity by a factor of 4. The element coordinate is controlled by the adopted method from [63]. However, the configuration of sub-array, i.e., a quarter as shown in Fig. 3.32, is chosen 4×7 instead of 3×9, which latter shows better PSLL

performance. The configuration here is similar to the thinned array in [56], which is optimized also by M-cGA in Section 3.4.1.

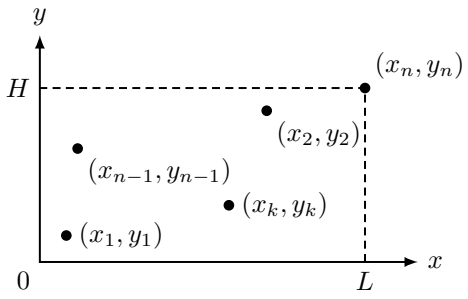

Figure 3.32: *Coordinates of elements in subarray of sparse planar array.*

The design object is to minimize the peak side-lobe level (PSLL) in two main planes, i.e., xz-, and yz-planes. Therefore, the fitness function is the sum of PSLLs in two planes, as explained in [56, 63], and also in Section 3.4.1. The array has been synthesized using the M-BOA with a population of 100 individuals; 30 independent trials have been considered, each of 500 iterations.

In Fig. 3.33, the average convergency curve of the M-BOA over the 30 independent trials along with the best and worst convergency curves has been reported; M-BOA can achieve very good solution e.g. -50.5 dB for the best case. Note that the optimal solution obtained here is much lower than those reported in previous works [56, 63] as could be seen from Table 3.12, in which the sum of PSLLs obtained with different methods is reported. The performance of M-BOA is comparable to M-cGA, since both of them are able to obtain fitness scores below -50 dB.

In Fig. 3.34, it is shown the array factors obtained by M-BOA. The PSLLs of the optimal solution are both lower than -20 dB (-22 dB in yz-plane and -28.5 dB in xz-plane) which is considerably lower than the result of $\mathrm{PSL} = -15.86$ dB in yz-plane in [63]. Moreover, the side-lobe levels on both planes are more "uniform" than those of M-cGA, shown in Fig. 3.18.

Table 3.12: *Obtained best PSLs by different methods.*

Sum of PSLs (dB)			
GA [56]	**MGA** [63]	**M-cGA**	**M-BOA**
-39.83	-45.45	-50.6	-50.5

3.5 Conclusions

In this chapter, two new optimization algorithms have been developed and their applications have been demonstrated by several mathematical and EM examples. By integrating learning mechanism, M-cGA shows better performance than its predecessors and can be efficiently applied to array thinning problems. The obtained results reveal that M-cGA is able to control PSLs of large arrays or planar arrays with pre-defined

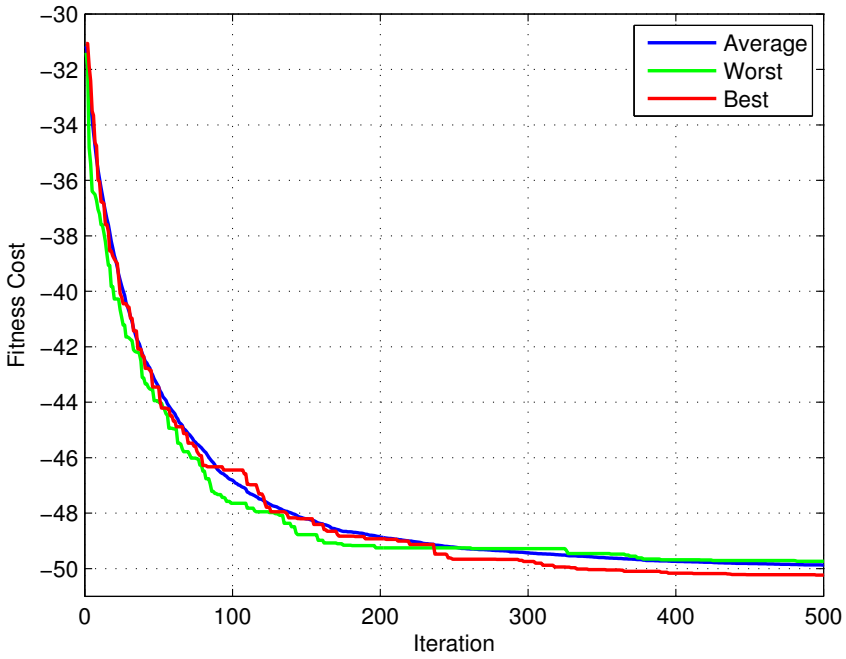

Figure 3.33: *Convergence of M-BOA.*

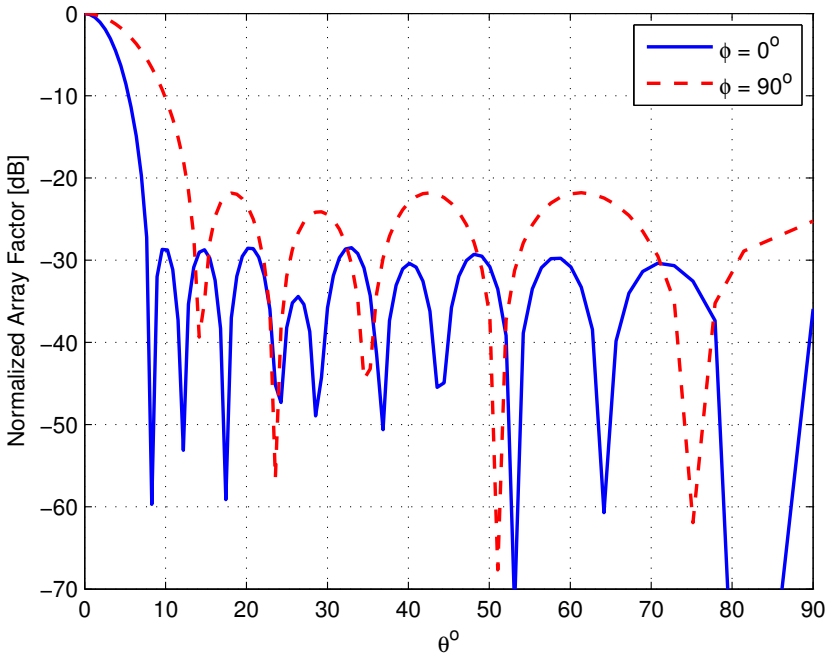

Figure 3.34: *Array Factor of optimal array at two main planes.*

constraints. Moreover, the computational cost required by M-cGA is greatly reduced with respect to other methods, which is important for applications such as scanning arrays.

The M-BOA has also been introduced: it shows improved performances with respect to the standard BOA, as well as other optimization algorithms as the GA and the PSO, both for what concerns the computational cost and the solution quality. Moreover, it has been shown, considering different examples, that this method seems particularly suitable for the design of sparse arrays, since it allows also to easily include the array number of elements among the optimization parameters.

Both proposed algorithms have shown their effectiveness for solving different EM problems. M-cGA is suitable for binary or discrete problems where the PVs are easily defined and controlled. M-BOA found their application to continuous cases, in which parameters can be even real or complex. From this view, M-BOA is potentially applicable for design of passive reflectarray antennas where element's dimensions are adjusted continuously, M-cGA is suitable for optimizing reconfigurable reflectarray antennas, in which the state of controllable devices could be discrete e.g. using MEMS devices.

CHAPTER 4

Passive Reflectarray Antennas

Reflectarray antennas (RA) are nowadays a quite popular technology, used in several applications, due to a significant number of attractive properties, such as low cost, low weight, conformal deployment and the possibility of introducing suitable reconfigurable capabilities. Unfortunately, they present also some intrinsic limitations and drawbacks compared to other solutions, and in particular a relatively narrow bandwidth. The bandwidth could be enlarged, but generally with a drastic increase of the structure complexity e.g. multi-layer structures.

Therefore, the objective of this chapter is to design a single layer passive reflectarray, in which the re-radiating elements have unconventional shape and enough degrees of freedom to compensate both the spatial and frequency phase variation of the re-radiated field. In particular, the work here is focused on a re-radiating elements consisting of two concentric square rings in which two different and quite independent geometric parameters are varied.

This chapter will start with an overview of reflectarray antenna design with historical development and current state of the art. Then in the second section, the double square ring unit cell will be introduced as a promising RA element. In the third section, design methods are presented. In this work, the double parameter design and optimization algorithm are combined for designing the reflectarray. Finally, two reflectarray configurations with horn feed are designed and numerical results are presented at the end of this chapter.

4.1 Reflectarray Antennas Design

The development of reflectarray antennas (RAs) started since 1963 when the first RA design consisting of variable length shorted waveguide components has been proposed

by Kennedy et al. [2]. Thanks to the improvements in antenna design technologies, in recent decades, RAs have been designed with printed technology, which greatly reduces the complexity of Kennedy's design. Printed patches have been implemented as RAs elements; by varying their lengths or attaching stubs to them, the responses of these patches can be tuned such that an arbitrary phase shift can be introduced. Patch antennas, however, are intrinsically narrow-band, and has contribute to the overall narrow-band characteristic of the whole RA structure.

In general, there are two reported approaches to overcome this well-known drawback of RAs. The first one implements multi-layer designs [7, 8], which stacks several patch layers to form the RA surface. Stacked patch RAs can improve the phase range and phase behavior of RA elementary, therefore the bandwidth of RA could be increased. This approach, however, increases the complexity of the RAs, i.e., multi-layer structure. The second approach, on the opposite, uses single layer design of multi-resonant structures, for example a unit cell consisting of double rings, or double square rings. These structures offer more than one degree of freedom to control the phase of the reflected wave. However, in all reported works, the RAs are often designed with only one variable parameter, which results in the lack of bandwidth for some applications.

4.2 Double Square Ring Element

In view of previous section, single-layer structures are highly desired for the design of reflectarray antennas. Among all the different types of patches that have been considered for this purpose, particular interest has been devoted to concentric rings of different shape, since this kind of choice looks promising as an effective compromise between a moderate increase of the complexity of the single patch geometry and its phase compensation capabilities. Furthermore, this type of radiating elements intrinsically posses different degrees of freedom, since the size and the width of the single rings could be varied independently; moreover it has a reduced resonance size and finally it has been seen that if such kind of elements are used in a multi-layer structure, in which the elements of each layer work in a different frequency band, they do not affect each others, allowing the realization of a multi-layer, multi-band structure.

4.2.1 Unit Cell Design

The RA re-radiating element considered in this work is of the type sketched in Fig. 4.1, and it consists of two square concentric rings, each one characterized by its side length ℓ and width w.

The considered unit cell's dimension is 15×15 mm, which is equal to $0.587\lambda \times 0.587\lambda$ at 11.75 GHz, the desired center frequency. To improve the re-radiating elements performances, a two layer dielectric structure has been used, consisting in a substrate characterized by height $h_1 = 5$ mm and relative dielectric constant $\varepsilon_{r1} = 1.1$ and in a cover with $h_2 = 0.85$ mm and $\varepsilon_{r2} = 2.5$.

To derive to this configuration, various design stages have been carried out. Initially, the unit cell was chosen with dimension of 12×12 mm, and printed on a substrate $h_1 = 3$ mm and relative dielectric constant $\varepsilon_{r1} = 1.1$, and the upper substrate. The

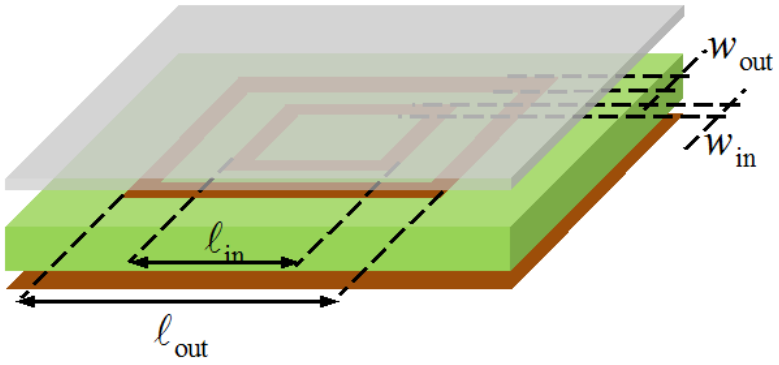

Figure 4.1: *Geometry of the considered re-radiating element.*

design is then investigated to define the best configuration of the unit cell, i.e. the widths of the rings w_{out}, w_{in} and dimension of the unit cell.

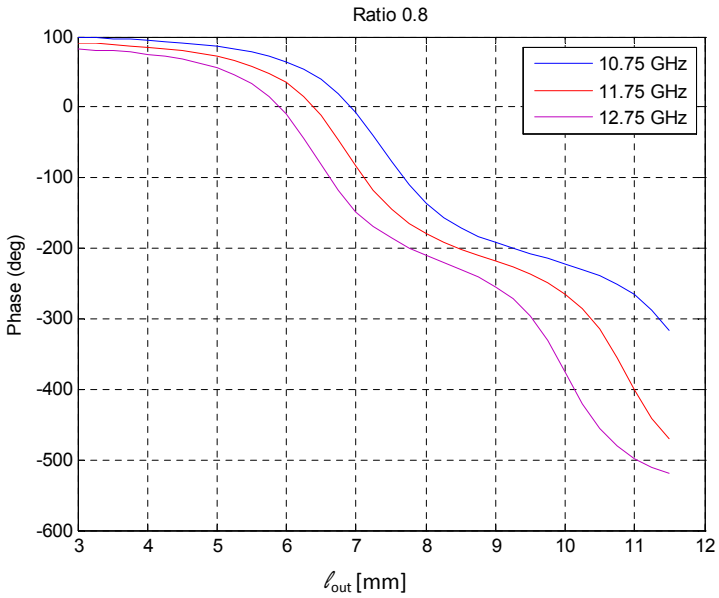

Figure 4.2: *Phase variation provided as a function of outer ring, at different frequencies, and Ratio = 0.8.*

Fig. 4.2 and Fig. 4.3 plot the reflected phase at different frequencies and different ratios between the outer ring and its width. Here, Ratio denotes for the ratio $(\ell_{out} - w_{out})/\ell_{out}$, and $(\ell_{in} - w_{in})/\ell_{in}$, so the ring's widths are proportional to their dimensions. While the ratio between the inner ℓ_{in} and outer ring ℓ_{out} is fixed to 0.5. It is shown that for lower Ratio, the phase curve is smoother, while the phase range is remained larger than 360° for all frequencies even when Ratio = 0.8. The Ratio is then assigned a value of 0.8, i.e the ring's widths are equal to 0.2 of their dimensions.

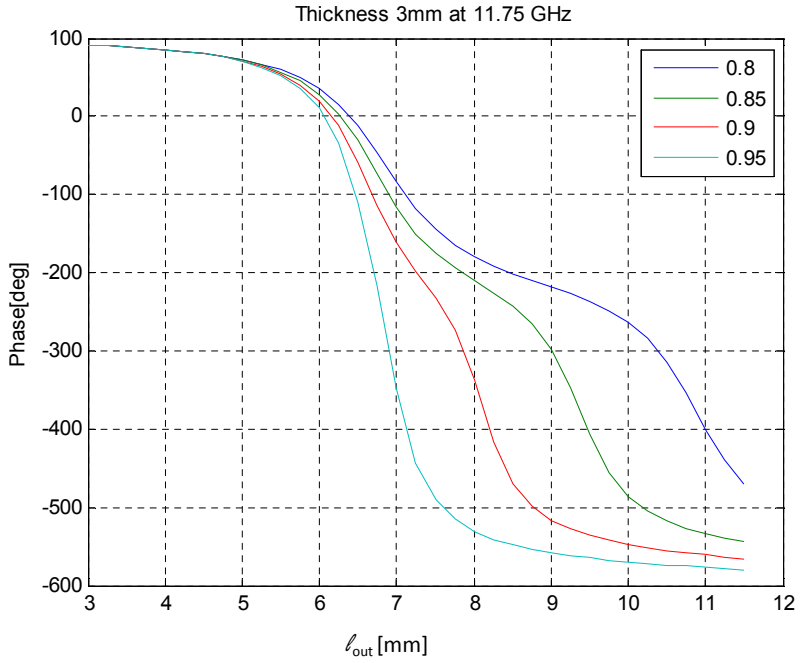

Figure 4.3: *Phase variation provided as a function of outer ring at center frequencies, and different Ratio*

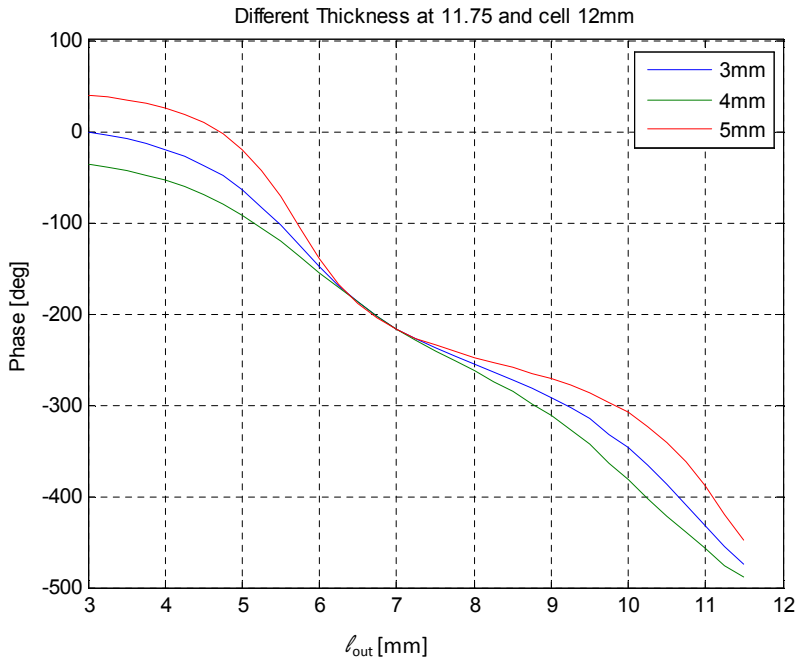

Figure 4.4: *Phase variation provided as a function of outer ring, at center frequency and different thickness.*

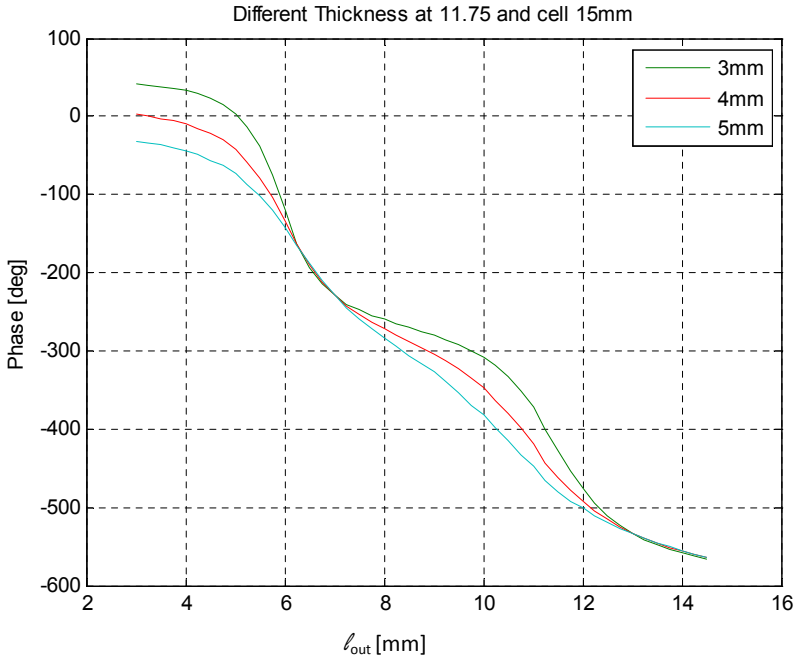

Figure 4.5: *Phase variation provided as a function of outer ring, at center frequency and different thickness.*

The unit cell is then simulated with different substrate's thickness and different cell sizes. Fig. 4.4 plots the reflected phase of a 12 mm cell at center frequency with different substrate thicknesses, while Fig. 4.5 shows the same reflected phase of a 15 mm cell. It is seen that the phase curve is smoother with thicker substrate, while the phase range is narrower. For a lager cell size, e.g. 15 cm, the phase range is enlarged. With the size of 15 mm, the phase range is more than $600\circ$, which is more than enough for the RA design, even with substrate thickness of 5 mm. The unit cell is then chosen with dimension of 15×15 mm and thickness $h_1 = 5$ mm, while the Ratio between the ring's width and its dimension is 0.2. The unit cell is then used to design passive reflectarrays in the next section.

4.2.2 Simulated Results

The structure in Fig. 4.1 is characterized by several degrees of freedom, i.e., the two lengths, the two widths and the aspect ratios, that are not completely independent. Since their effectiveness in controlling the phase of the re-radiated field is not electromagnetically equivalent, the first analysis carried out was concentrated to figure out which set of all the possible different geometrical parameters of a configuration of two concentric rings may present the best phase variation.

In order to obtain this result, for all of them the phase of the re-radiated field has been computed with a suitable set of different couples of geometrical parameters, considering the element embedded in an infinite periodic lattice and adopting a full wave MoM approach. Examples of these results are reported in Fig. 4.6, and Fig. 4.7 where the phase variation provided is reported as a function of the the size ℓ_{out} of the outer-

most ring and the aspect ratio p, that relates the size of the inner ring to that of the outer one, i.e., $\ell_{in} = p \cdot \ell_{out}$; the two ring widths (w_{out}, w_{in} in Fig. 4.1) have been adjusted proportionally to the size of the relative ring. These couple of geometrical parameters, (ℓ_{out}, p), are used to design the RAs, later on.

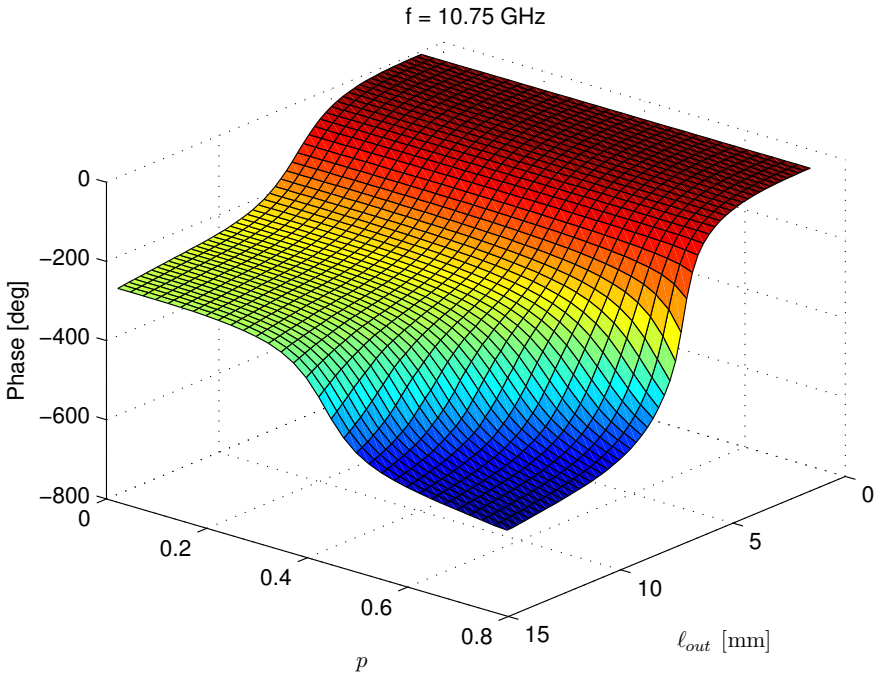

Figure 4.6: *Phase variation provided at 10.75 GHz as a function of two geometrical parameters.*

Fig. 4.8 and Fig. 4.9 show the phase variation with respect to the variation of the side length ℓ_{out}, for a fixed value of the aspect ratio p and with respect to the variation of p, having fixed ℓ_{out}, respectively. The three curves in the two figures refer to different frequencies. From these results it is possible to conclude that all these phase curves present a significant phase range, more remarkable when ℓ_{out} is varied, running from around $300°$ to more than $600°$, and an important quasi-linear behavior: moreover, curves corresponding different frequencies are almost parallel.

The design of each re-radiating element in an RA implies the choice of those ℓ_{out} and p values that give the proper phase shift, to compensate both the phase delay introduced by the distance between the feed and the element and the variation due to the frequency. This choice requires not only the phase maps like the one shown in Fig. 4.6, but also those like the one in Fig. 4.10, in which the difference between the curves of the phase variation with the two selected geometrical parameters computed at the central frequency and at an extreme of the band are plotted. Adopting the design procedure introduced in [16], and also described in next Section 4.3.1, it is therefore possible to first find the proper values of ℓ_{out} that provides the compensation of the phase delay introduced by the path between the feed and each element, and then it is possible to

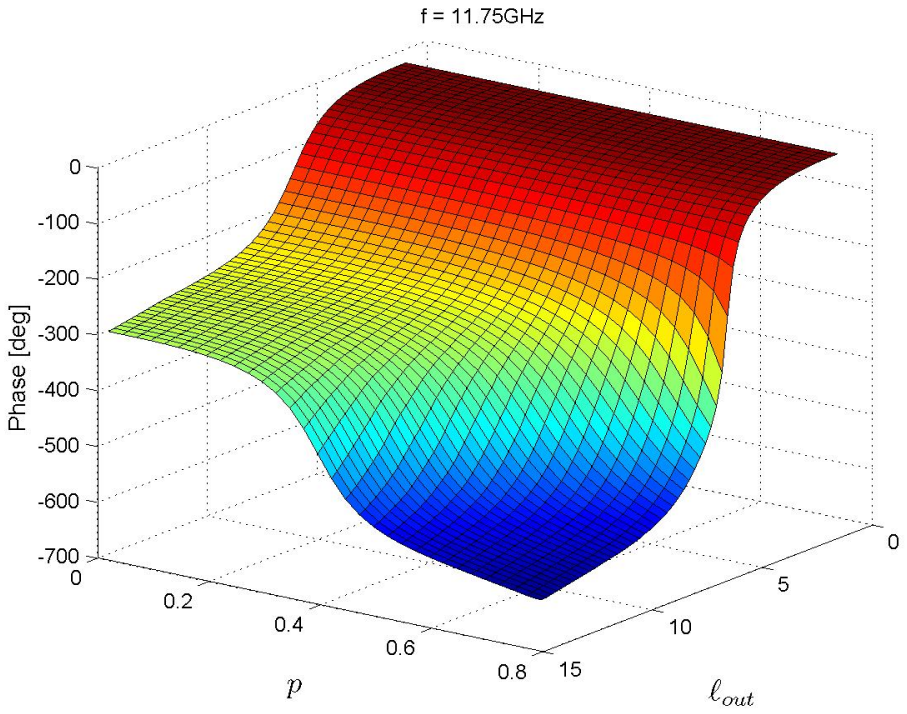

Figure 4.7: *Phase variation provided at 11.75 GHz as a function of two geometrical parameters.*

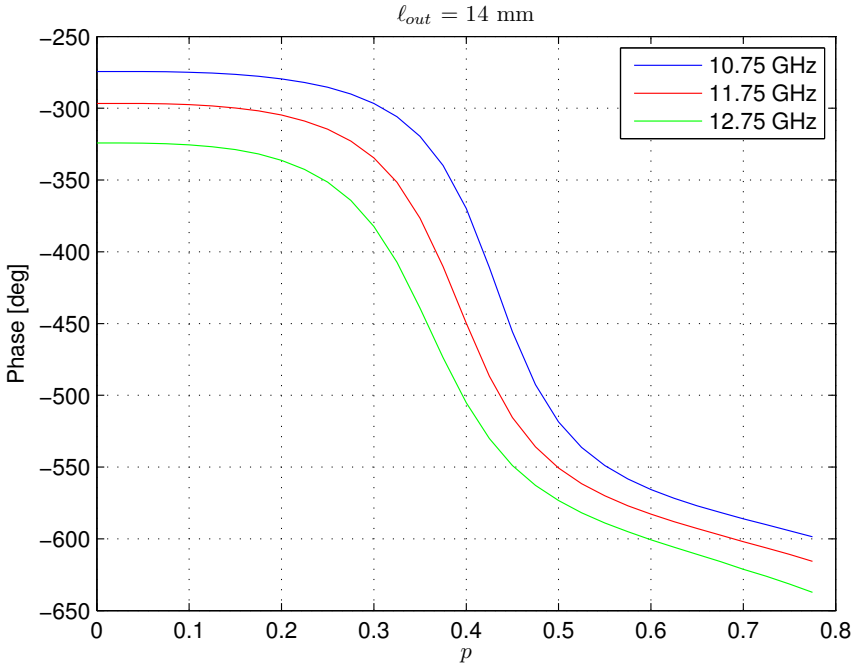

Figure 4.8: *Phase variation provided as a function p.*

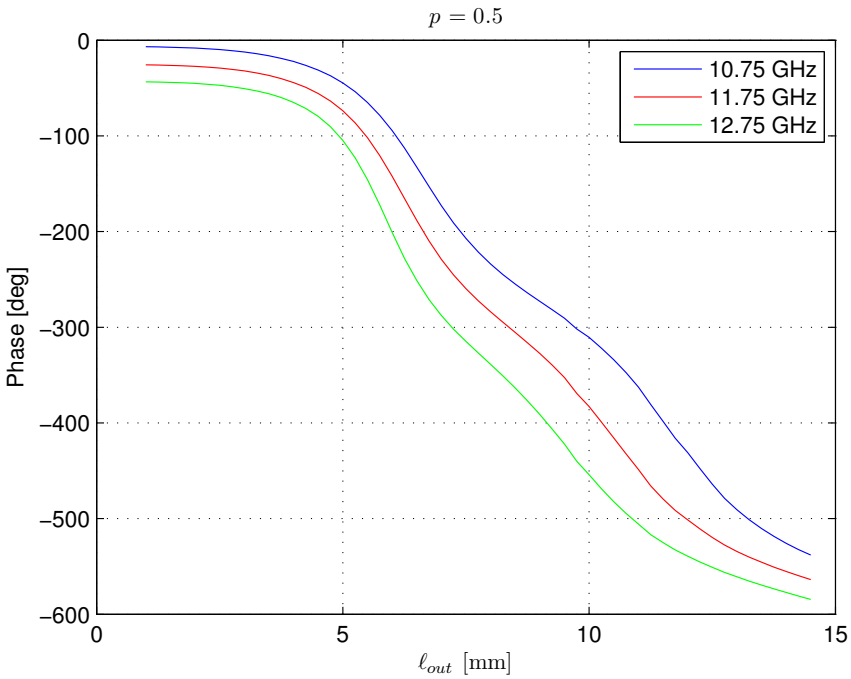

Figure 4.9: *Phase variation provided a as a function of* ℓ_{out}.

select the values of p to assure the proper variation with frequency of this phase.

4.3 Design method

Despite of the large number of degrees of freedom, in most of the RAs in which concentric rings are used, only one geometric parameter is independently varied [13–15], while the others are changed proportionally: in this way it is possible to easily enlarge the bandwidth, but not enough to fulfill the requirements in several applications. These are the reasons why in the framework of this chapter we consider as radiating element a concentric double square ring configuration, in which at least two geometrical parameters are varied. In this way, it is possible to compensate with one parameter the spatial phase shift and with the other the frequency variation of the incident field phase, so that the re-radiated field remains almost the same over the whole bandwidth, overcoming the previously considered limitations. In other words, this means that each element of the array has to provide a phase contribution to the re-radiated field that varies both with the element position and with the frequency.

To effectively control all degrees of freedom for reflectarray design, in this section, double parameter design method will be implemented. By applying this method, the reflectarray antennas have shown improvement in bandwidth as will be shown in the next section. At the end of this section, other design methods such as the application of optimization algorithms and artificial neural network (ANN) will be also reviewed.

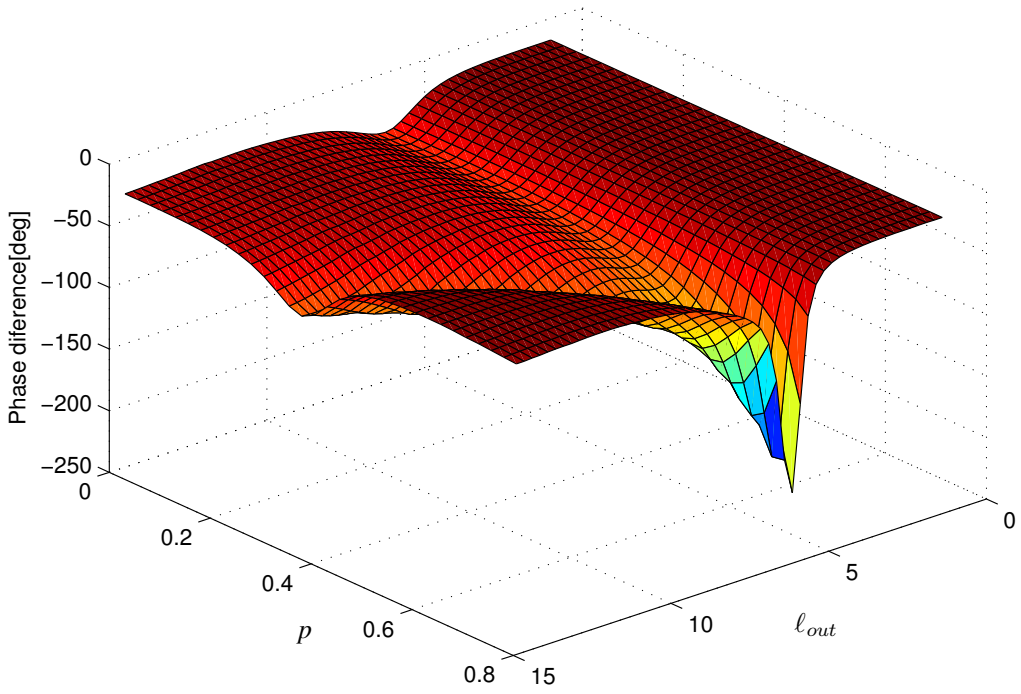

Figure 4.10: *Difference between the phase at the central frequency and at one extreme of the band as a function of ℓ_{out} and p.*

4.3.1 Double Parameter Design

The method was first mentioned in [16], where two degrees of freedom are controlled to compensate the phase requirements at different frequencies. For sake of simplicity, in this sub-section, the method is explained using the double square ring unit cell, and two of its parameters, ℓ_{out} and p.

Initially, the phase ϕ_1 of reflected field at specific frequency f_1 is calculated versus two geometrical parameters, as previously shown in Fig. 4.11. For each required phase delay, a set of geometrical values $s = (\ell_{out}, p)$ is selected. To illustrate this, the set of all the geometrical values providing phase delay $\phi_1 = 400°$ is plotted as a red line in Fig. 4.11.

The same procedure has been used to generate the phase ϕ_2 of the reflected field at frequency f_2 versus ℓ_{out} and p. Then, a map of phase difference $\Delta\phi_{12}$ between ϕ_1 and ϕ_2 is created, as previously shown in Fig. 4.12 . The set of geometrical values pairs selected is used to identify the phase differences that can be achieved with radiating element for a fixed phase delay at the second frequency (i.e., the green line in Fig. 4.12). The cross points between the red line (the set selected from the first step) and the green line are the values of (ℓ_{out}, p) that compensate the required phase delay ϕ_1 at frequency f_1 and the phase difference between ϕ_1 and ϕ_2. In other words, elements with pair values (ℓ_{out}, p) will compensate phase required at frequencies f_1 and f_2, which implies

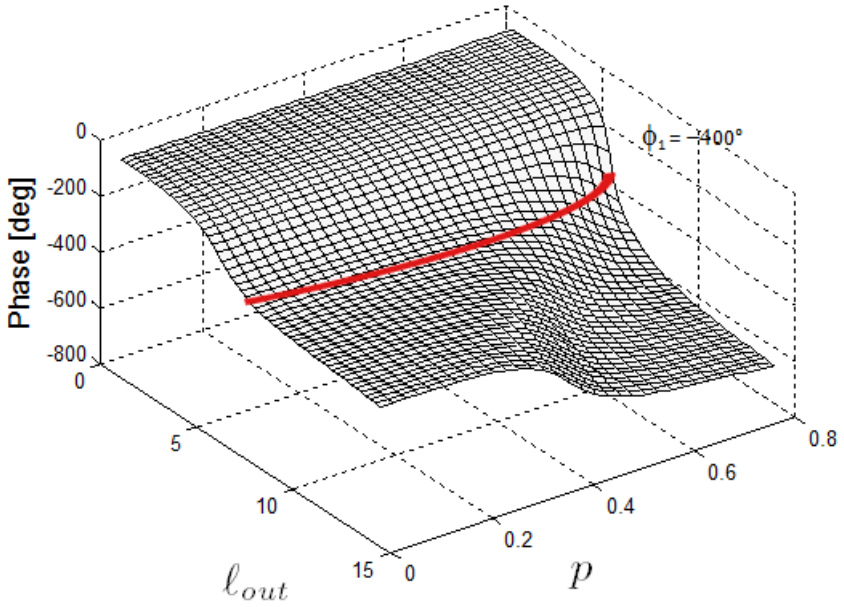

Figure 4.11: *The set of ℓ_{out} and p values providing the required phase ϕ_1 at frequency f_1.*

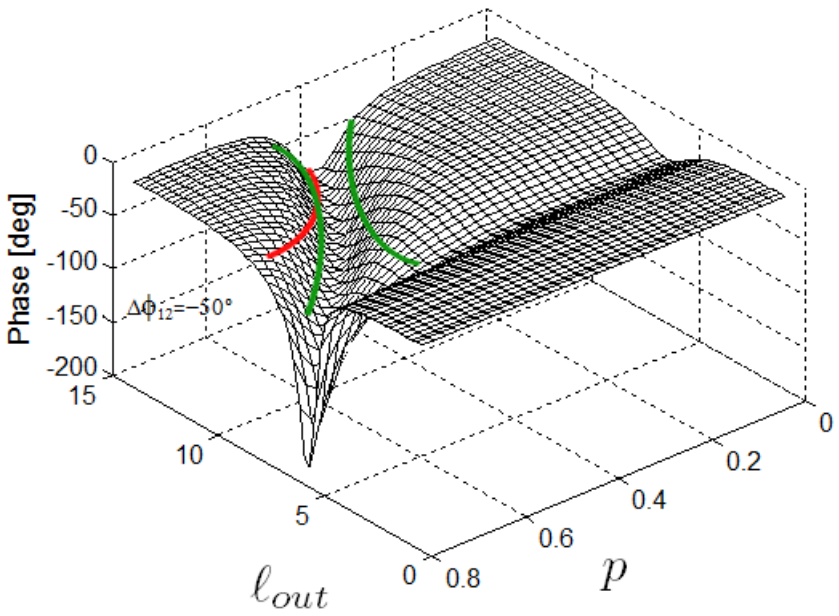

Figure 4.12: *The set of ℓ_{out} and p values providing the required phase ϕ_1 and $\Delta\phi_{12}$at the considered frequencies f_1 and f_2 vs. .*

that the RAs bandwidth could be ensured for the entire designed band.

4.3.2 Application of Artificial Neural Network

Generally, the reflectarray design can be divided into two steps: the characterization of the reflectarray unit cell with respect to design parameters e.g. physical dimensions, incident wave etc., and the design of the entire structure, which could be managed by phase-only synthesis (POS) or by means of optimization. The characterization of the unit cell is to map the phase and the amplitude of the reflection coefficient of the unit cell to the selected geometrical parameters (these maps are then called look-up tables). This step is often performed by a full wave method of moment approach and applying the local periodic (LP) assumption, i.e., the element is embedded in an infinite environment on which a plane wave impinges. The generation of the look-up table is computationally expensive, since it requires to perform the full-wave analysis of the periodic array several times for multiple values of geometrical parameters, as well as for different frequencies, and angles of incidence. Moreover, the storage of data occupied by these simulations requires a large amount of dynamic memory. Finally, if the design of RAs is carried out by means of optimization using stochastic-based algorithms, the reflection coefficient sampling rate needs to be high.

In order to reduce the computational time and memory consumption, the application of artificial neural network (ANN) has been proposed in literature, relating the behavior of RA unit cell and its geometrical parameters [15, 77–79]. These works demonstrate the applicability of ANN in modeling the RA re-radiating elements. With the help of the ANN, the amplitude and phase of the reflection coefficient can be reconstructed precisely, taking into account the effect of different angles of incident wave, and for different polarizations. For the detail description of ANN, the reader is referred to [80, 81], this sub-section is devoted to explain the implementation of ANN to reflectarray design.

The general ANN model, applying to characterize RA unit cell, is depicted in Fig. 4.13. The inputs for the network are selected design parameters, e.g. physical dimensions. The angle of incidence can be included since it differs from one element to the other, especially at the RA's borders and when the RA's electrical size is large. The outputs are generally the phase and amplitude of the reflection coefficients for each polarization. The network can consist in multiple hidden layers with bias. The input composition in each neuron is made by a nonlinear weighted sum

$$f(x) = k(x)\left(\sum_i w_i g_i(x)\right), \tag{4.1}$$

where $k(x)$ is a nonlinear activation function which models the activity of biological neurons in the network and w_i are the weights, which are the coefficients connecting nodes in the network.

The ANN works properly when for any set of inputs, it produces the desired outputs. It means the connections between the different nodes in the network are set properly, i.e., the weights w_i have been correctly chosen by the same training procedure. After training, the ANN can be seen as a black box: when a set of design parameters input to the box, we obtain a set of outputs, which visualize properly the behavior of RA elements. The ANN is now ready to act as EM modeling tool box for selecting the correct design parameters for every RA element.

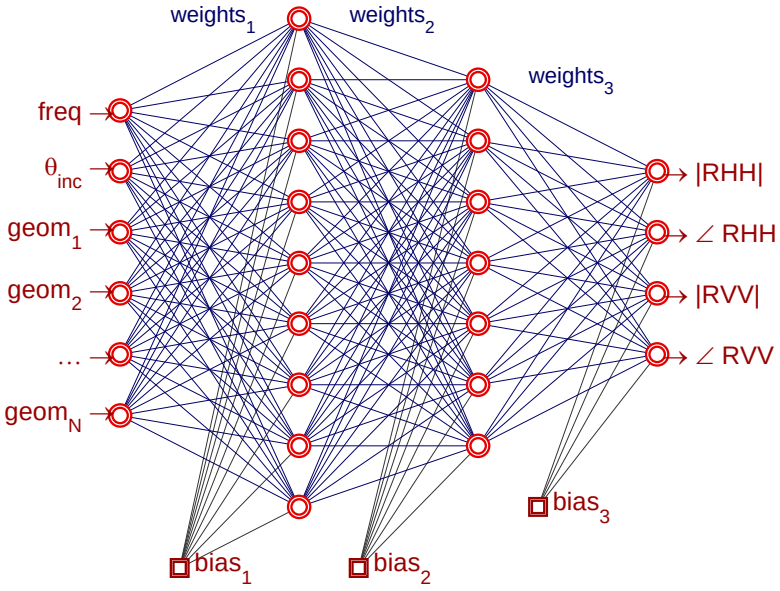

Figure 4.13: *A typical Multi-layer Perceptron structure of ANN, with 2 hidden layers.*

To show the effectiveness of this approach, Fig. 4.14 reports the comparison between full-wave HFSS simulation and ANN surrogate model for phase values in 3 considered frequencies. The ANN structure consists of 4 inputs, 2 outputs neurons and 2 hidden layers of 11 and 9 neurons respectively. The inputs are the angle of incident, the frequency and two geometrical parameters, i.e. ℓ_{out}, p, while the outputs are the magnitude and phase of reflection coefficient.

4.3.3 Optimization of Reflectarray Antennas

The design of the entire reflectarray can be done: either directly by controlling the phase of each element to create the desired beam, i.e., phase-only synthesis, or indirectly by means of optimization, i.e., synthesis using optimization algorithms [24,25,82,83]. The advantage of using global optimizers is that they are able to handle a large number of degrees of freedom and provide a configuration, which satisfied pre-defined constraints.

Fig. 4.15 shows the block diagram of the implementation of global optimization algorithm to design the reflectarray antennas. Optimization algorithms can be used in setting parameters for elements in the array in order to produce the phase required to create desired beam e.g. pencil, contour beams, etc. The required phases are computed by fast methods such as phase-only synthesis (POS) or projection matrix algorithm (PMA). This is a popular approach to integrate an optimizer since the design procedure only works with RA elements [23,25,79]. Moreover, available data such as the look-up tables or the ANN (as described in Section 4.3.2) or equivalent model of RA element could be included to accelerate the optimization process. An example of application of

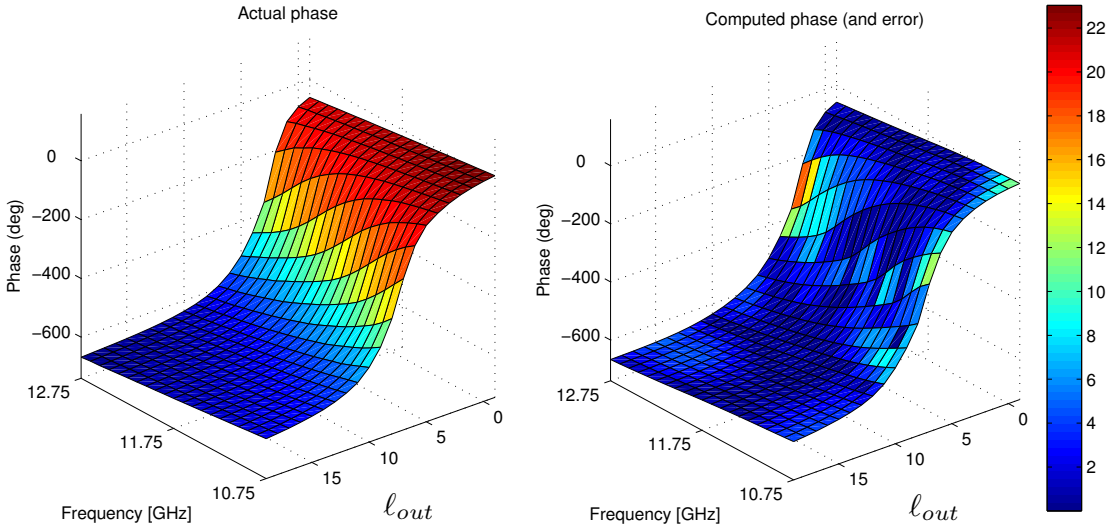

Figure 4.14: *Phase characterization by ANN.*

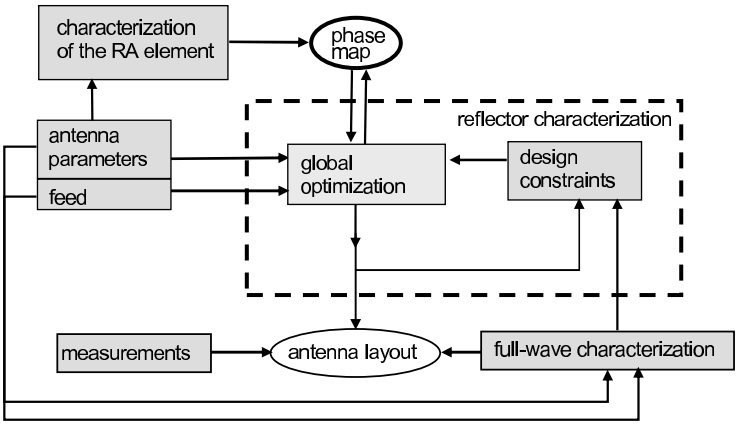

Figure 4.15: *Block diagram of the design procedure integrating global optimization algorithm.*

ANN is shown in Fig. 4.16, where the ANN replaces the data from maps in Fig. 4.15. This approach, however, often exploits the analysis of RA's elements, which is based on the local periodic (LP) assumption, and therefore neglects mutual coupling between elements. This affects the performance of the RA e.g. resulting high side-lobe level.

Alternatively, global optimization can be applied to the design of entire array (global level) by considering the RA as an object and all parameters relating to elements are variables. By controlling these parameters, the optimizers try to find the best configuration that fits the design constraints, which is validated by full-wave simulation. However, this approach is normally very time consuming, since there are hundreds or even thousands of variables characterizing an RA and also the evaluation performed by full-wave simulator is time consuming. The advantage is that the design will take into

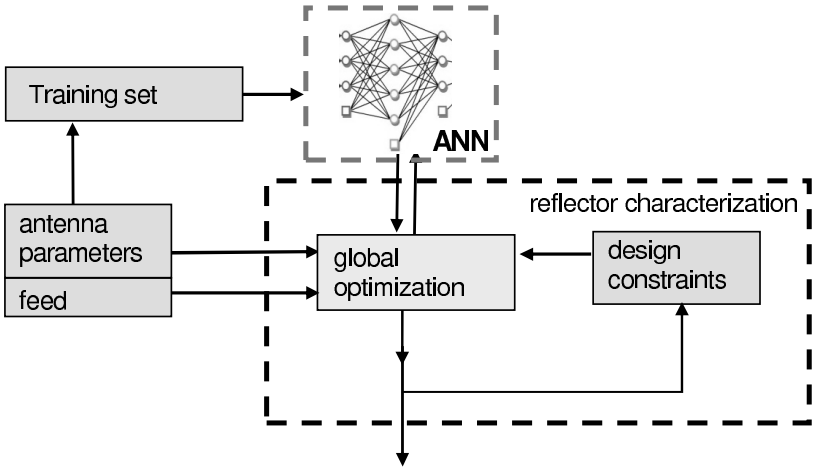

Figure 4.16: *Part of the block diagram in 4.15 modified by the introduction of ANN.*

account all aspect of the array, therefore, the final design would satisfy all constraints. This approach is applied in the next chapter for the design of reconfigurable reflectarray antennas.

4.4 Reflectarray Implementation

From the previous sections, the double square ring unit cell has shown a good phase behavior with several degrees of freedom which allows the potential application of the double parameter approach to design RAs. In this section, reflectarray designs will be realized using this unit cell combined with the design methods described above. The design of horn antenna, which is used later as the feed for the RAs, is presented first. Following, the implementation of these design methods to determine geometrical parameters for each element in the array is carried out.

4.4.1 Horn Antenna Design

For the following RA designs, a horn antenna is implemented as the feed, designed to operate at X band and cover the design frequency band $10.75-12.75$ GHz for RAs. The feed is pyramidal horn, which follows the design method described in ([26], Chapter 13). The prototype of horn antenna is depicted in Fig. 4.17, while its parameters are listed in Table 4.1. In Fig. 4.18, it is plotted the radiation patterns of the designed horn at two main plane cuts at 11.75 GHz. The phase center of the horn is determined at a distance of 136.5 mm from the port.

Table 4.1: *Parameter for horn antenna (in mm).*

a	b	l	a_1	b_1	ρ
15	10.134	30	74	50	120

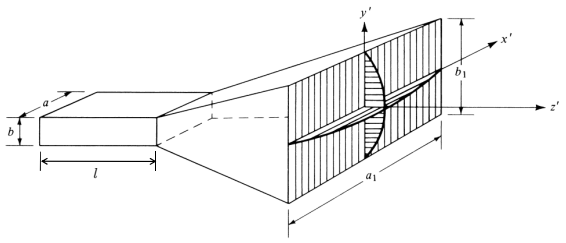

(a) Pyramid horn

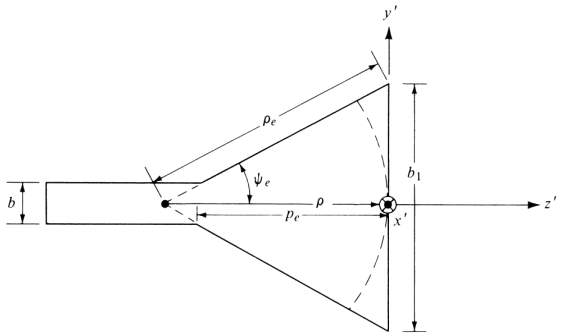

(b) E-plane view

Figure 4.17: *Pyramid horn antenna (from [26]).*

4.4.2 Implementation

In this chapter, passive RAs are designed with pencil beams scanned to a pre-defined direction. The phase required for each element is determined by the phased array theory presented in Section 2.1:

$$\phi_R(x_i, y_i) = k_0(d_i - (x_i \cos\varphi_b + y_i \sin\varphi_b) \sin\ \theta_b) \tag{4.2}$$

where k_0 is the propagation constant in vacuum, (x_i, y_i) are the coordinates of element i, d_i is the distance from the phase center of the feed to the cell, and $\phi_R(x_i, y_i)$ is the phase shift required for element i, and ϕ_b, θ_b is the direction of the beam. Other beam patterns such as contour beam could be synthesized in the same manner (the required phase could be found by phase-only synthesis).

Two parameters, i.e., ℓ_{out} and p, are manipulated to obtain the required phase for every element. The double parameter design method is implemented in order to enhance the bandwidth of reflectarray.

4.5 Numerical Results

In this section, numerical results of reflectarray antennas designed in the previous sections will be presented. The design of a re-radiated surface, consisting of 5×5 array of double square ring elements with plane wave excitation, is shown first to prove the effect of design method to improve the RA gain. Then, the designs of two RA configurations with horn feed will be presented. Numerical results of these RAs will show the wide-band characteristic of the double square ring elements.

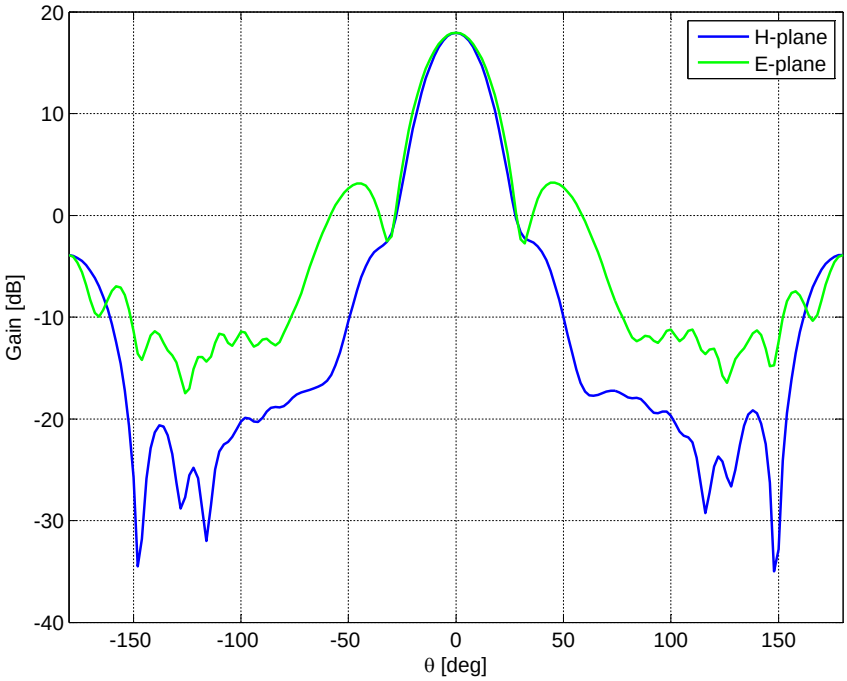

Figure 4.18: *Radiation pattern of horn antenna at two main plain cuts.*

4.5.1 Reflective Surface Design

As a proof of the concepts summarized in the previous sections, and in particular of the real possibility to enhance the bandwidth with the use of the introduced double parameter method, design of a reflective surface has first been considered. The surface consists in 5×5 array of double square ring elements on which, for the sake of simplicity, the incident field is a plane wave impinging orthogonally to the plane. The layout of the reflective surface is shown in Fig. 4.19, the elements have been design to redirect the incident wave to scan at an angle of 20° with respect to the normal. Two different approaches are applied to design the surface for maximizing the gain in the frequency band $10.75 - 12.75$ GHz, that corresponds to a bandwidth of 17%

In Fig. 4.20, it is shown the frequency behavior of the maximum gain on the entire frequency band computed using the dual-parameters re-radiating elements and compared with the gain of similar surface, in which only ℓ_{out} has been used as degree of freedom. It is possible to see that the gain variation is less than 1 dB for the whole considered bandwidth. Moreover, the exploitation of two degrees of freedom of RA's elements allows an increase of gain of almost 1 dB.

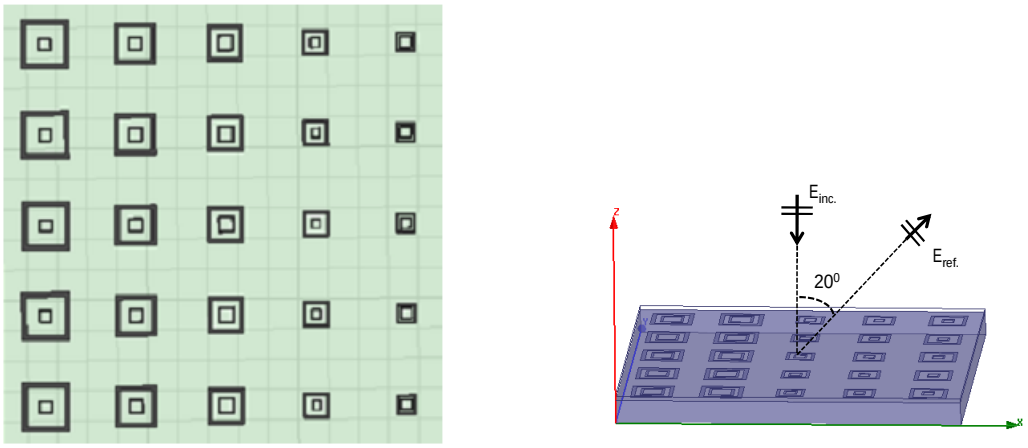

(a) (b)

Figure 4.19: *Prototype of* 5×5 *reflective surface with plane-wave incident.*

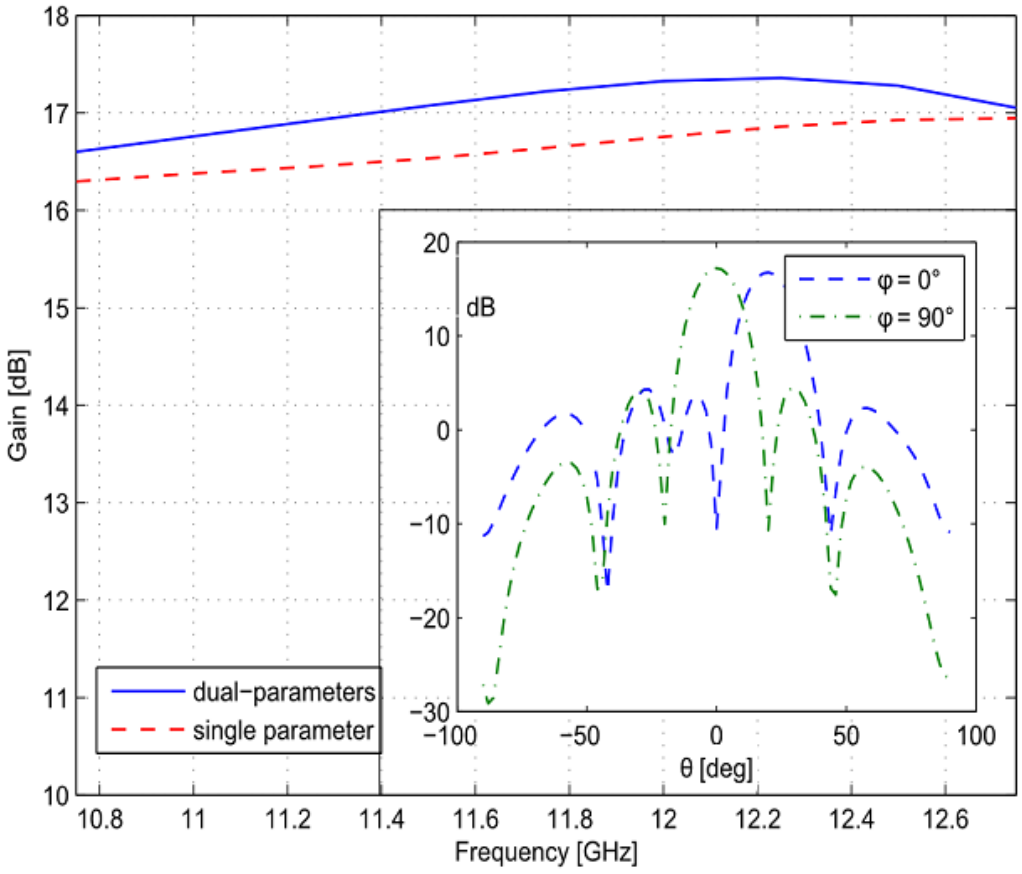

Figure 4.20: *Gain comparison for* 5×5 *reflective surface. Inset: radiation pattern of dual-parameter antenna at central frequency.*

4.5.2 Reflectarray Antennas Designs

In order to experimentally validate the synthesis concepts previously detailed, two reflectarray configurations of different size have been considered. Both of them are off-set fed, since in that case the distances between the feeder and the lower and upper sides of the reflector are quite different, and the frequency compensation of the introduced delays is more complex to achieve. With the same aim of considering the worst case, the planar reflectors have been designed in such a way that the direction of maximum radiation is slanted with respect to the broadside: in this way it is possible to check if the direction of maximum radiation remains the same at the different frequency, due to the proper compensation of the re-radiated field phase.

16×16 Reflectarray Antenna

The first considered RA design is the configuration depicted in Fig. 4.21, consisting in a 16×16 planar reflector fed by a rectangular horn located at a distance of 390 mm along the z-axis and of 125 mm along the x-axis from the center of the coordinate system, which is coincident with the central point of the reflector.

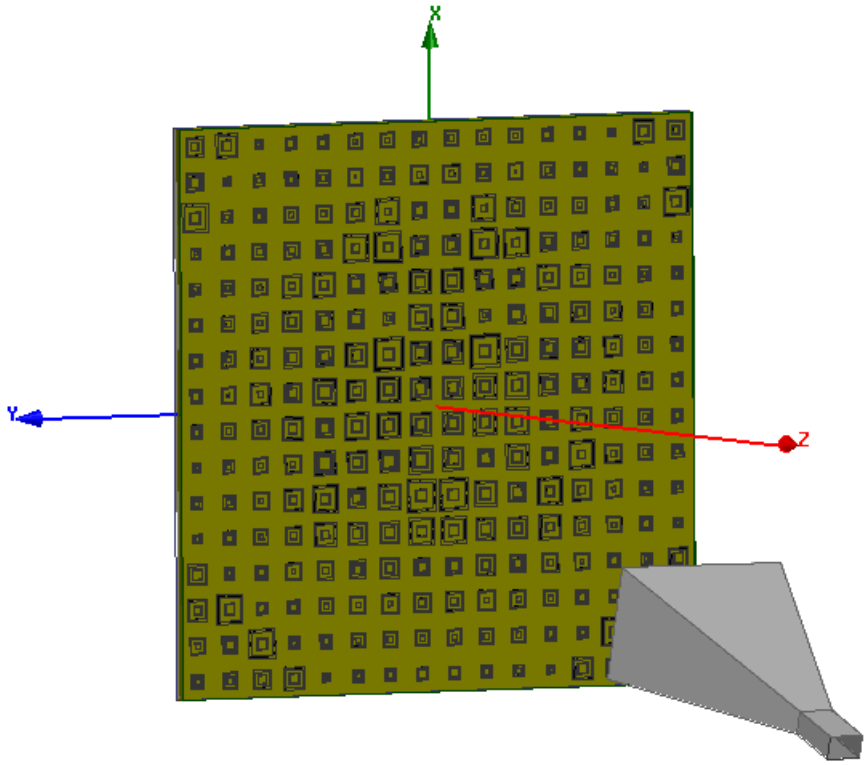

Figure 4.21: *View of the designed* 16×16 *RA geometry.*

The structure has been designed using the two degrees of freedom of the double ring re-radiating elements to obtain the maximum re-radiation in a direction tilted of 18° with respect to the normal and to minimize the gain variation in the frequency range $10.75 - 12.75$ GHz, as reported in Fig. 4.23.

The entire RA has been analyzed using a full wave simulator and the radiation patterns for different frequencies have been computed. In Fig. 4.23, the radiation patterns in the plane $\phi = 0°$ computed at the extremes and at the center of the frequency band, are shown: in this case, not only the gain variation is really small, lower than 0.5 dB in the entire band, but the side lobe level remains almost constant and below -18 dB. Compared to the radiation pattern obtained by 1 parameter design method Fig. 4.24 and Fig. 4.25, the gain is higher while the side-lobe levels are managed lower by using double parameter method. The results confirm the effectiveness of the proposed method for passive reflectarray design.

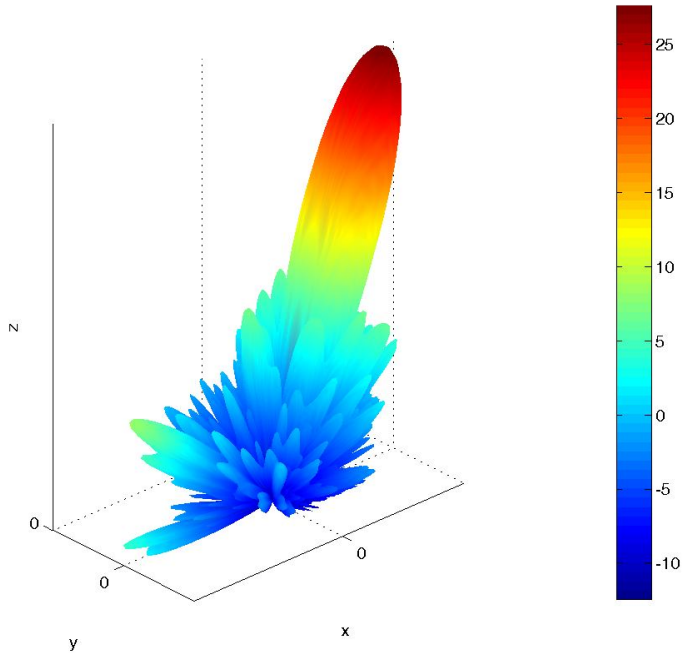

Figure 4.22: *3-D radiation patterns of the 16×16 RA computed at the central frequency.*

32×32 Reflectarray Antenna

The second considered configuration is the 32×32 planar reflector shown in Fig. 4.26. In this case the rectangular horn located at a distance of 671 mm along the z-axis and of 217.5 mm along the x-axis from the center of the coordinate system, which is coincident with the central point of the reflector. As in the previous design, to improve the re-radiating elements performances, the same dual layer dielectric structure has been used, consisting in a substrate characterized by height $h_1 = 5$ mm and relative dielectric constant $\varepsilon_{r1} = 1.1$ and in a cover with $h_2 = 0.85$ mm and $\varepsilon_{r2} = 2.5$. As in the previous case, the planar reflector has been optimized to work in the frequency band $10.75 - 12.75$ GHz, and to have a direction of maximum radiation tilted $18°$ off broadside.

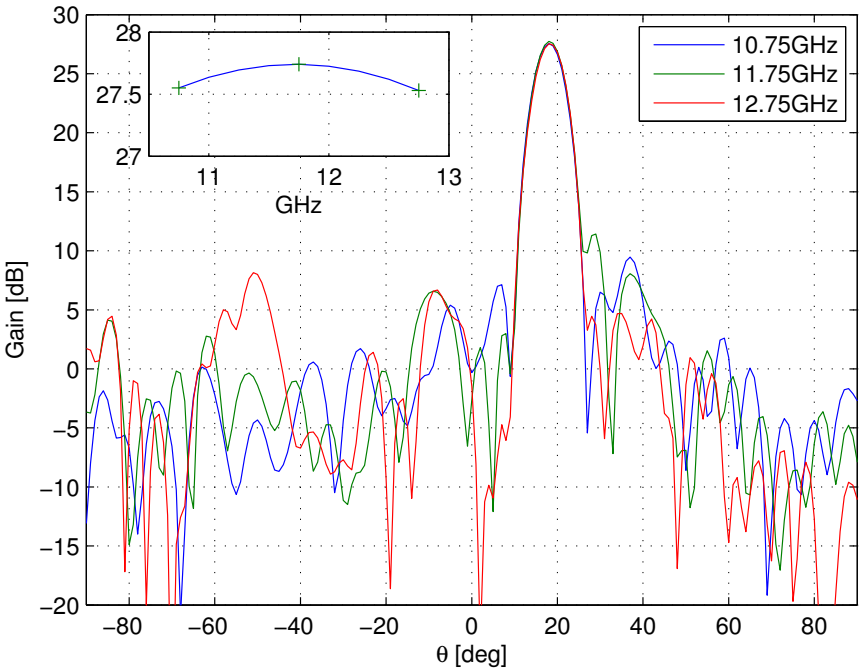

Figure 4.23: *Radiation patterns of the 16×16 RA designed by double parameter method, computed at three different frequencies in the plane $\phi = 0°$. Inset: gain frequency variation*

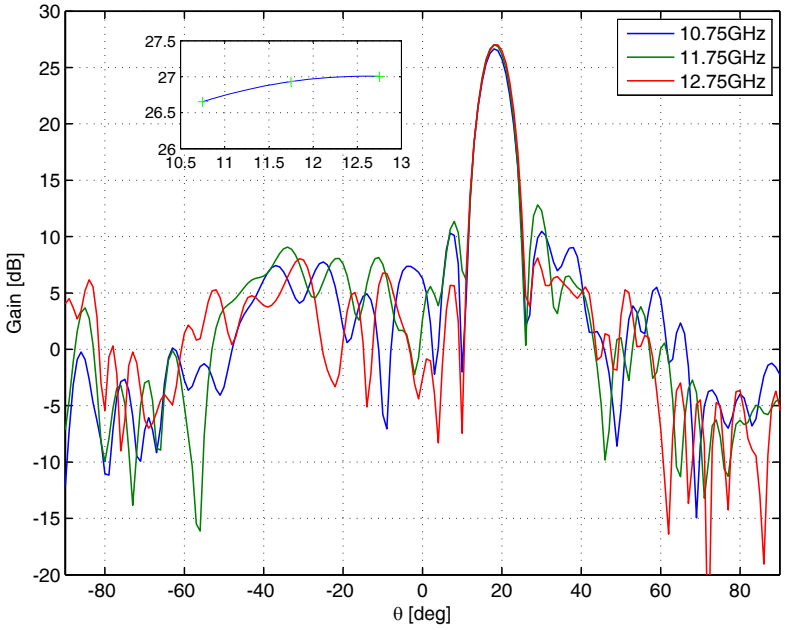

Figure 4.24: *Radiation patterns of the 16×16 RA designed by 1-parameter method, computed at three different frequencies in the plane $\phi = 0°$. Inset: gain frequency variation.*

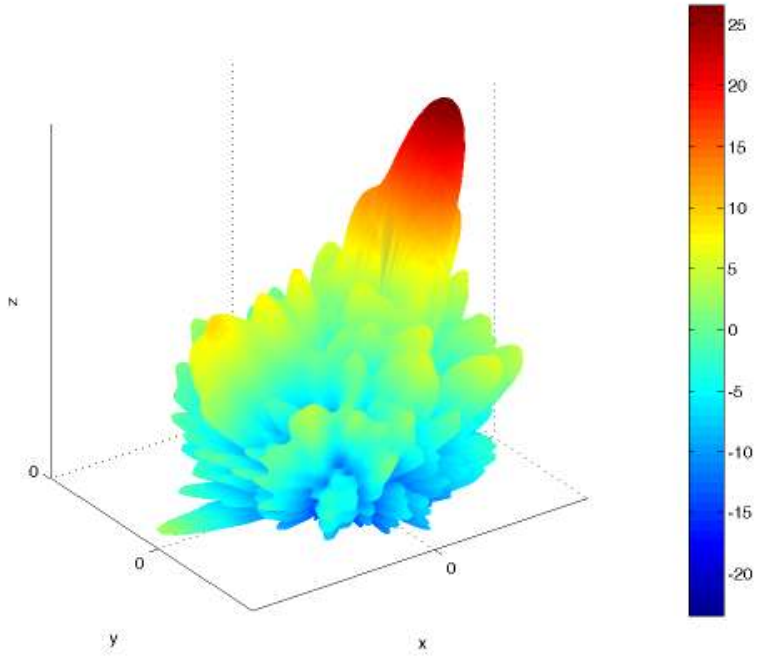

Figure 4.25: *3-D radiation patterns of the 16×16 RA designed by 1-parameter method computed at the central frequency.*

In Fig. 4.27, the 3D radiation pattern of the reflectarray, computed at the central frequency, is reported, showing the high directivity of the designed structure and the absence of unwanted high lobes apart from those around the maximum.

Finally, in Fig. 4.28, the cuts in the vertical plane for three different frequency values are shown: the main lobe is almost coincident in the three cases, and no shift of main beam occurs changing frequency. The side lobes increase slightly with the frequency, but in any case they are well controlled. In the figure inset it is reported the frequency behavior of the gain, showing that also in this case it remains almost constant over the entire bandwidth. Finally, the aperture efficiencies are reproted Table 4.2 for both designs, which are acceptable since one of the limitations of passive RA is low efficiency due to the spillover, cross polar and illumination losses.

Table 4.2: *Aperture Efficiency.*

RA16	RA32
53.6%	40.03%

4.6 Conclusions

In this chapter, the step by step design procedure of passive reflectarray antennas has been presented. The double square ring element has been proposed as a unit cell for

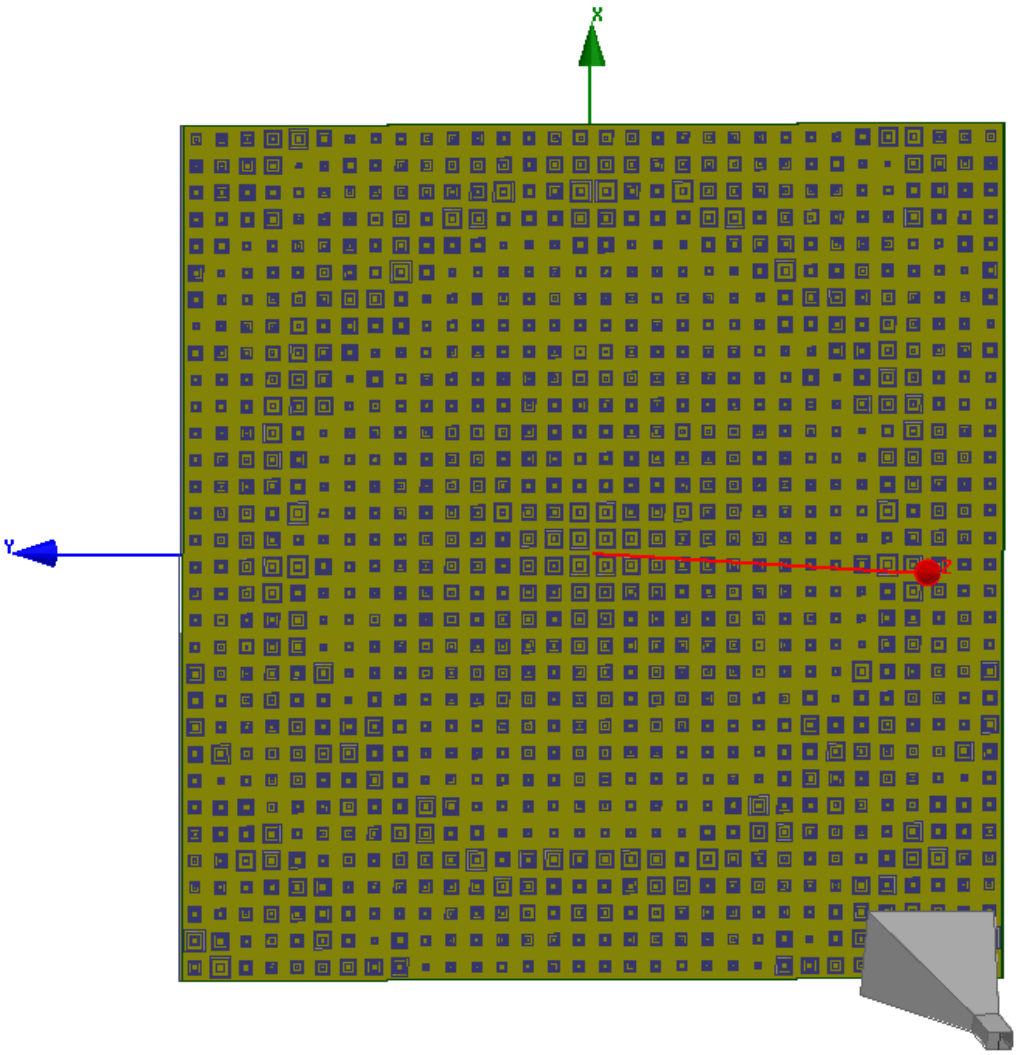

Figure 4.26: *View of the designed* 32×32 *RA geometry.*

passive phase compensation. This element is classified as a single layer structure with two square rings printed on the same layer. The unit cell offers a good phase range and several degrees of freedom for antenna design. ANN surrogate model is used to get a fast description of reflection coefficient.

The double parameter design method has also been introduced which effectively manages design parameters of double square ring element to enhance the gain bandwidth of reflectarray antennas. The example of the reflective surface has shown that by applying this design method, gain can be improved by almost 1 dB over the whole bandwidth.

We also presented numerical results of two different passive RA configurations. The results have shown the effectiveness of the design method and performance of the proposed unit cell. A large bandwidth, i.e., more than 17% of 1 dB gain bandwidth has been achieved for both RA designs. Moreover, these results are validated by Ansoft

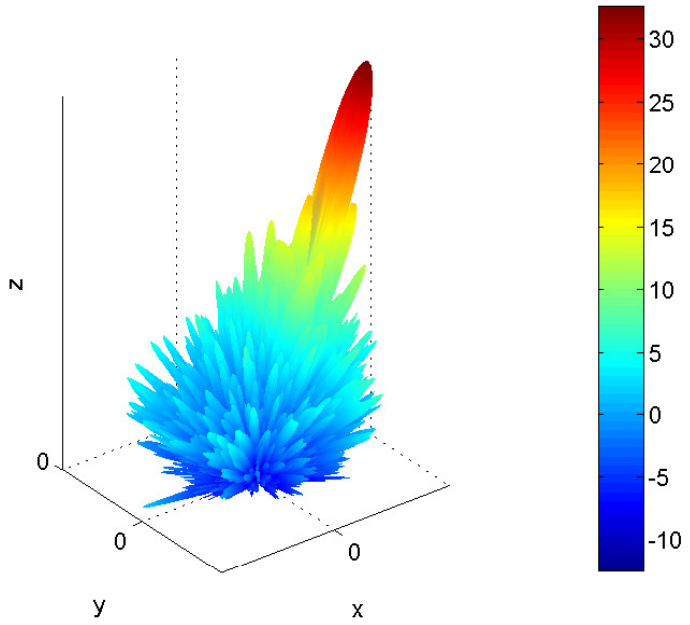

Figure 4.27: *3-D radiation patterns of the 32×32 RA computed at the central frequency.*

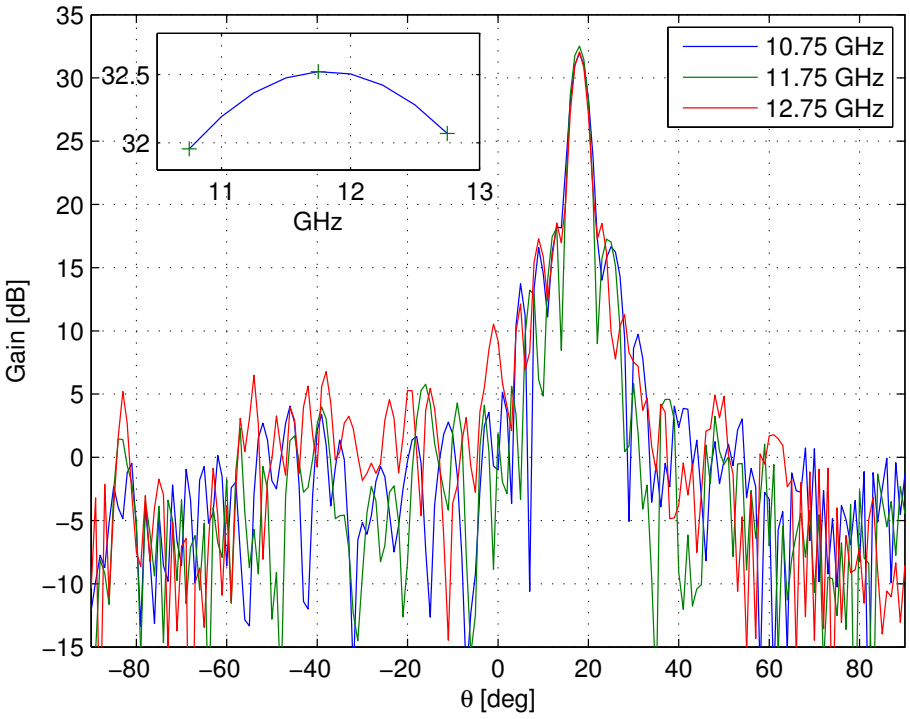

Figure 4.28: *Radiation patterns of the 32×32 RA computed at three different frequencies in the plane* $\phi = 0°$. *Inset: gain frequency variation.*

HFSS simulation.

CHAPTER 5

Reconfigurable Reflectarray Antennas

The previous chapter has addressed the advantages of reflectarray antennas over traditional reflector due to their attractive qualities, e.g. low-cost, light weight, good efficiency, high gain, and ease of manufacturing. In more recent years, the possibility of reconfigurability has been investigated, too. By integrating elements such as varactor diodes, PIN diode switches, or micro-electro-mechanical system (MEMS) to array element (scatter), the arrays are able to synthesize different patterns on the same structure. This has enabled reflectarrays to be applied to several complex communication systems such as satellite communication systems, radars.

In reconfigurable reflectarray antenna (RRA), each element is loaded with one or more electronic switch to reconfigure its electrical properties. Therefore, the design of the RRA unit cell is the core of design procedure. The element has to show not only good phase behavior for array design, but also to be simple to integrate with the switches. Here, a unit cell consisting of three dipole has been adopted as the RRA element. The analysis of this element combining with varactor diodes has shown potential application for RRA.

In this chapter, the design and the analysis of three dipole unit cell and its application to RRA is presented. The chapter starts with a review on RRA design, where different methods are listed. Then, the RRA unit cell based on tunable resonator approach implementing varactors is presented. Next, the optimization of the infinite reflective surface, in which the Floquet harmonics of the structure are suppressed by optimization procedure, is presented. Finally, the use of the proposed element for the RRA design is described. This adopted design procedure is based on the combination of method of moment and optimization routine will be implemented as RRA design method. Numerical results and conclusions are addressed at the end of this chapter.

5.1 Introduction

The introduction of RRA has dated back to 1977, when Phelan [84] implemented rotation technique to spiral cell of reflectarray to reconfigure circularly polarized wave. With enabled technologies, in recent years, several alternative solutions for RRA have been proposed including the use of varactor diode, PIN diode, and more recently developed MEMS. This significant progress has allowed RRAs to be used in various areas. Similarly to passive RA design, there are three main approaches that could be adopted to obtain the phase shift in RRAs: tunable resonator, guided-wave approach, and rotation technique [85].

The first approach consists in changing the resonant frequency of elements. Instead of changing the physical dimensions of the resonator as in passive RA, RRA elements use electronic switches to attain this phase shift. The idea is using these devices to vary the effective electrical length of the resonator, so that the reflection phase change as well. Devices such as varactor diode, PIN diode or MEMS could be implemented in this approach. The first attempt to integrate varactor diode to RRA is presented in [86], however the design only achieved 180° of phase range. Larger phase range can be achieved by using different loading configurations [87–89] with the same concept of varactor-loaded patch. It is also possible to use MEMS varactor for this kind of approach.

Alternatively, the phase shift of the RRA elements can be controlled by using guided-wave approach. The concept is again similar to the one applied in fixed reflectarray design, which uses delay line to shift the phase of reflected wave. The impinging wave is first transformed by the antenna into a guided-wave, that is then phase shifted using delay line and re-radiate. The delay line in case of RRA is control by varactor diode to create different phase shift. This approach offers several advantages over the first one, as the possibility to attain more than 360° of phase range [90, 91] using coupled aperture. Moreover, using this technique, wide-band behavior can be achieved since the delay line can provide true-time delay capability.

The third approach is based on the use of rotation techniques. The concept is the same as implemented in passive RA, in which different phase shift for circular-polarized wave is generated by rotating elements [92, 93]. In RRA, independent rotation of each element is carried out by electrical means to create electromagnetic rotation of element instead of geometry rotation. This was first done in [84] by using diodes in rotation-invariant geometry. Other designs have been proposed so far, however there is no full reflectarray with beam-scanning using this technique.

The RRA, in any case, present their trivial drawbacks such as the complexity of the design since electronic devices and their controlling network that have to be integrated into the array platform. The quantization effect is also another well known problem for RRA. The phase errors at each element due to the finite number of available phases result in decreasing the gain and increasing the side lobe levels. Though, the RRA are still very attractive for modern communication systems. So far, research on RRA is mainly focused on single band, single polarization, and now is extending to multi-band operation, polarization manipulation, and amplification, which promises wide range of applications of RRA.

5.2 Unit Cell Design

As mentioned in the previous section, the most important part of the design of reconfigurable reflectarray antennas is the unit cell design, which allows the integration of electronic components into RRA for controlling the reflected phase. After considering and analyzing different possible configurations for RRA unit cell, the one consisting of three printed dipoles has been chosen, since it could be easy for manufacturing and integrating with electronic devices. The three dipoles are parallelly printed on a same dielectric layer and each of them is loaded with a varactor that acts as phase shifter. The introduction of three varactors is also an advantage of the proposed design, since the unit cell now offers more degrees of freedom to control the phase variation and the possible reconfigurability.

5.2.1 Three-dipole Unit Cell

The considered RRA unit cell was first proposed in [94, 95] as passive reflectarray element. The three printed dipoles form a multi-resonant structure: by controlling the length of the dipoles and the ratio between the center dipole and the two satellite dipoles, the unit cell has shown a good phase behavior with more than 500° of phase range with very low losses. The implementation of this unit cell to passive RA has shown the achievement of wide bandwidth in the X-band, and a good performance of RA design. Taking as a reference the results in [94, 95] the "passive" RA unit cell has been firstly analyzed and designed to work at a frequency of 5.5 GHz.

The element structure is sketched in Fig. 5.1, where its dimension are shown. The dipole width is 3 mm, while their length is varied to compensate the phase shift. Figs. 5.2–5.3 plot the phase and amplitude of the reflection coefficient versus the length of the center dipole. The results confirm the good phase response of the element over a wide frequency band.

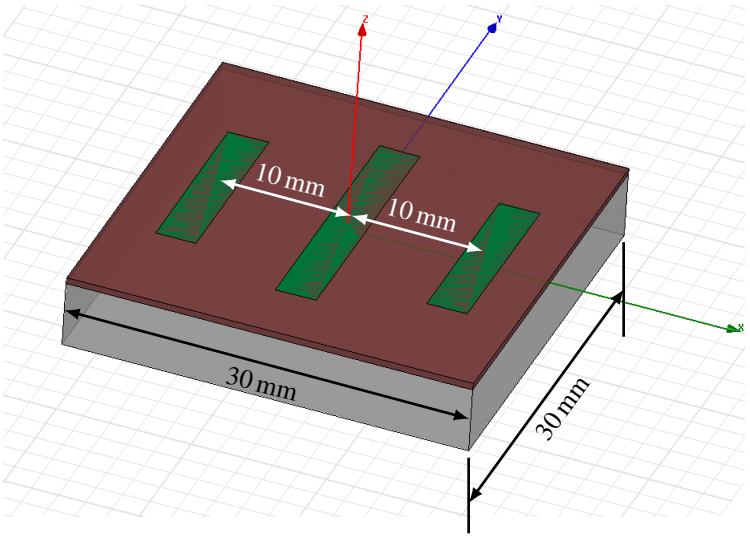

Figure 5.1: *Three-dipole unit cell.*

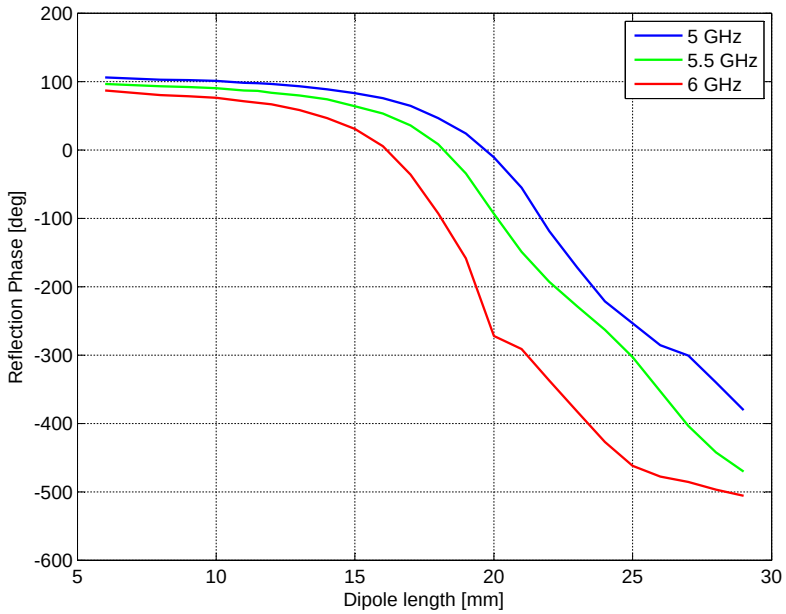

Figure 5.2: *Phase of the reflection coefficient for the three-dipole unit cell.*

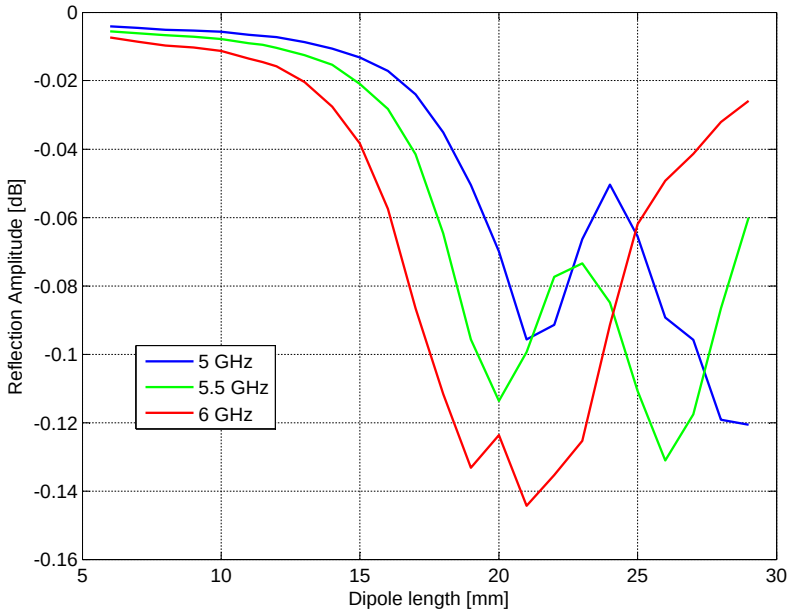

Figure 5.3: *Amplitude of the reflection coefficient for three-dipole unit cell.*

5.2.2 Reconfigurable Unit Cell

If instead of varying the length of the dipoles, each one is loaded with a tunable reactance, realized by a varactor diode, it is possible at the same time to compensate the phase shift and to provide the reconfigurability. The RRA element considered in this work is therefore modified as illustrated in Fig. 5.4, and it consists of three dipoles with attached varactors, backed by air substrate and ground plane. The element is designed at frequency of 5.5 GHz, and the cell dimension is $5.5\lambda \times 5.5\lambda$.

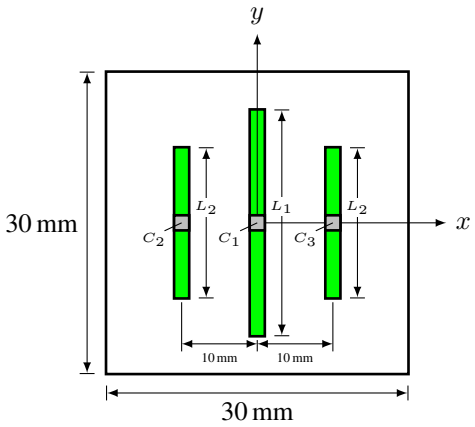

Figure 5.4: *RRA unit cell.*

The tunable resonator approach is applied in this case; the capacitance of varactors are varied to obtain different phase of reflected wave. Thank to the three degrees of freedom, in addition to provide the desired phase shift and the possibility to reconfigure the RA, this unit cell also allows to control of the mutual coupling between adjacent cells as shown in next section. Moreover, this enables the application of the design method mentioned in Section 4.3 to the design of RRA.

5.2.3 Simulated Results

In RRA design, the physical dimensions of the element are fixed since the control part is performed by electronic means. Therefore, the first step is to define the proper values for all geometry parameters, i.e., the length, width of the dipoles, as well as their ratio need to be defined. Fig. 5.5 and Fig. 5.6 show examples of the reflection phase of the RRA element for different lengths of dipoles, and different ratios between the center and two satellite dipoles. In this case, three varactors are set to the same value, and are varied simultaneously in between (0.1–2) pF. By extensive analysis, all design parameters are defined as follows: the main dipole length L_1 equals to 28 mm, while the ratio between the main dipole and two satellite dipoles L_2/L_1 is 0.8, and the air substrate thickness is 5.5 mm.

As mentioned above, three varactors can be manipulated independently to control the phase of the reflection coefficient. Fig. 5.7 shows a graph of the phase variation as

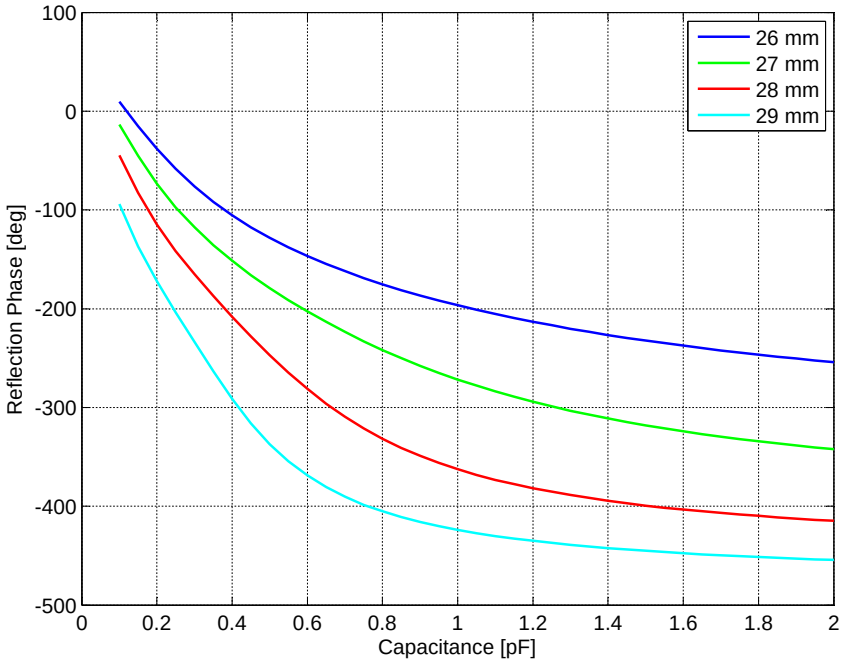

Figure 5.5: *Phase of the reflection coefficient of the RRA unit cell:for different values of the center dipole's length*

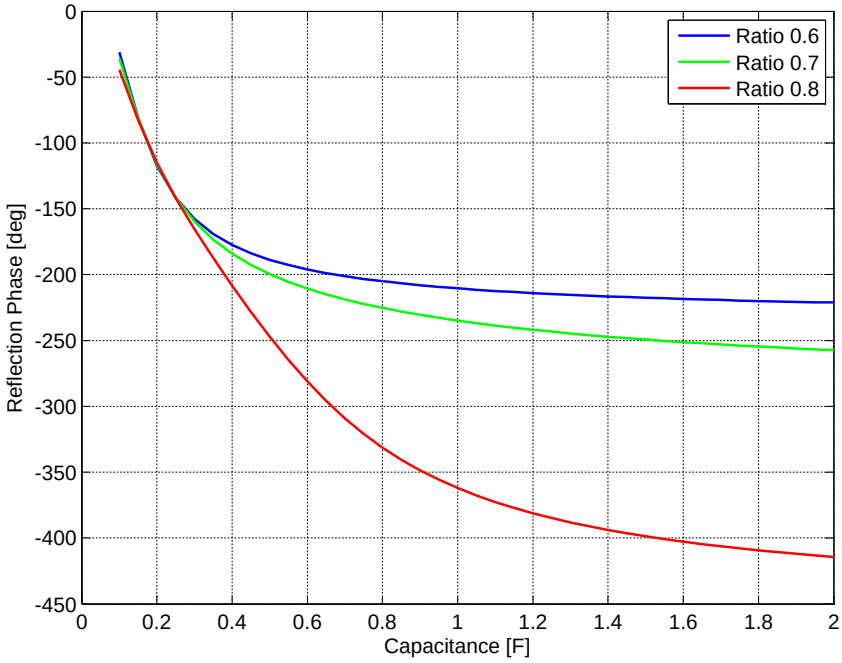

Figure 5.6: *Phase of the reflection coefficient of the RRA unit cell for different values of the ratio* L_2/L_1.

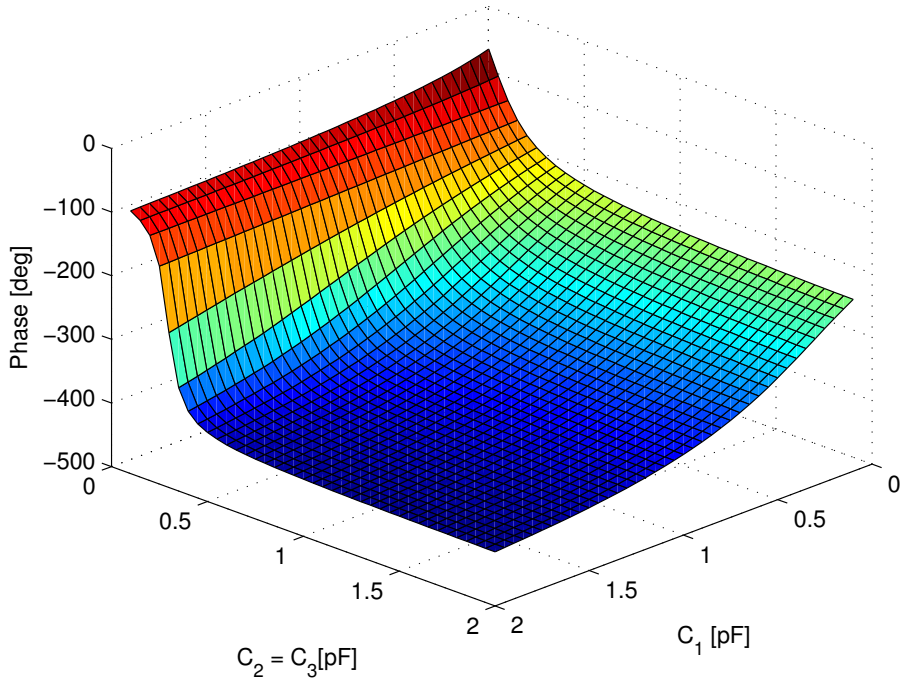

Figure 5.7: *Phase variation provided at* 5.5 *GHz as function of the two varactor parameters*

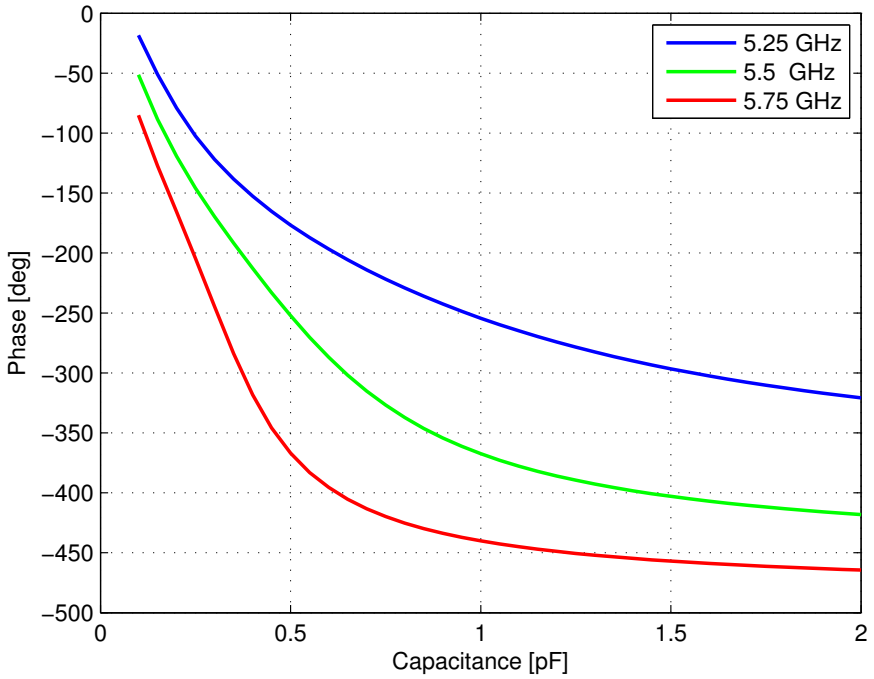

Figure 5.8: *Phase variation provided at* 5.5 *GHz as function of the varactor parameter (assuming the three varactors have a same value).*

a function of the capacitance values of the center dipole and those of the two satellite ones assuming two satellite varactors have a same value.

Fig. 5.8 illustrates the phase curve at different frequencies when the three varactors are equally varied, i.e., along the diagonal in Fig. 5.7. It is possible to see that the phase range for the design is around 370° at the center frequency, which is favorable for array phasing. In all cases, a varactor is characterized by a variable capacitor, an inductor, $L = 0.4\,\text{nH}$, and a resistor, R, which is assumed to be 0. A more realistic modeling could be employed but the current analysis, the ideal model without losses is sufficiently accurate.

5.3 Infinite Reflective Surface

The analysis and the design of reflectarray antennas often makes the assumption of local periodicity (LP), which assumes that all elements are identical [22]. The unit cell of a reflectarray is analyzed first in an infinite environment with a full-wave approach, which captures the mutual coupling effects between identical elements. The data from this analysis is then used for selecting elements that produce the necessary scattering characteristics for the array. The final configuration, therefore, consists of different elements with potentially strong variation in geometries or loads from element to element. This changes the mutual coupling between elements, which violates the LP assumption, and affects the performance of the reflectarray.

To circumvent this problem, the surrounded element [96, 97] and extended local periodicity methods [98] have been proposed. These methods attempt to include the real environment in the element analysis, so that, the data obtained from the unit cell analysis more accurately takes into account the effect of an element's neighbors. The achieved results show an improvement in the array performances. However, the design of a reflectarray is still based on the analysis of a local region of elements and the final far-field pattern can still show discrepancies with respect to that obtained by the full-wave simulation or measurements of the entire RA.

In this section, the design of a surface with a periodic phase gradient to illustrate the effect of the LP violation. Though the structure is not the same as a reflectarray, this is the first step to understanding the mutual coupling effect and the way to control it. The analysis of the periodic structure can be used to assist in the design of optimized RAs later. To control the mutual coupling in the proposed structure, an optimization scheme is integrated into the design process. Moreover, to speed up the optimization process, the scattering matrix technique is employed.

5.3.1 Reflective Surface

The structure considered is shown in Fig. 5.9, which consists of 1×3 sub-array with master/slave boundaries on the four surrounding walls, i.e., simulating an infinite environment.

The 1×3 sub-array was chosen to produce 120° inter-element phase shifts, which results in large electrical differences between the adjacent elements and purposeful strong violations of the LP assumption. The array is phased such that the phase periodicity along the X-axis equal to the length of the sub-array, W_x. From the Floquet analysis in

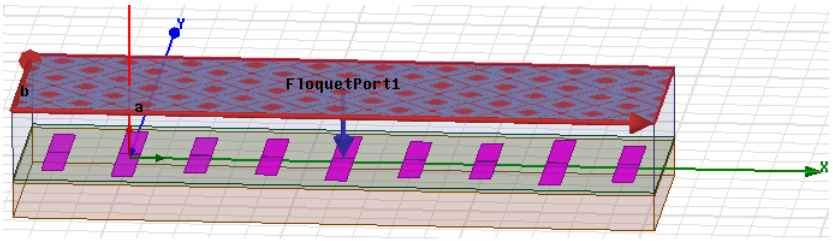

Figure 5.9: 1×3 *Sub-array*

Section 2.3, the direction of propagating modes are determined as

$$\theta_p = \sin^{-1}\left(\frac{2p\pi}{kW}\right) \tag{5.1}$$

where W is phase periodicity and k is the wave number. From Eqn. (5.1), the modes p that propagate can be determined by calculating the values of p which result in

$$\left|\frac{2p\pi}{kW}\right| \leq 1 \tag{5.2}$$

5.3.2 Floquet Harmonics

From Eqn. (5.1) and Eqn. (5.2), the propagating modes, p, for the structure in Fig. 5.9 are $-1,\ 0,\ 1$, and the desired direction is given by $p = 1$ (since $W = W_x = 3 \times 0.55\lambda$). An incident plane wave is assumed to normally impinge the reflectarray surface and then is reflected at an angle θ_1 ($p = 1$ in Eqn. 5.1). To simulate and capture the incident and reflected waves of the structure, a Floquet port is employed as shown in Fig. 5.9. The incident plane wave is generated by mode TE_0 of the Floquet port and the reflected power will be coupled to mode TE_p, where $p = -1, 0, 1$. By considering each mode as a separate port, the coupled power to each mode from the incident, TE_0 mode can be directly obtained from a multi-port scattering matrix representation.

To illustrate the existence of Floquet harmonics in this type of structure, an initial array of unloaded dipoles is designed. The results are shown in Fig. 5.10, which illustrates the Floquet harmonics of an infinite dipole array for different phase offsets (i.e., the sub-array is first phased with the first element's phase set to $0°$, then $30°$, $60°$, and so on). This is to illustrate the impact of varying the local geometry on the harmonic magnitudes.

The same procedure is applied to the designs of the 1×3 arrays of square patch and of the RRA unit cell proposed in this chapter. Fig. 5.11 and Fig. 5.12 show the Floquet harmonic behavior of these structures with different phase offsets. The phase offsets are varied in the same way as the case of unloaded dipole array. It is clear that for all the cases, the Floquet harmonics do exist on the phased gradient surface. Moreover, depending on the interaction between elements (mutual coupling), the power coupled to a same mode is different, which means by proper controlling the mutual coupling, it is possible also to control these Floquet harmonics. From these results, it can be seen that significant power is transmitted to mode TE_{-1}, therefore, in order to improve the

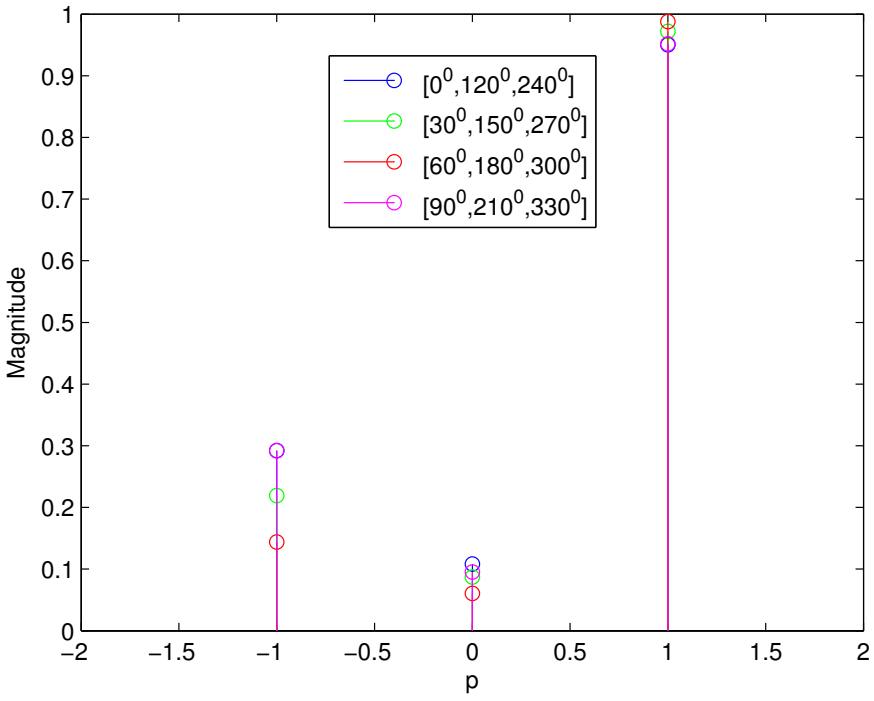

(a) Linear

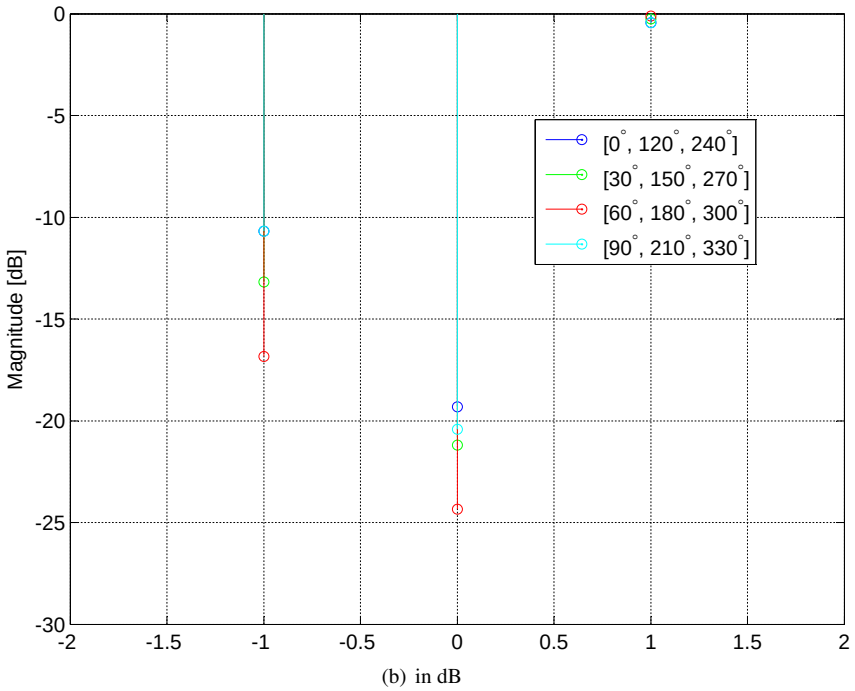

(b) in dB

Figure 5.10: *Floquet harmonics of the 1×3 unloaded dipole array*

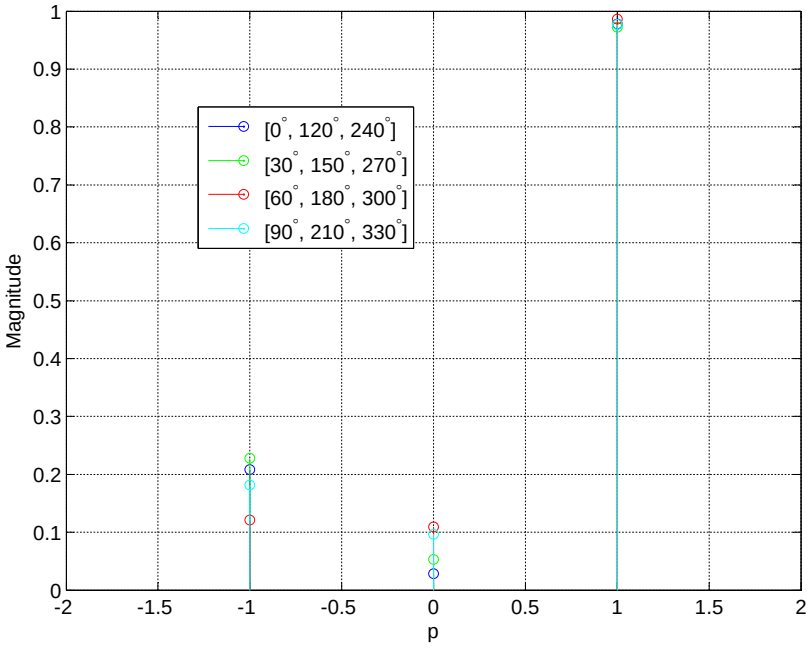

Figure 5.11: *Floquet harmonics of the 1×3 square patch array*

efficiency of coupling to the desired $p = 1$ mode, the other two harmonics, $p = -1, 0$, have to be suppressed.

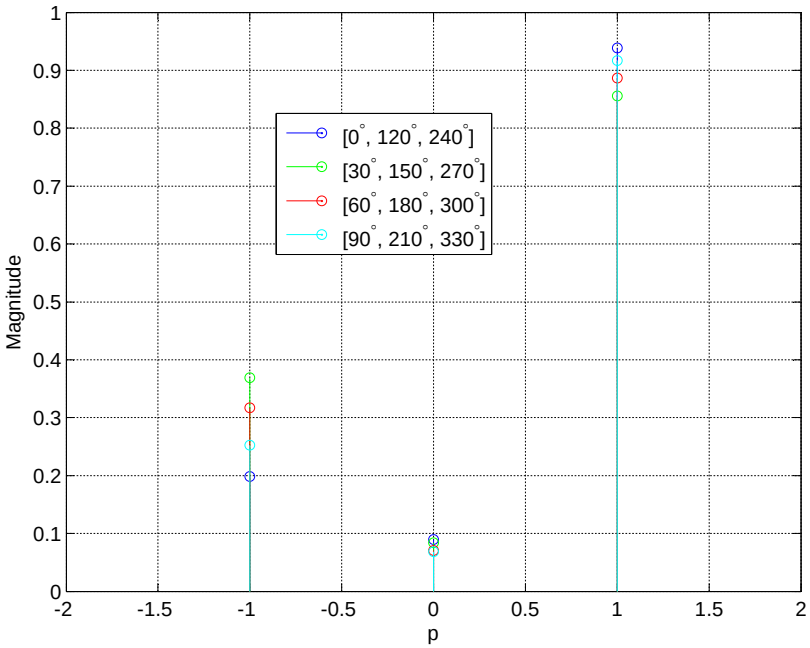

Figure 5.12: *Floquet harmonics of the 1×3 array of loaded three-dipole element.*

5.4 Reconfigurable Reflectarray Implementation

As illustrated in the previous section, the violation of local periodicity results in the existence of Floquet harmonics in the phase gradient periodic structure. The same conclusion could be drawn for the case of finite reflectarray antennas, since the elements in the array are different in phase to shape the desired beam. As a results, the RA performance is affected: the real RA pattern is different from the predicted one, and it generally presents higher side lobe level. To overcome with this problem, in this section, a new approach based on the method of moment (MoM) combined with an optimization algorithm is proposed as a design tool for enhancing the RRA's performances. The proposed method will be detailed with other approaches in the following.

5.4.1 RRA Design Methods

Generally, the design of RRAs could implement the same procedures as described for passive RAs. The design is based on the analysis of the single element and the phase shift to create desired beam patterns. The phase shift is calculated using phase-only synthesis techniques such as the intersection approach, or the projection matrix algorithm. For example, to create pencil beam, the RA design Eqn. 4.2 is used to find the phase required for each element to compensate the spatial and frequency differences. This approach, however, suffers from the same limitation as demonstrated in previous section. Moreover, the phase quantization effect could be an issue because this results in an additional increase in phase error.

Recently, the work in [99] has shown that the phase calculated using element analysis is no longer correct in the finite array environment. The paper pointed out that the phase after reflection will differ from that calculated using LP assumption. As a result, radiation pattern shown discrepancies as already pointed out. Moreover, the amplitude of the reflected wave does not only depend on the position of the element with respect to the feed, but also on the phase offset. Therefore, phase offset can be considered as a degree of freedom for the design. This method will be briefly summarized here and be used as a reference method to compare the results obtained by the here proposed approach.

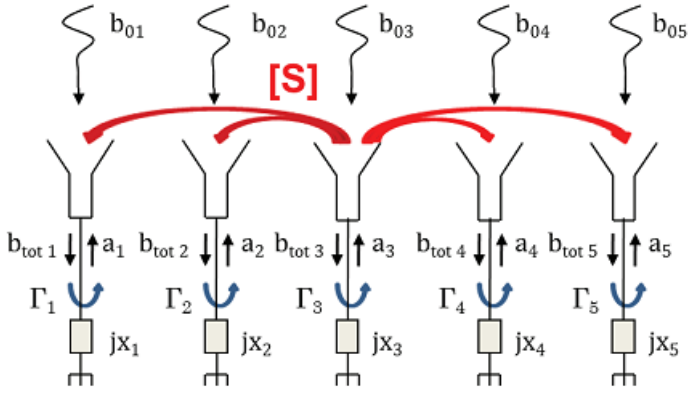

Figure 5.13: *Scheme for the scattering matrix characterization of the RA elements behavior, Y. Abdallah, et al. [99].*

The method is described for the design of the RA with identical elements, which are loaded by reactance to serve as phase shifter. The procedure to calculate the reactive load is summarized below. At first, the method replaces all reactance components by lumped ports, and characterizes the relation between ports by means of scattering elements as shown in Fig. 5.13. Here, $\vec{b}_{0i}$ represents the incident wave from feed to element i^{th}, $\vec{a}_i$ denotes the excitation wave after reflection of incident wave at element i^{th}. The "total" incident wave enters each element is the sum of the incident from the feed and the mutual coupling from element's neighbors as follows:

$$\vec{b}_{tot} = \vec{b}_0 + [S]\vec{a} \tag{5.3}$$

where the excitation weightings $\vec{a_i}$ are the reflected from total coupled waves.

$$\vec{a} = [\Gamma]\vec{b}_{tot} \tag{5.4}$$

substituting Eqn. 5.4 into Eqn. 5.3, we have:

$$[\Gamma]^{-1}\vec{a} = \vec{b}_0 + [S]\vec{a} \tag{5.5}$$

and assuming $|\Gamma| = 1$

$$\mid \vec{a} \mid = \mid \vec{b}_0 + [S]\vec{a} \mid \tag{5.6}$$

Solving Eqn. 5.6 with respect to the excitation $\vec{a}$, the reactive loads, $X_{m,n}$, can be found through $\vec{a}$ and Γ

$$\Gamma_{m,n} = \frac{a_{m,n}}{b_{tot,m,n}} \tag{5.7}$$

$$X_{m,n} = \frac{j\Gamma_{m,n} - 50}{j\Gamma_{m,n} + 50} \tag{5.8}$$

The method could properly account for the effects of all elements in the array, and therefore it attains the correct phase and amplitude of the wave after reflection ($\vec{a}$). As a consequent, the results have shown an improvement in side lobe area of the RA pattern with respect to the traditional RA design method. The method, however, is applicable for the case where there is only one port attach to each element (single dipole or patch). It becomes very complex in which any unit cell consists of more elements, as the considered case here, since the number of ports drastically increases, if the interaction among the elements of a single cell has to be taken into account as well.

As mentioned in the previous chapter, optimization algorithms could be integrated in the RA design procedure to provide a fully integrated design tool. Especially for RRA, when geometrical parameters are fixed and only the electronic switches are adjusted, optimization routines can be applied to control the performance of the RRAs effectively. The values or states of these electronic devices are considered as variables to be optimized by the global optimization algorithms in order to create the desired beam patterns.

5.4.2 Optimization of RRA

The optimization scheme for RRA design is shown in Fig. 5.14. At the beginning, initial RRA configurations are generated based on he phase-only synthesis approach. They are good starting points, since the array main beams could be properly formed using the calculated phase. The optimization, therefore, needs only to adjust the values/states of electronic components to maintain the desired beam, and control the side-lobe area. To guarantee an accurate description of the entire RRA, MoM is implemented in the evaluation of RRA design. Each configuration is, therefore, computed by MoM, and the radiation pattern will be used to score the fitness function, which are the input for optimization's operators. New set of RRA configurations are then generated by optimizer and the procedure continues until the problem's constraints are satisfied.

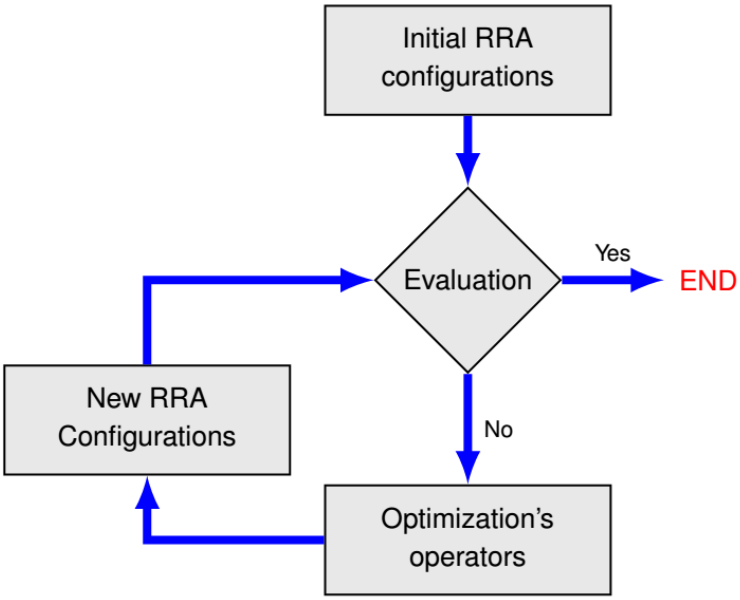

Figure 5.14: *RRA design scheme using optimization algorithms*

Generally, the fitness function is defined as:

$$f = \sum_{u} \sum_{v} \left(|E(u,v)| - Mask(u,v) \right)^2 \tag{5.9}$$

represents the error between the computed radiation pattern and the mask at each step of the optimization process and for different individuals of the population. This function takes into account the pattern of all points in the visible space, i.e., $u^2 + v^2 \leq 1$, and where the pattern is greater than mask, i.e., $(u,v) \in |E(u,v)| \geq Mask(u,v)$. The $Mask$ is defined as shown in 5.15, with specified beam-width and side-lobe level. Since the main beam constraints are generally reached with the initial step, the optimization essentially focus on the reduction of the side-lobe level and maintain the beam.

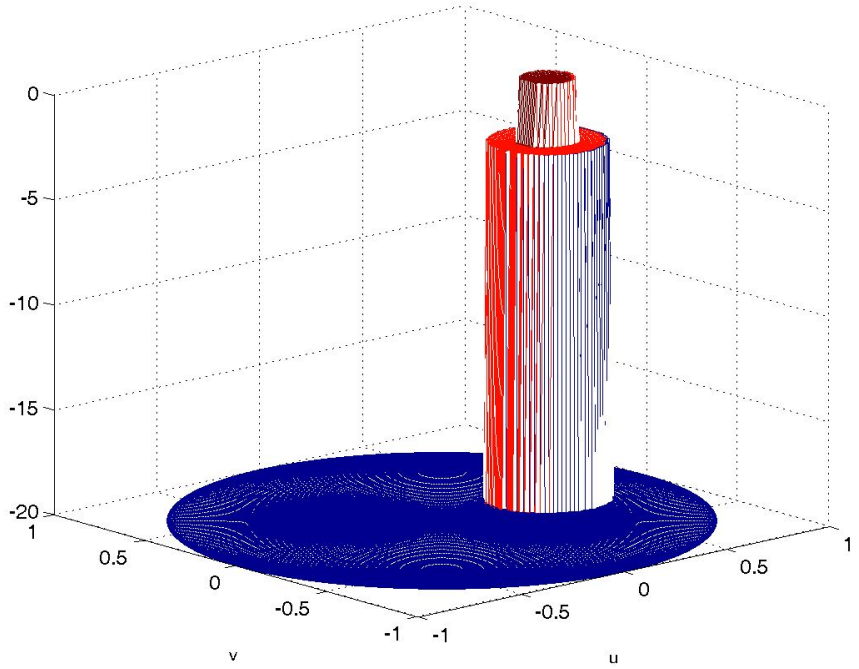

Figure 5.15: *Desired mask for optimizing RRAs*

5.5 Numerical Results

In this section, numerical results of the RRA designs will be presented. The first example considered is the optimization of an infinite reflective surface. The design has been chosen to prove the ability to reduce the Floquet harmonics by means of optimization and the possibility to control the mutual coupling. Following, two designs of 8×8 RRA with two different elements, i.e., single dipole and three-dipole unit cell are presented.

5.5.1 Optimization of infinite reflective surface

From Floquet theory, it is known that when the phase periodicity of an infinite structure is greater than one wavelength, there will be propagating Floquet harmonics. Floquet harmonics in the infinite structure correspond to side-lobes in the finite structure. Therefore, there is a need to suppress these harmonics in the infinite array especially when scanning the array. In this section, a process of optimizing an infinite reflective surface based on the unit cell described in Section 5.2.2 is introduced, which greatly reduces these harmonics.

In this work, an approach based on the generalized scattering matrix is proposed to effectively manage all RRA elements: all the varactors are substituted by lumped ports, and a multi-port analysis including the Floquet port and the associated harmonics is performed. This results in a generalized scattering matrix [100] including the lumped ports and Floquet ports. Using signal flow graphs, the lumped ports can be loaded with suitable reactance and the coupling from the $p = 0$ mode to the other Floquet

modes can be estimated. Hence, the impact of varying the varactor capacitances on the Floquet modes can be easily computed once the multi-port scattering matrix has been determined, which makes the optimization of the structure much more computationally feasible.

Next, all the dipoles are loaded with the reactance as shown in Fig. 5.4 and the loads that produce the required phase shifts while minimizing the amplitudes of the undesired Floquet harmonics are determined employing the M-BOA, introduced in Section 3.3.2. The results are shown in Fig. 5.16, which compares the prediction from the scattering matrix method to full-wave simulations with Ansys HFSS. The full-wave simulations include lumped-element capacitance in the dipoles set to the optimized values. Good correlation between proposed method and HFSS is found, which confirms its effectiveness and accuracy. Moreover, the results confirm that the undesired Floquet harmonics are greatly reduced.

A further step is that of trying to optimize the structure over the frequency band ranging from 5 to 6 GHz, in such a way that the power transfer to the undesired Floquet harmonics is minimized on the entire band. Fig. 5.17 shows the power coupled to different modes at different frequencies. The power coupled to mode -1 and mode 0 are below 0.1 (-20 dB) for the frequency band from $5.2 - 6$ GHz, and most of energy is transferred to mode 1, which is the desired direction. Therefore, by dynamically controlling the capacitance values of these varactors, the Floquet harmonics are suppressed over a large bandwidth.

5.5.2 8×8 Reflectarray of Loaded Dipole Elements

The first RRA configuration considered is an 8×8 array of single dipoles loaded with reactance as phase shifter. The array layout is shown in Fig. 5.18, where the unit cell consist of only one dipole which has similar dimension as the center dipole of the cell plotted in Fig. 5.4. The array is placed at a distance of 294.5 mm from the $X-Y$ plane, while the feed is located at the origin of the reference system and has a $\cos\theta$ pattern. A more accurate feed pattern could be assumed, but here the simple case has been considered with the purpose to compare the proposed method with other approaches presented in Section 5.4. The method based on the element analysis (local periodicity assumption), and the method from [99] are respectively named as method 1 and method 2.

Fig. 5.19 shows the evaluation of the RRA performances by the two methods 1 and 2 as a function of the phase offset. The fitness function defined in Eqn. 5.9 is used to evaluate the RRA radiation patterns. It is clear that the RRA performance depends on phase offset, therefore the phase offset could be a degree of freedom for the design. Moreover, by selecting the best results of each method over the phase offset range, the method 2 (the approach from [99]) showed better result than the method 1 based on element analysis (local periodic assumption), which indicates that the RRA performance could be improved by accurately defining the phase for each element.

The proposed approach using optimization algorithm is then carried out to design the RRA. The M-BOA [51] is applied to adjust these continuous values of varactors. Fig. 5.20 compares the optimized results with the best results obtained by method 2

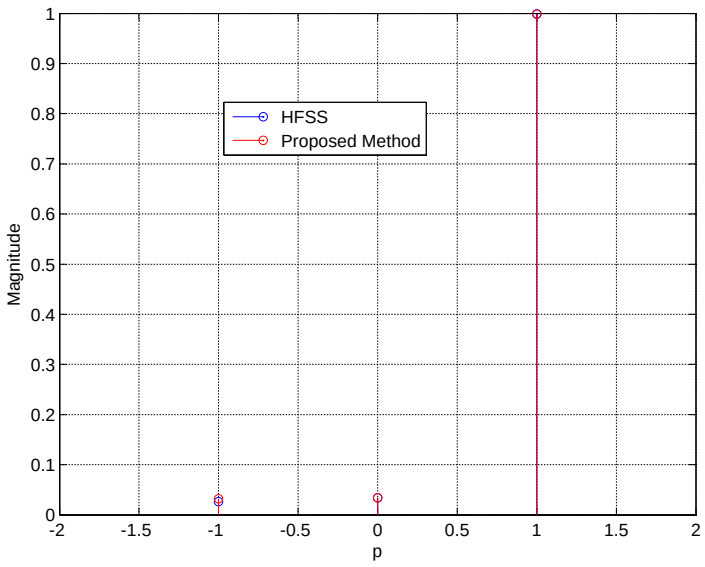

(a)

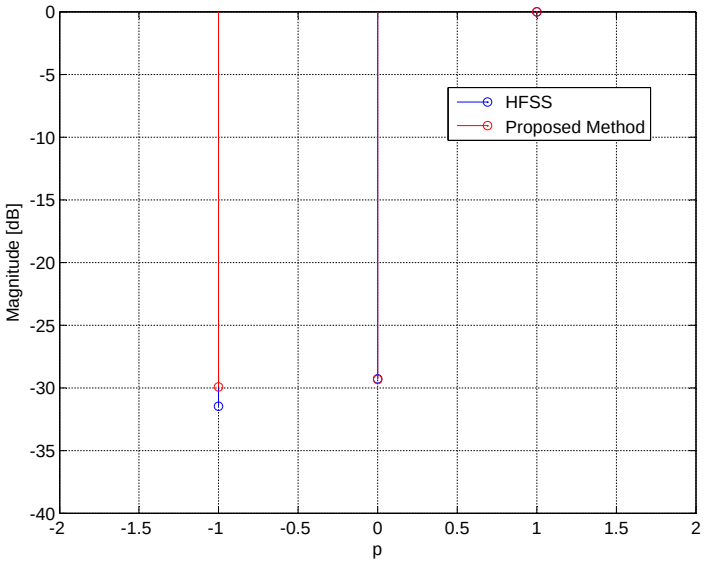

(b) in dB

Figure 5.16: *Optimized results of Infinite Reflective Surface*

(the best configuration of method 2 is picked up from Fig. 5.19). By using optimization approach, an improvement in side-lobe level is observed, especially remarkable for the 1^{st} side-lobe. The results do not show a breakthrough, but rather they reveal the possibility to enhance the RRA performance by properly controlling the phase shifters.

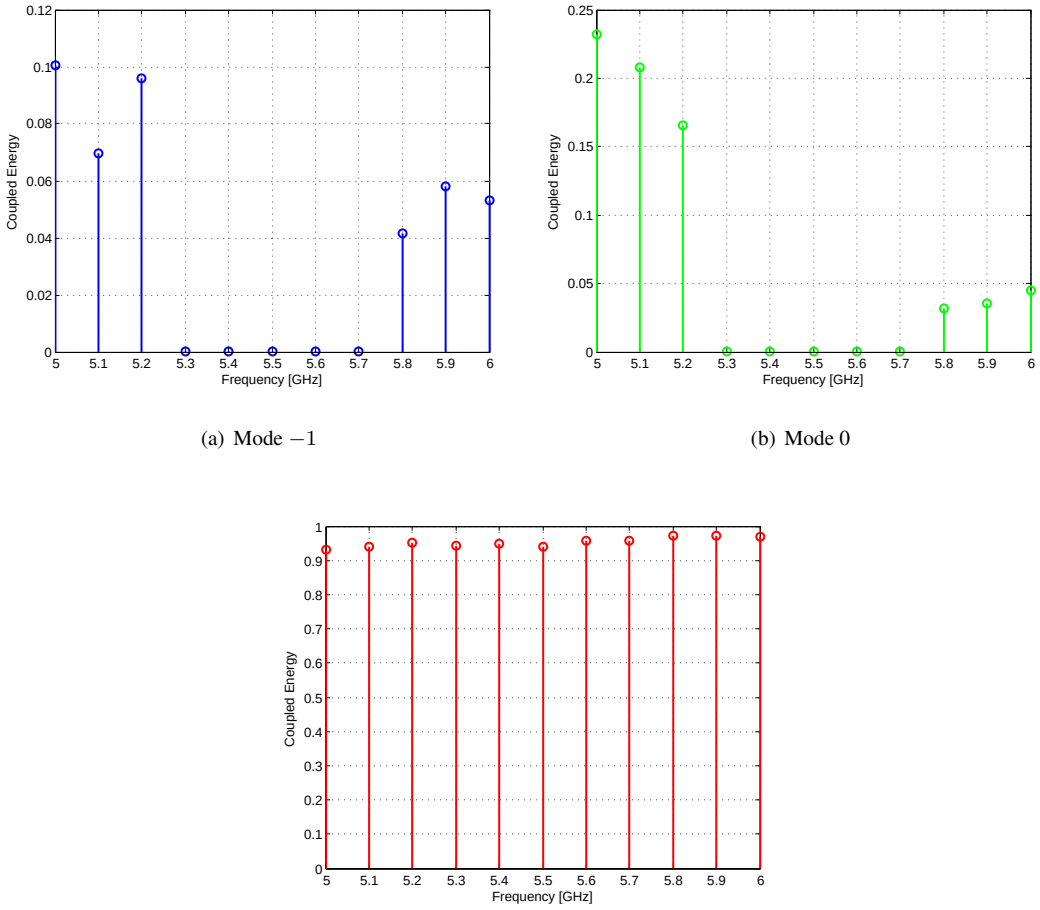

(a) Mode -1

(b) Mode 0

(c) Mode 1

Figure 5.17: *Power coupled to Floquet harmonics at different frequencies*

5.5.3 8×8 Reflectarray of Loaded Three-Dipole Elements

The design of an 8×8 RRA with three-dipole elements is finally considered and has a same configuration described in Section 5.5.2, but with the three-dipole unit cell instead of single dipole elements, as depicted in Fig. 5.21. Each dipole is loaded with a varactor, and could be manipulated independently to provide different phase shift. The two satellite dipoles have been considered loaded with the same valued varactors in order to reduce the complexity of controlling network and accelerate the optimization process. As mention above, the method in [99] is computationally expensive to apply to three-dipole element, therefore, the optimization has been applied here only to the element analysis approach, and the results have been compared with those of method 1.

Fig. 5.22 plots the radiation pattern of the best configurations obtained by method 1 and optimization approach in the $\phi = 0°$ plane. The RRA configuration obtained by the optimization approach maintains the main beam scanning in direction $\theta = 150°$, while

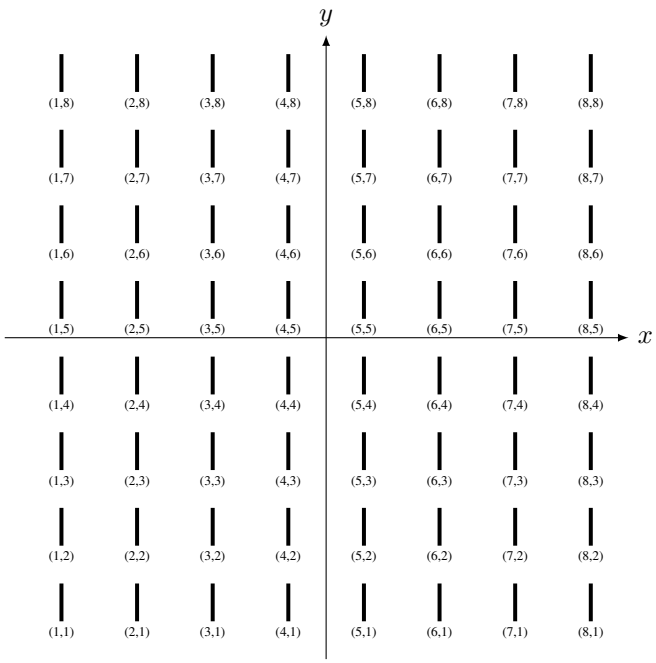

Figure 5.18: *Layout of the* 8×8 *RRA using single dipoles as elements.*

it manages to keep the side-lobe level lower than the RRA designed using method 1. A detailed comparison in the side-lobe area is shown in Fig. 5.23 where the differences of radiation patterns obtained by optimization and method 1 are plotted. The side-lobe level is well controlled by optimization design method, where the difference is greater than zero. It is worthy to notice that in some points the difference is lower than 0: this generally occurs in correspondence of zeros of the radiation patterns that are irrelevant for comparison. The radiation pattern in two planes, $\theta = 79^\circ$ and $\theta = 86^\circ$, are plotted in Fig. 5.24, and Fig. 5.25. Also in these cases, the results relative to the RRA designed with the optimization approach outperform those obtained with method 1.

5.6 Conclusions

In this chapter, the design of reconfigurable reflectarray antennas has been considered. The RRA unit cell consisting of three dipoles loaded with varactors that can be varied independently to create different phase shift for the element has been proposed for the RRA design.

The design of infinite reflective surface implementing the proposed element is presented. From the Floquet analysis and full-wave simulation, it has been demonstrated that the Floquet harmonics exist on this kind of structures. This was taken to illustrate the mutual coupling effect in periodic structures, and reflectarray as well, which is the results of the violation of local periodic assumption. These Floquet harmonics over a wide frequency band could be controlled by optimizing the structure, for instance with M-BOA. The results reveal the possibility to improve RRA performance by properly

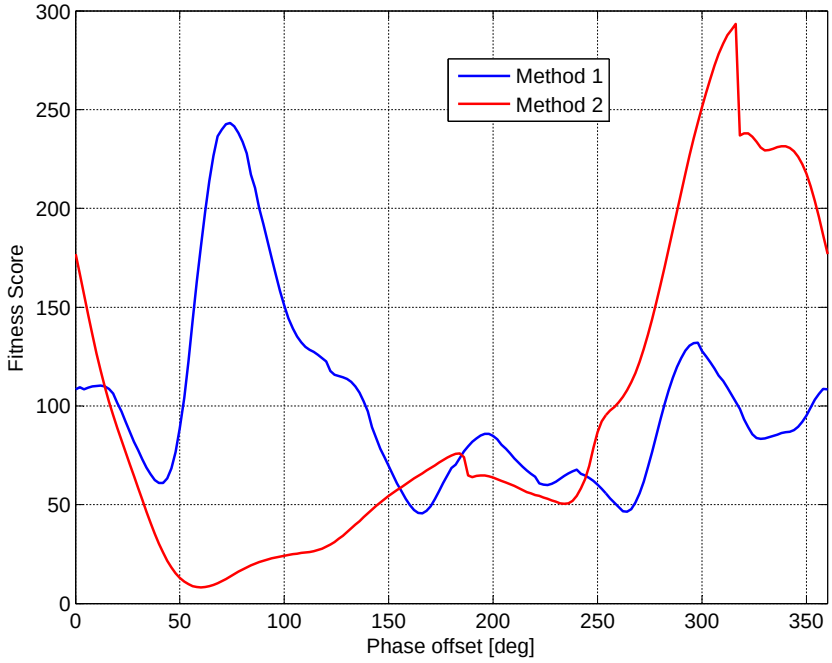

Figure 5.19: *Fitness score vs. phase offset*

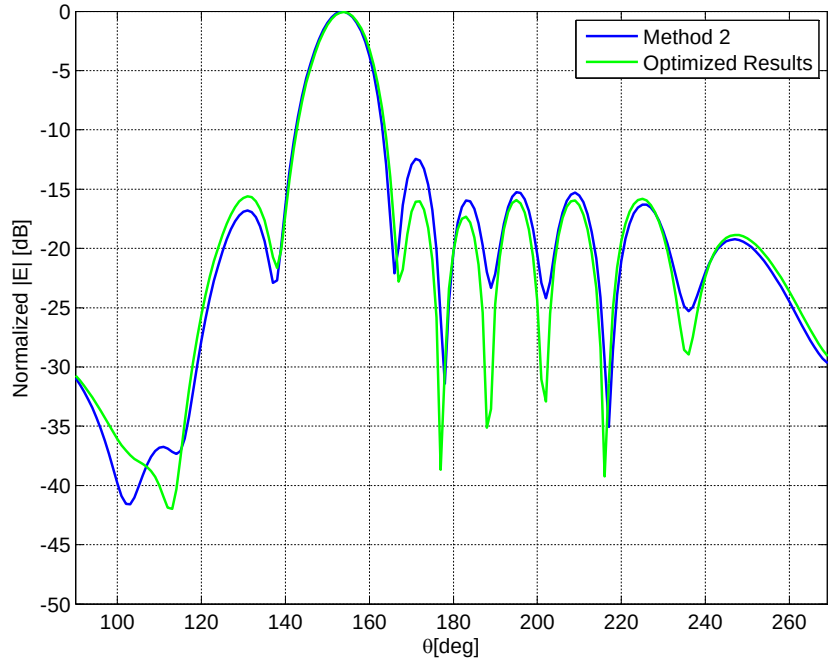

Figure 5.20: *Radiation pattern of the 8×8 RRA in $\phi = 0^\circ$ cut plane*

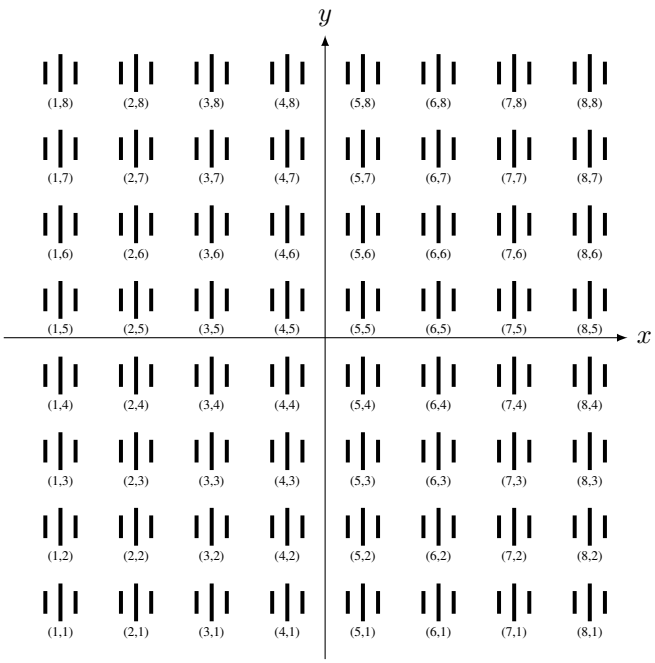

Figure 5.21: *Layout of the* 8×8 *RRA with three-dipole elements.*

controlling the mutual coupling effect between elements.

To verify this idea, two RRA configurations have been designed with different methods. The results showed an improvement in side-lobe area using optimization design method. All the results, however, have been computed by full-wave approach

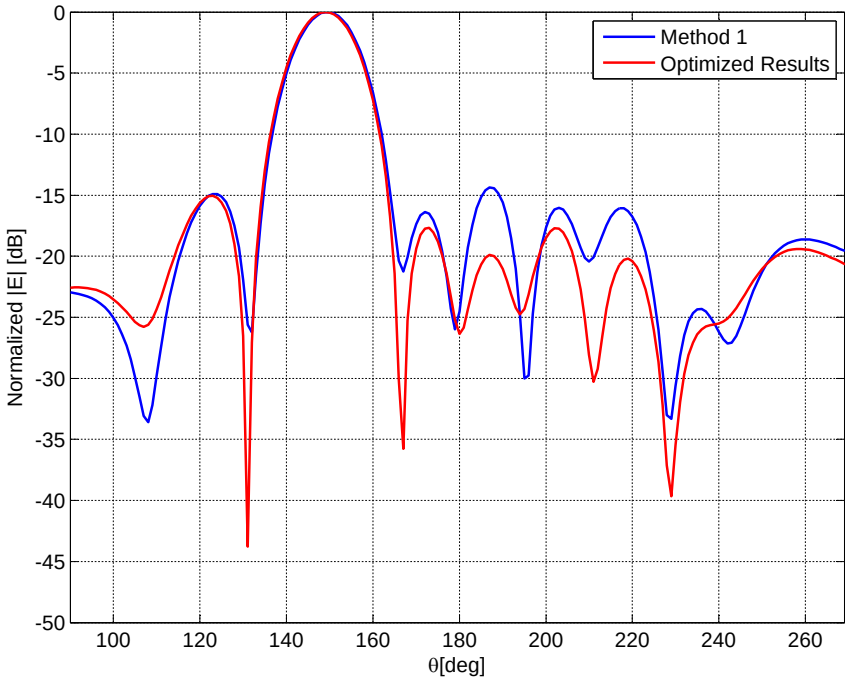

Figure 5.22: *Radiation pattern in the $\phi = 0°$ plane cut*

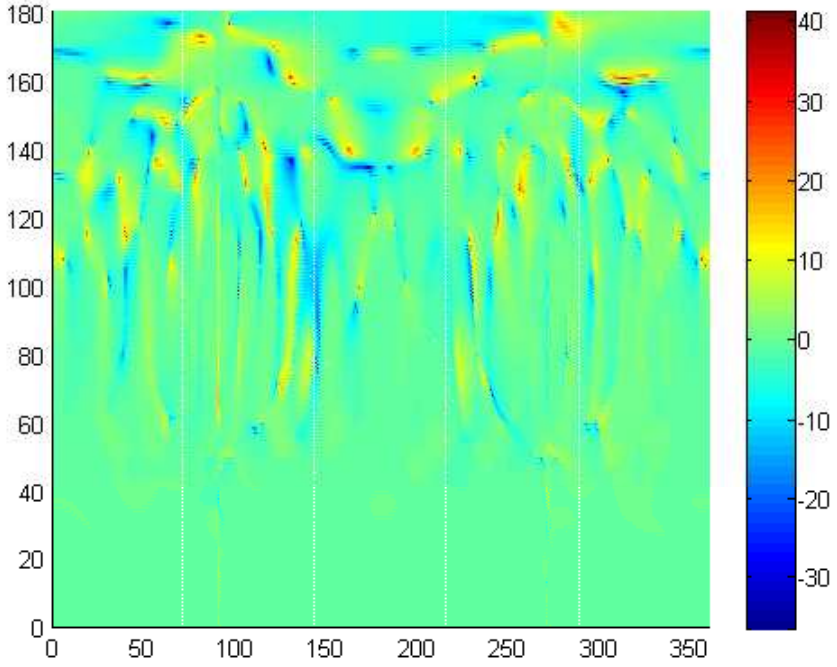

Figure 5.23: *Radiation difference between the two approaches*

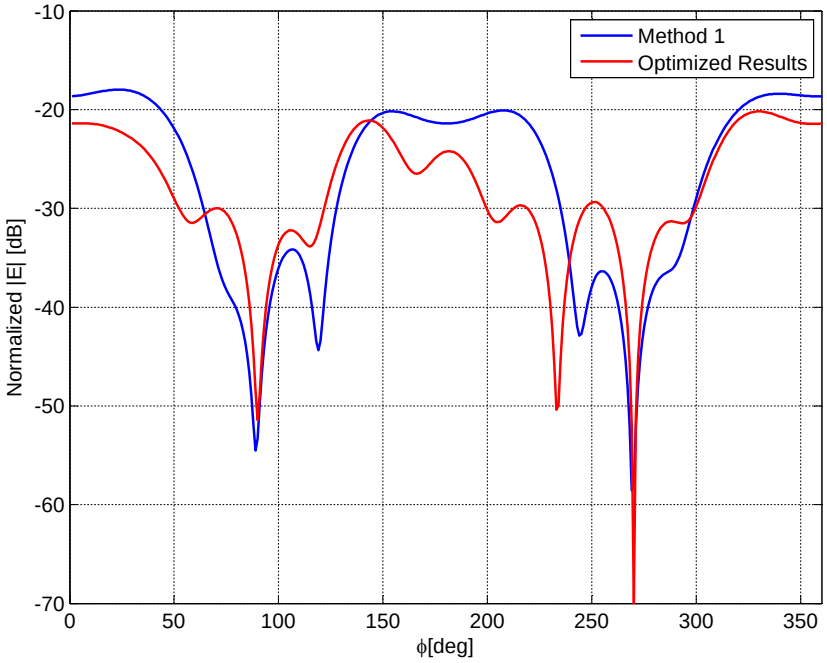

Figure 5.24: *Radiation pattern in the $\theta = 79^\circ$ plane cut*

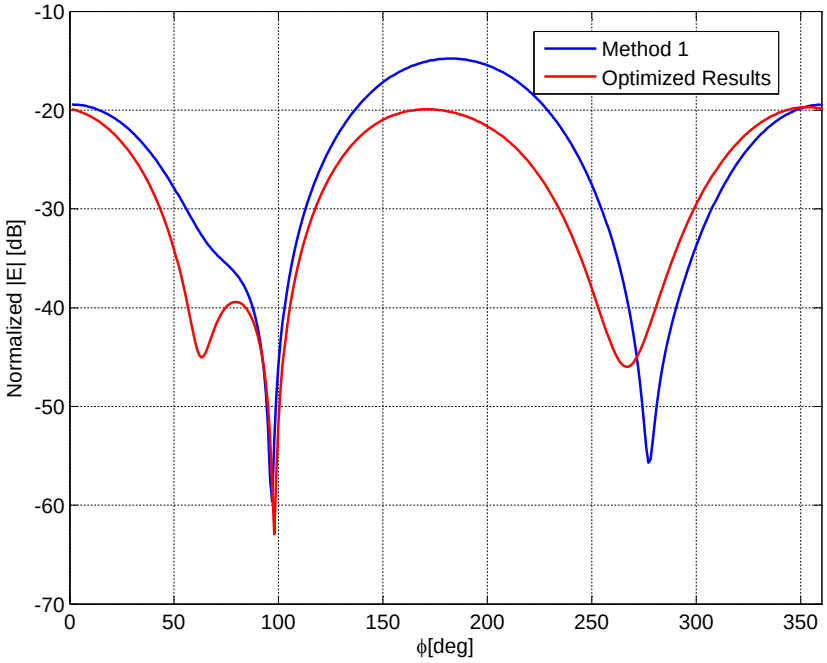

Figure 5.25: *Radiation pattern in the $\theta = 86^\circ$ plane cut*

CHAPTER 6

Conclusions

The goal of this thesis is to demonstrate the possibility to implement global optimization algorithms to antenna designs, with a particular focus on reflectarray antennas. To support the designs of complex EM problems, the first objective is to develop new optimization algorithms, which overcome the limitations of the best available population-based global optimizers. These algorithm are then tested with EM problems to prove their performances. The second objective is to design a single layer reflectarray with improved bandwidth, and finally, the application of optimization algorithms to design reflectarray antennas was the last objective.

In Chapter 3, two new optimization algorithms significantly improved from their ancestors have been presented. The first considered algorithm is the compact genetic algorithm (cGA). CGA implements the probability vector (PV) to represent the population, which greatly reduces the occupied memory by the algorithm, however cGA could not improve in term of solution quality with respect to simple genetic algorithm (sGA). The improved version of cGA by implementing more than one PV, and integrating a learning mechanism in updating process has been proposed. The idea is to use more than one PV to enhance the exploration properties of the algorithm and increase the ability to avoid the local optimum. The improved version showed its excellent performance compared to its ancestors, and also GAs when applied to mathematical and EM problems, including thinned array syntheses. The obtained results showed that the improved version of cGA not only provides better results, but also at a reduced computational cost.

Moreover, in the Chapter 3, another optimization algorithm has been deeply investigated, and a significantly new version has been proposed, the modified Bayesian optimization algorithm (M-BOA). This is a derivation of the original BOA by suitably introducing a mutation scheme to prevent the diversity of new generated population.

The M-BOA overcomes the drawback of BOA when the starting points are not good, or when it has been trapped in local minimum. This shows the effectiveness of the mutation scheme in population-based algorithms. M-BOA has been successfully implemented to several EM design problems such as filter design, linear array syntheses, or sparse array syntheses. The optimized results revealed that the M-BOA not only provides the optimum solution, but it can also estimate the requirement to obtain these solutions, as it has been shown in linear array syntheses. Both the considered algorithms showed their potential application to EM problem where hundred of parameters have to be managed.

In Chapter 4, the double square ring element for passive reflectarray design has been investigated. The considered element possesses a good phase behavior over a wide frequency range, which it yields a large reflectarray bandwidth. Moreover, the proposed unit cell offers several degrees of freedom for RA design, and it allows the application of double parameter design method to passive RA design. The application of double parameter design ensures the performance of the reflectarray over a defined frequency range. Numerical results of 16×16 array and 32×32 proved the effectiveness of the chosen element and of the design method. The reflectarrays implemented this unit cell achieved 17% 1dB gain bandwidth over the whole desired band.

Finally, in Chapter 5, the application of the optimization to RA design has been proposed for reconfigurable reflectarrays (RRA). A new RRA element, consisting of three dipoles loaded with varactors, has been presented. The considered element is a single-layer structure, which allows easily to introduce the controlling network for these varactors. Additionally, the RRA unit cell offers a continuous phase range of more than 360°. The proposed element has been first implemented for the design of a reflective surface. Though designing such a surface is not quite the same as designing an RA, this step showed the possibility to controlling the mutual coupling effect between elements in array by properly control the varactors of each elements. Through the design, it shows the interaction between elements in RA is significant, and can be controlled by properly design or by means of optimization. Finally, the designs of 8×8 RRA with singe dipole element and three-dipole element have proved this idea. The optimized design showed an improvement in side-lobe suppression.

Through these investigations, the original goals and objectives have been achieved:

- Two new optimization algorithms have been developed, which showed better performance with respect to their ancestors, and are promising for the optimization of EM problems.

- The double square ring unit cell has been proposed for the passive reflectarray design. Numerical results showed good frequency behavior of the whole RA designs.

- Finally, the three-dipole unit cell has been proposed for RRA design. The implementation of optimization algorithm to RA design is also presented through the design of infinite reflective surface and two entire RRAs.

6.1 Contributions

The work presented in this thesis produced several publications in both journals and conferences papers, as listed below.

Journal Papers

1. B. V. Ha, P. Pirinoli, R E. Zich, M. Mussetta, "Direct Synthesis of Dual-parameter Concentric Ring RA with Enhanced Bandwidth," *International Journal on Antenna and Propagation (IJAP)*, 2012, doi:10.1155/2012/535673.

2. B. V. Ha, P. Pirinoli, R. E. Zich, M. Mussetta, F. Grimaccia, "Modified Bayesian Optimization Algorithm for Sparse Linear Antenna Design," *Progress In Electromagnetics Research (PIER-B)*, vol. 54, pp. 385-405, 2013.

3. B. V. Ha, P. Pirinoli, R. E. Zich, M. Mussetta, "Application of Improved Compact Genetic Algorithm to Thinned Array Synthesis," (in preparation for IEEE AWPL Letter).

Conference Papers

4. B. V. Ha, P. Pirinoli, M. Mussetta, R. E. Zich, "Dual-Parameter Concentric Ring RA Elements", *Proc. European Conf. Antennas Propag. EuCAP*, Prague, 26-30 March, 2012.

5. B. V. Ha, M. M. Maglio, R. E. Zich, "Contactless Energy Transfer in Adverse Environment Using Rectanna," *Proc. Asia-Pacific Electromag. Compatibility APEMC*, Singapore, 21-24 May, 2012 .

6. B. V. Ha, M. M. Maglio, M. Mussetta, P. Pirinoli, R. E. Zich, "Modified Bayesian Optimization Algorithm for EMC Complex System Design," *Proc. Asia-Pacific Electromag. Compatibility APEMC*, Singapore, 21-24 May, 2012.

7. B. V. Ha, P. Pirinoli, M. Mussetta, R. E. Zich, "Design of Single Layer RA with Enhanced Bandwidth," *IEEE AP-S*, Chicago, July 8-14, 2012.

8. B. V. Ha, P. Pirinoli, M. Mussetta, R. E. Zich, "Modified Bayesian Optimization Algorithm for Antenna Design," *IEEE AP-S*, Chicago, July 8-14, 2012.

9. B. V. Ha, R. E. Zich, P. Pirinoli, M. Mussetta, D. N. Chien, "Improved Compact Genetic Algorithm for Complex System Design," *Proc. Inter. Conf. Commu. Elect.*, Hue, Vietnam, August 1-3, 2012.

10. B. V. Ha, M. Mussetta, F. Grimaccia, P. Pirinoli, R. E. Zich, "Modified Bayesian Optimization Algorithm for Planar Array Design," *Proc. Inter. Conf. Commu. Elect.*, Hue, Viet Nam, August 1-3, 2012.

11. B. V. Ha, P. Pirinoli, M. Mussetta, R. E. Zich, D. N. Chien "Reflectarray antenna for X-band satellite communication," *Proc. Inter. Conf. Commu. Elect.*, Hue, Viet Nam, August 1-3, 2012.

12. B. V. Ha, R. E. Zich, M. Mussetta, P. Pirinoli, "Improved Compact Genetic Algorithm for Thinned Array Design," *Proc. European Conf. Antennas Propag. EuCAP*, Gothenburg, Sweden, Apr. 8-12, 2013.

13. B. V. Ha, R. E. Zich, M. Mussetta, P. Pirinoli, D. N. Chien, "Thinning Array using Improved Compact Genetic Algorithm," *IEEE AP-S*, Orlando, FL, July 8-14, 2013.

14. B. V. Ha, R. E. Zich, M. Mussetta, P. Pirinoli, "Linear Sparse Array Synthesis using Modified Bayesian Optimization Algorithm," *IEEE AP-S*, Orlando, FL, July 8-14, 2013.

15. B. V. Ha, R. E. Zich, M. Mussetta, P. Pirinoli, "Synthesis of Sparse Planar Array using Modified Bayesian Optimization Algorithm," *Proc. Inter. Conf. Elect. Advance App.*, Torino, Sept. 9-13, 2013.

APPENDIX $\mathcal{A}$

Benchmark Functions

The expressions of the standard cost function used in Section 3.3.3 are:

– **Ackley** function ($N = 15$)

$$f(X) = 10 + e - 20e^{-0.2\sqrt{\frac{1}{N}\sum_i {x_i}^2}} - e^{\frac{1}{N}\sum_i \cos(2\pi x_i)}$$

– **Rosenbrock** function ($N = 15$)

$$f(X) = \sum_{i=1}^{N} \left(100(x_{2i} - x_{2i-1}^2)^2 + (1 - x_{2i-1})^2\right)$$

– **Rastrigin** function ($N = 15$)

$$f(X) = \sum_{i=1}^{N} \left(x_i^2 - 10\cos(2\pi x_i) + 10\right)$$

– **Shekel** function ($N = 9$)

$$f(X) = 12 - \sum_{i=1}^{N} \left((X - a_i)^T (X - a_i) + c_i\right)^{-1}$$

where $X = (x_1, x_2)$ is the variable vector, a_i are vectors of i^{th} locel minima and c_i are constant proportional to minimum $f((a_i)^T) \approx 12 - \frac{1}{c_i}$. There are 9 minima at points $(-3, -3), (-3, 0), (-3, +3), \ldots, (+3, +3)$.

APPENDIX $\mathcal{B}$

Generalized Scattering Matrix

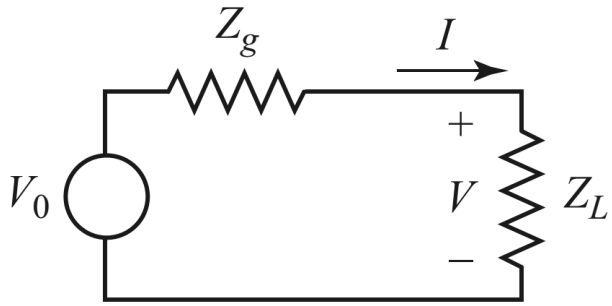

Figure B.1: *A generator with impedance Z_g connected to a load impedance Z_L*

In the Fig. B.1 there is no defined characteristic impedance, nor is there a voltage reflection coefficient, or incident and reflected voltage or current waves. It is possible, however, to define a new set of waves, called *power waves*, which have useful properties when dealing with power transfer between a generator and a load.

The incident and reflected power wave amplitudes a and b are defined as the following linear transformations of the total voltage and current:

$$a = \frac{V + Z_R I}{2\sqrt{R_R}} \tag{B.1a}$$

$$b = \frac{V - Z_R^* I}{2\sqrt{R_R}} \tag{B.1b}$$

where $Z_R = R_R + jX_R$ is known as the *reference impedance*.

The reflection coefficient, Γ_p, for the reflected power wave can be found by using (B.1) and the fact that $V = Z_L I$ at the load:

$$\Gamma_p = \frac{b}{a} = \frac{V - Z_R^* I}{V + Z_R I} = \frac{Z_L - Z_R^*}{ZL + Z_R} \tag{B.2}$$

Equation (B.2) suggests that choosing the reference impedance as the conjugate of the load impedance,

$$Z_R = Z_L^*, \tag{B.3}$$

will have the useful effect of making the reflected power wave amplitude go to zero.

To define the scattering matrix for power waves for an N-port network, we assume the reference impedance for port *i* is Z_{Ri}. Then, analogous to (B.1), we define the power wave amplitude vectors in terms of the total voltage and current vectors:

$$[a] = [F]([V] + [Z_R][I]) \tag{B.4a}$$

$$[b] = [F]([V] - [Z_R^*][I]) \tag{B.4b}$$

where [F] is a diagonal matrix with elements $1/2\sqrt{Re\{Z_{Ri}\}}$ and $[Z_R]$ is a diagonal matrix with elements Z_{Ri}.
By the impedance matrix relation that $[V] = [Z][I]$, (B.4) can be written as

$$[b] = [F]([Z] - [Z_R]^*)([Z] + [Z_R])^{-1}[F]^{-1}[a] \tag{B.5}$$

Because the scattering matrix for power waves, $[S_p]$, should relate $[b]$ to $[a]$, we have

$$[S_p] = [F]([Z] - [Z_R]^*)([Z] + [Z_R])^{-1}[F]^{-1} \tag{B.6}$$

The ordinary scattering matrix for a network can first be converted to an impedance matrix, then converted to the generalized power wave scattering matrix using (B.6).

For multi-port network simulated in HFSS, the impedance matrix is directly obtained from full-wave simulation, while the *reference impedance* is the input impedance Z_o for active port, and is the impedance characteristic of lumped element loading at lumped port e.g. RLC circuit represent for varactor diode .

Bibliography

[1] J. Huang, and J. A. Encinar. *Reflectarray Antennas*. Wiley-IEEE Press, 2007.

[2] D. Berry, R. Malech, and W. Kenedy. The reflectarray antenna. *IEEE Trans. Antennas Propag.*, 11(6):645–651, 1963.

[3] H. R. Phelan. *US Patent*. US3925784, 1975.

[4] C. S. Malagisi. *US Patent*. US4053895, 1977.

[5] J. Huang. Bandwidth study of microstrip reflectarray and a novel phased reflectarray concept. *IEEE Int. Symposium Antennas Propagat.*, pages 582–585, 1995.

[6] D. M. Pozar. Bandwidth of reflectarrays. *IEEE Electronic Letters*, 39(21):1490–1491, 2003.

[7] J. A. Encinar. Design of two-layer printed reflectarrays using patches of variable size. *IEEE Trans. Antennas Propag.*, 49(10):1403–1410, 2001.

[8] J. A. Encinar, and J. A. Zornoza. Broadband design of three-layer printed reflectarrays. *IEEE Trans. Antennas Propag.*, 51(7):1662–1664, 2003.

[9] J. A. Encinar, M. Arrebola, L. F. de la Fuente, and G. Toso. A transmit-receive reflectarray antenna for direct broadcast satellite applications. *IEEE Trans. Antennas Propag.*, 59(9):3255–3264, 2011.

[10] L. S. Ren, Y. C. Jiao, F. Li, J. J. Zhao, and G. Zhao. A dual-layer t-shaped element for broadband circularly polarized reflectarray with linearly polarized feed. *IEEE Antennas Wireless Propag. Letters*, 10:407–410, 2011.

[11] L. Moustafa, R. Gillard, F. Peris, R. Loison, H. Legay, and E. Girard. The phoenix cell: A new reflectarray cell with large bandwidth and rebirth capabilities. *IEEE Antennas Wireless Propag. Letters*, 10:71–74, 2011.

[12] S. H. Yusop, N. Misran, M. T. Islam, and M. Y. Ismail. Analysis on split concept of reflectarray antenna element for bandwidth enhancement. *IEEE Proc. Int. Conf. Space Scie. and Commu.*, pages 273–276, 2011.

[13] M. E. Bialkowski, and K. H. Sayidmarie. Investigations into phase characteristics of a single-layer reflectarray employing patch or ring elements of variable size. *IEEE Trans. Antennas Propag.*, 56(11):3366–3372, 2008.

[14] D. Zhou, Z. Niu, and R. Li. Investigation on a single-layer microstrip circular-patch/ring-combination reflectarray element. *Proc. CSQRWC.*, pages 664–667, 2011.

[15] M. Mussetta, P. Pirinoli, P. T. Cong, M. Orefice, R. E. Zich. Characterization of microstrip reflectarray square ring elements by means of an artificial neural network. *Proc. of Fourth Europ. Conf. on Antennas Propag.*, pages 1–4, 2010.

[16] P. De Vita, A. Freni, G. L. Dassano, P. Pirinoli, R. E. Zich. Broadband element for high-gain single-layer printed reflectarray antenna. *IEEE Electronics Letters*, 43(23), 2007.

[17] D. M. Pozar. Wideband reflectarrays using artificial impedance surfaces. *IEEE Electronic Letters*, 43(3):148–149, 2007.

[18] F. Venneri, S. Costanzo, G. D. Massa, and G. Amedola. Aperture-coupled reflectarrays with enhanced bandwidth features. *Journal of Electromagnetic Waves and Applications*, 22(11-12), 2008.

[19] G. Zhao, Y. C. Jaio, F. Zhang, and F. S. Zhang. Broadband reflectarray antennas using double-layer sub-wavelength patch elements. *IEEE Electronic Letters*, 9:1139–1142, 2010.

[20] P. Nayeri, F. Yang, and A. Z. Elsherbeni. Bandwidth improvement of reflectarray antennas using closely spaced elements. *Progress In Electromagnetic Reseach C*, 18:19–29, 2011.

[21] J. Ethier, M. R. Chaharmir, and J. Shaker. Reflectarray design comprised of sub-wavelength coupled resonant square loop elements. *IEEE Electronic Letters*, 47(22):1215–1217, 2011.

[22] D. M. Pozar, S. D. Targonski, and H. D. Syrigos. Design of millimeter wave microstrip reflectarrays. *IEEE Trans. Antennas Propag.*, 45(2):287–296, 1997.

[23] M. Zhou, S. B. Sorensen, O. S. Kim, E. Jogensen, P. Meincke, and O. Breinbjerg. Direct optimization of printed reflectarrays for contoured beam satellite antenna applications. *IEEE Trans. Antennas Propag.*, 61(4):1995–2004, 2013.

[24] M. Mussetta, G. Dassano, P. Pirinoli, R. E. Zich, and M. Orefice. 18 ghz microstrip reflectarray: Ga optimization and experimental measurements. *Proc. Journes Int. de Nice sur les Antennas*, pages 240–241, 2004.

[25] P. Nayeri, F. Yang, and A. Z. Elsherbeni. Design of single-feed reflectarray antennas with asymetric multiple beams using the particle swarm optimization method. *IEEE Trans. Antennas Propag.*, 61(9):4598–4605, 2013.

[26] Constantine A. Balanis. *Antenna Theory: Analysis and Design, 3rd Edition*. John Wiley & Son, 2005.

[27] Arun K. Bhattacharyya. *Phased Array Antennas: Floquet Analysis, Synthesis, BFNs, and Active Array System*. Wiley & Sons Inc., 2006.

[28] H. Unz. Linear arrays with arbitrarily distributed elements. *IEEE Trans. Antennas Propag.*, 8:222–223, 1960.

[29] D. G. Leeper. Isophoric arrays-massively thinned phased arrays with well-controlled side-lobes. *IEEE Trans. Antennas Propag.*, 47(12):1825–1835, 1999.

[30] D. E. Goldberg. *Genetic Algorithms in search, optimization and machine learning*. Addison – Wiley, 1989.

[31] J. Kennedy, and R.C. Eberhart. *Swarm Intelligence*. Morgan Kaufmann: SanFrancisco, CA, 2001.

[32] M. Dorigo, V. Maniezzo, and A. Colorni. The ant system: Optimization by a colony of cooperating agents. *IEEE Trans. Syst, Man, Cybern. B*, 26(2):29–41, 1996.

[33] Selleri, S., M. Mussetta, P. Pirinoli, R.E. Zich, and M. Matekovits. Differentiated meta-pso method for array optimization. *IEEE Trans. Antennas Prop.*, 56(1):67–75, 2008.

[34] Y. S. Ong, and A. J. Kean. Meta-lamarckian learning in memetic algorithms. *IEEE Trans. Evol.Comput.*, 8(2):99–110, 2004.

[35] A. Basak, S. Pal, S. Das, A. Abraham, and V. Snasel. A modified invasive weed optimization algorithm for time-modulated linear antenna array synthesis. *IEEE Proc. Congr. Evol. Comput.*, pages 1–8, 2010.

[36] D. Simon. Biogeography-based optimization. *IEEE Trans. Evol. Comput.*, 12(6):702–713, 2008.

[37] F. Grimaccia, M. Mussetta, and R. E. Zich. Genetic swarm optimization: Self adaptive hybrid evolutionary algorithm for electromagnetics. *IEEE Trans. Antennas Propag.*, 55(3):781–785, 2007.

[38] Y. H. Lee, B. J. Cahill, S. J. Porter, and A. C. Marvin. Novel evolutionary learning technique for multi-objective array antenna optimization. *Progress In Electromagnetics Research*, 48:125–144, 2004.

[39] J. R. Perez-Lopez, and J. Basterrechea. Hybrid particle swarm-based algorithms and their application to linear array synthesis. *Progress In Electromagnetics Research*, 90:63–74, 2009.

[40] K. A. De Jong. *An analysis of the behavior of a class of Genetic adaptive systems*. University of Michigan, 1975. PhD thesis.

[41] Mühlenbein, H. and G. Paaß. From recombination of genes to the estimation of distributions i. binary parameters. *Parallel Problem Solving from Nature*, pages 178–187, 1996.

[42] G. R. Harik, F. G. Lobo, and D. E. Goldberg. The compact genetic algorithm. *IEEE Trans. Evol. Comput.*, 3(4):287–297, 1999.

[43] C. W. Ahn, and R. S. Ramakrishna. Elitism-based compact genetic algorithm. *IEEE Trans. Evol. Comput.*, 7(4):367–385, 2003.

[44] G. Shi, and Q. Ren. Research on compact genetic algorithm in continuous domain. *IEEE World Congr. Comput. Intel.*, pages 793–780, 2008.

[45] B. V. Ha, R. E. Zich, M. Mussetta, P. Pirinoli, and D. N. Chien. Improved compact genetic algorithm for em complex system design. *Proc. Int. Conf. Commu. and Elect.*, pages 389–392, 2012.

[46] M. Pelikan, D. E. Goldberg, and E. Cant-Paz. Boa: The bayesian optimization algorithm. *Proc. Genetics Evol. Comput. Conf. GECCO*, pages 525–532, 1999.

[47] M. Pelikan. *Bayesian Optimization Algorithm: Toward a New Generation of Evolutionary Algorithms*. Springer, 2005.

[48] J. Pearl. *Probabilistic reasoning in intelligent systems: networks of plausible inference*. Morgan Kaufman, 1988.

[49] D. Heckerman, D. Geiger, and D. M. Chickering. *Learning bayesian networks: the combination of knowledge and statistical data*. Microsoft Research, Redmond, WA, 1994. Technical Report MSR-TR-94-09.

[50] S. Baluja. *Population based incremental learning: A method for integrating genetic search based function optimization and competitive learning*. Carnegie Mellon University, Pittsburgh, PA, 1994. Technical Report No. CMUCS-94-163.

[51] B. V. Ha, M. Mussetta, P. Pirinoli, and R. E. Zich. Modified bayesian optimization algorithm for microstrip filter design. *Proc. AP-S Symp.*, 2012.

[52] Y. T. Lo. A mathemetical theory of antenna arrays with randomly spaced element. *IEEE Trans. Antennas Propag.*, 12(3):257–268, 1964.

[53] O. Quevedo-Teruel, and E. Rajo-Iglesias. Ant colony optimization in thinned array synthesis with minimum sidelobe level. *IEEE Antennas Wireless Proga. Letters*, 5(1):349–352, 2006.

[54] B. Steinberg. Comparison between the peak sidelobe of random array and algorithmically designed aperiodic array. *IEEE Trans. Antennas Propag.*, 21(3):366–370, 1973.

[55] S. Holm, B. Elgetun, and G. Dahl. Properties of the beampattern of weight- and layout-optimized sparse arrays. *IEEE Trans. Ultra. Ferroelectr. Freq. Control.*, 44(5):983–991, 1997.

[56] Randy L. Haupt. Thinned arrays using genetic algorithms. *IEEE Trans. Antennas Propag.*, 42(7):993–999, 1994.

[57] A. Trucco. Thinning and weighting of large planar arrays by simulated annealing. *IEEE Trans. Ultra. Ferroelectr. Freq. Control.*, 6(2):347–355, 1999.

[58] A. Trucco, and V. Murino. Stochastic optimization of linear sparse arrays. *IEEE J. OceanEng.*, 24(3):291–299, 1999.

[59] S. Caorsi, A. Lommi, A. Massa, and Pastorino. Peak sidelobe reduction with a hybrid approach based on gas and different sets. *IEEE Trans. Antennas Propag.*, 52(4):1116–1121, 2004.

[60] G. Oliveri and A. Massa. Genetic algorithm (ga)-enhanced almost difference set (ads)-based approach for array thinning. *IET Microwave, Antennas Propag.*, 5(3):305–315, 2011.

[61] B. V. Ha, R. E. Zich, M. Mussetta, and P. Pirinoli. Improved compact genetic algorithm for thinned array design. *Proc. Eur. Conf. Antennas Propag.*, pages 1807–1808, 2013.

[62] B. V. Ha, R. E. Zich, M. Mussetta, P. Pirinoli, and D. N. Chien. Thinning array using improved compact genetic algorithm. *IEEE Proc. AP-S Int. Symp.*, 2013.

[63] K. Chen, X. Yun, Z. He, and C. Han. Synthesis of sparse planar array using modified real genetic algorithm. *IEEE Trans. Antennas Propag.*, 55(4):1067–1073, 2007.

[64] P. C. Magnusson, G. C. Alexander, and V. K. Tripathi. *Transmission lines and wave propagation, 3rd Edition*. CRC Press, 1992.

[65] Gies, D. and Y. Rahmat-Samii. Particle swarm optimization for reconfigurable phase-differentiated array design. *Microw. Opt. Tech. Letters*, 38(3):168–175, 2008.

[66] W. W. Chung, F. Yang, and A. Z. Elsherbeni. Linear antenna array synthesis using taguchis method: a novel optimization technique in electromagnetics. *IEEE Trans. Antennas Propag.*, 55(3):723–730, 2007.

[67] Y. Liu, Q. H. Liu, and Z. Nie. Reducing the number of elements in a linear antenna array by the matrix pencil method. *IEEE Trans. Antennas Propag.*, 56(9):2955–2962, 2008.

[68] Y. Liu, Q. H. Liu, and Z. Nie. Reducing the number of elements in the synthesis of shaped-beam patterns by forward-backward matrix pencil method. *IEEE Trans. Antennas Propag.*, 58(2):604–608, 2010.

[69] C. Chung-Yong, and P. M. Goggans. Using bayesian inference for linear antenna array design. *IEEE Trans. Antennas Propag.*, 59(9):3211–3217, 2011.

[70] K. K. Yan, and Y. Lu. Sidelobe reduction in array-pattern synthesis using genetic algorithm. *IEEE Trans. Antennas Propag.*, 45(7):1117–1122, 1997.

[71] F. J. Ares-Pena, A. Rodriguez-Gonzalez, E. Villanueva-Lopez, and S. R. Rengarjan. Genetic algorithms in the design and optimization of antenna array patterns. *IEEE Trans. Antennas Propag.*, 47(3):506–510, 1999.

[72] M. Donelli, S. Caorsi, F. D. Natale , G. Franceschini, and A. Massa. A versatile enhanced genetic algorithm for planar array design. *Journal of Electromagnetic Waves and Applications*, 18:1533–1548, 2004.

[73] D. W. Boeringer, D. H. Werner, and D. W. Machuga. A simultaneous parameter adaptation scheme for genetic algorithms with application to phased array synthesis. *IEEE Trans. Antennas Propag.*, 53(1):356–371, 2005.

[74] M. M. Khodier, and C. G. Christodoulou. Linear array geometry synthesis with minimum sidelobe level and null control using particle swarm optimization. *IEEE Trans. Antennas Propag.*, 53(8):2674–2679, 2005.

[75] M. Donelli, R. Azaro, L. Fimognari, and A. Massa. A planar electronically reconfigurable wi-fi band antenna based on parasitic microstrip structures. *IEEE Antennas and Wireless Propag. Letters*, 6:623–626, 2007.

[76] W. Zhang, L. Li, and F. Li. Reducing the number of elements in linear and planar antenna arrays with sparseness constrained optimization. *IEEE Trans. Antennas Propag.*, 59(8):3106–3111, 2011.

[77] D. Caputo, A. Pirisi, M. Mussetta, A. Freni, P. Pirinoli, and R. E. Zich. Neural network characterization of microstrip patches for reflectarray optimization. *Proc. 3rd European Conf. Antennas Propag. (EuCAP)*, pages 2520–2522, 2009.

[78] P. Robustillo, J. Zapata, J. A. Encinar, and J. Rubio. Ann characterization of multi-layer reflectarray elements for contoured-beam space antennas in the ku-band. *IEEE Trans. Antennas Propag.*, 60(7):3205–3214, 2012.

[79] A. Freni, M. Mussetta, and P. Pirinoli. Neural network characterization of reflectarray antennas. *Int. Journal Antennas Propag.*, 2012(ID541354), 2012.

[80] Haykin. *Neural Networks: A comprehensive foundation*. Upper Saddle River, NJ, Prentice-Hall, Inc., 1999.

[81] Q. J. Zhang, and K. C. Gupta. *Neural Networks for RF and microwave design*. Norwood, MA, Artech House, 2000.

[82] I. Barriuso, A. L. Gutierrez, M. Lanza, J. R. Perez, L. Valle, M. Domingo, and J. Basterrechea. Comparison of heuristic methods when applied to the design of reflectarrays. *Proc. 5th European Conf. Antennas Propag. (EuCAP)*, pages 970–974, 2011.

[83] Y. Aoki, H. Deguchi, M. Tsuji. Reflectarray with arbitrarily-shaped conductive element optimized by genetic algorithm. *IEEE A-P. Symposium*, pages 960–963, 2011.

[84] H. R. Phelan. Spiraphase reflectarray for multitarget radar. *Microwave Journal*, 20, 1977.

[85] S. V. Hum, J. Perruisseau-Carrier. Reconfigurable reflectarrays and array lenses for dynamic antenna beam control: a review (accepted). *IEEE Trans. Antennas Propag.*, 2013.

[86] L. Boccia, F. Venneri, G. Amendola, and G. Di Massa. Application of varactor diode for reflectarray phase control. *IEEE Proc. AP.-Symposium*, pages 132–135, 2002.

[87] S. V. Hum, M. Okoniewski, and R. J. Davies. Modeling and design of electronically tunable reflectarray. *IEEE Trans. Antennas Propag.*, 55(8):2200–2210, 2007.

[88] O. G. Vendik, and M. Parnes. A phase shifter with one tunable component for a reflectarray antenna. *IEEE Trans. Antennas Propag. Mag.*, 50(4):53–65, 2008.

[89] L. Boccia, G. Amendola, and G. Di Massa. Performance improvement for a varactor-loaded reflectarray element. *IEEE Trans. Antennas Propag.*, 58(2):585–589, 2010.

[90] M. Riel, and J. Laurin. Design of an electronically beam scanning reflectarray using aperture-coupled elements. *IEEE Trans. Antennas Propag.*, 55(5):1260–1266, 2007.

[91] E. Carrasco, M. Barba, and J. A. Encinar. X-band reflectarray antenna with switching-beam using pin diodes and gathered elements. *IEEE Trans. Antennas Propag.*, 60(12):5700–5708, 2012.

[92] J. Huang, and R. J. Pogorzelski. A ka-band microstrip reflectarray with elements having variable rotation angles. *IEEE Trans. Antennas Propag.*, 46(5):650–656, 1998.

[93] C. Guclu, J. Perruisseau-Carrier, and O. Civi. Proof of concept of a dual-band circularly-polarized rf mems beam-switching reflectarray. *IEEE Trans. Antennas Propag.*, 60(11):5451–5455, 2012.

[94] L. Li, Q. Chen, Q. Yuan, K. Sawaya, T. Maruyama, R. Furuno, and S. Uebayashi. Novel broadband planar reflectarray with parasitic dipoles for wireless communication application. *IEEE Antennas Wireless Propag. Letters*, 8:881–885, 2009.

[95] E. Carrasco, M. Barba, J. A. Encinar, M. Arrebola, F. Rossi, and A. Frenni. Design, manufacture and test of a low-cost shaped-beam reflectarray using a single layer of varying-sized printed dipoles. *IEEE Trans. Antennas Propag.*, 61(6):3077–3085, 2013.

[96] M. A. Milon, D. Cadornet, R. Gillard and H. Legay. Surrounded-element approach for the simulation of reflectarray radiating cells. *IEEE Microw. Antennas Propag.*, 1(2):289–293, 2007.

[97] C. Yann, R. Loison, R. Gillard, L. Michele and J. P. Martinaud. A new approach for analyzing reconfigurable reflectarray antennas. *IEEE Trans. Antennas Propag.*, 60(7):3077–3085, 2012.

[98] M. Zhou, S. Sorensen, E. Jorgensen, P. Meincke, O. S, Kim and Breinbjerg. Analysis of printed reflectarrays using extended local periodicity. *Proc. Eur. Conf. Antennas Propag.*, pages 1408–1412, 2011.

[99] Y. Abdallah, C. Menudier, M. Thevenot, and T. Monediere. Investigations of the effects of mutual coupling in reflectarray antennas. *IEEE Antennas Propag. Mag.*, 55(2):49–61, 2013.

[100] D. M. Pozar. *Microwave Engineering, 4th Edition*. John Wiley & Son, Inc., 2011.